THE WOUND-ON-TENSION OF WINDERS WITH NIP ROLLERS

By

YAO REN
Bachelor of Science in Vehicle Engineering
Beijing Institute of Technology
Beijing, China
2006

Master of Science in General Mechanics and Foundation of Mechanics
Beijing Institute of Technology
Beijing, China
2008

Submitted to the Faculty of the
Graduate College of the
Oklahoma State University
in partial fulfillment of
the requirements for
the Degree of
DOCTOR OF PHILOSOPHY
December, 2016

THE WOUND-ON-TENSION OF WINDERS WITH NIP ROLLERS

Dissertation Approved:

Dr. J. K. Good

Dissertation Adviser

Dr. D. A. Lucca

Dr. R. P. Singh

Dr. R. Bulut

ACKNOWLEDGEMENTS

I would like to express my gratitude to my advisor, Dr. J. K. Good. I'm grateful for his guidance and sponsorship. His natural intuition to the essence of such many mechanics fields is something I always admire. His passion and devotion to those problems will always inspire me. I also feel hugely indebted for his patience and tolerance to allow me to choose a hard way to finish my study.

I would like to thank Dr. D. A. Lucca, Dr. R. P. Singh, and Dr. R. Bulut. Their respective artistic ways of lecturing the surface mechanics, advanced composites, and soil mechanics have led me to the wonderland of mechanics. And I sincerely appreciate their time and effort in serving my committee.

I want to thank Mr. Ron Markum's help in the experimental work. Without his help I can never finish those lab tests. Our lab is his kingdom. I appreciate he guided me through there and helped me develop my experimental skills there.

I am grateful to every colleague and friend I met during my study. Each of you has provided a different thinking paradigm to remind me being humble and always learning.

Last but most important, I would like to thank my wife Hui Ding. Through all those years, she's not only willing to share my happiness due to every step forward but more in every piece of failure and frustration I encountered. I am also thankful for my parents' all along support.

Name: YAO REN

Date of Degree: DECEMBER, 2016

Title of Study: THE WOUND-ON-TENSION OF WINDERS WITH NIP ROLLERS

Major Field: MECHANICAL AND AREOSPACE ENGINEERING

Abstract: Roll-to-roll (R2R) manufacturing is widely used to create products from traditional web materials such as plastic webs, metal foils, to the recent printed and flexible electronics. Winding or rewinding is a critical component in any R2R manufacturing. Webs may witness damage and defects due to inappropriate residual stresses in the wound rolls, which cause economic losses. Preventing those defects requires an accurate prediction of wound roll stresses. The Wound-On-Tension (WOT) is the tension in the outermost lap of a winding roll. It is the most influential input which determines the wound roll stresses. The WOT is dependent of winder types, material properties of web, winding parameters, and geometry of the winder. In this study, an explicit finite element code Abaqus/Explicit is used to develop a model which account for all those aspects. Winder types of pure center winder, center winder with nip, surface winder, and hybrid (torque differential) winder were studied. The WOT is found to be governed by the contact mechanics, specifically the slip/stick behavior, between web and nip and web layers themselves in the nip contact zone. The explicit Abaqus model developed successfully deals with this problem. Web material properties are known to be state dependent on stresses and have a significant impact on the WOT. This is first time accommodated by implementing a user-defined subroutine VUMAT in Abaqus. New test methods were developed for material properties that are critical to the WOT but difficult to measure. Experimental verification of the WOT was conducted and good agreement was found. A parametric model was developed by Abaqus Python scripting, which facilitates use of the model to predict WOT by analysts in research and industry.

Table of Contents

List of Figures

List of Tables

Chapter 1. Introduction

The internal stresses within winding rolls are known to be sensitive to the tension within each layer of material that is wound onto the roll. Observation has shown this tension level to be highly dependent on the type of winding equipment (a winder) used and the winder operating parameters. Winding defects have been coupled to internal stress levels within rolls. This dissertation is concerned with developing methods for predicting the tension in the outer layer of a winding roll. The focus will be on a class of winding equipment that employ impinged nip rollers into the outer surface of the winding roll. These winders comprise a very large portion of the winding equipment used in roll to roll (R2R) manufacturing processes. The tension developed in the outer layer of the winding roll by these winders is largely unknown and is governed by the science of contact mechanics and is much influenced by material behavior. The results of this research will be used in conjunction with existing winding models to predict wound roll stresses and hence to avoid defects and economic loss.

1.1 Background

Webs are defined herein as materials in the form of long, thin, and flexible strips. Webs can have considerable width (as wide as around 10 m) but even so will be inconsequential in comparison to their length (usually in the magnitude of kilometers). Paper, plastic films, textiles, and aluminum foils are some common examples of web

materials. Webs have a broad application in industry as well as our everyday life. Suppliers manufacture and process webs continuously on production lines, which enables not only the mass production of a rich variety of products, but also the automation of many manufacturing processes [1]. The most effective and convenient way to store the produced webs is to wind them into rolls [2], where miles of web can be stored in a compact volume. Figure 1-1 shows traditional rolls of metal web and more recent rolls of printed electronics. Many roll-to-roll manufacturing processes such as coating, laminating and printing are time dependent but all these processes may be necessary in manufacturing a given product. This necessitates the unwinding and rewinding of webs several times to facilitate the unique optimal velocity for each process. Potential damage due to residual winding stresses is possible each time the web is wound. Value is added to the web in each successive process and the loss associated with winding damage after the later web process is much greater than that associated with winding loss after the first process, which often is the creation of the web. Winding or rewinding is usually the last process in an R2R manufacturing; the potential damage and defects which may occur at this stage and the mechanism they are forming are worthy special investigation.

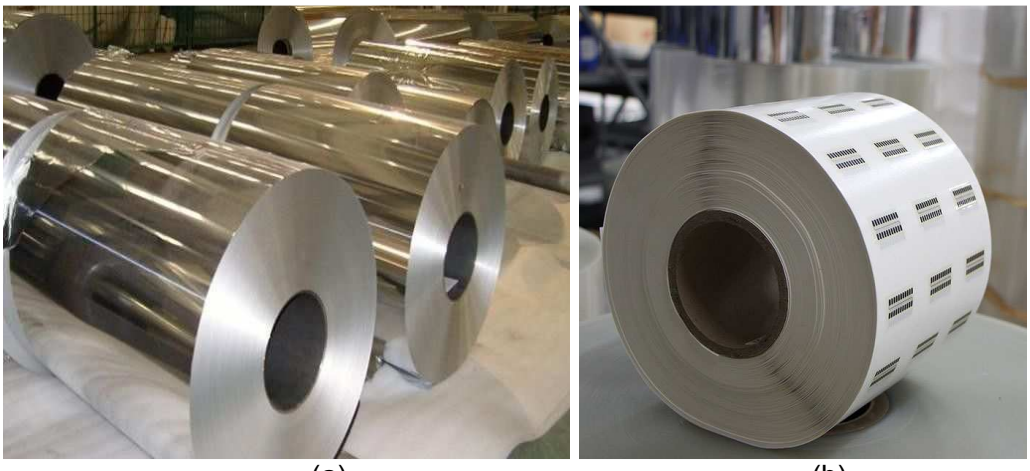

(a) (b)

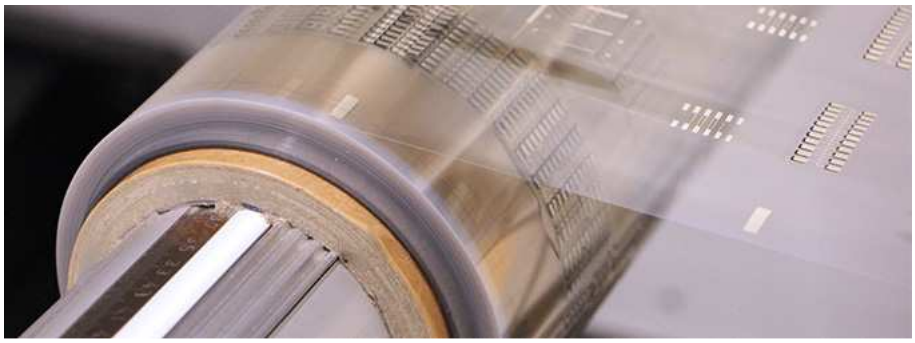

(c)

Figure 1-1 (a) Roll of metal web, (b) roll of printed electronics, (c) winding printed electronics

1.1.1 Conventions

Web handling and R2R manufacturing, as more an industrial field, have conventions and terms that are accepted by insiders by default but may be unfamiliar to others. This section briefly introduces necessary conventions and terms to facilitate our discussion within this thesis. As discussed earlier, the geometric state of the web during an R2R manufacturing would be mostly flat between unwind and rewind part, or a cylinder-like but actually a spiral in the roll. A Cartesian coordinate system is adopted for web in the flat state and a cylindrical coordinate system for web in the roll. Based on those two coordinate systems, the web behavior and material properties can be conveniently described. The two coordinate systems are shown in Figure 1-2. The axes of the Cartesian coordinate system are named by convention:

- MD: Machine Direction, the direction the web or material flow travels through an R2R manufacturing machine. It is also labeled as 1-axis.
- CMD: Cross Machine Direction, the direction in the web surface plane and perpendicular to MD. It coincides with the axial direction of the roll and is also labeled as 3-axis.

- ZD: Z Direction, the direction perpendicular to the web surface plane (out-of-plane direction) and forms a right-hand set with MD and CMD. It is also labeled as 2-axis.

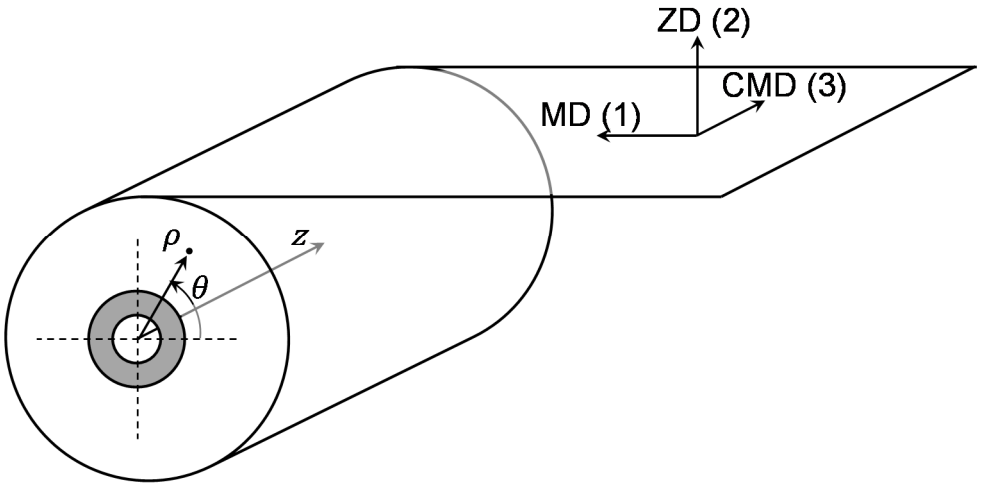

Figure 1-2 Coordinate system of web and wound roll

After the web is wound into a roll, the MD, ZD and CMD are transformed into the tangential direction, radial direction and axial direction respectively, followed web's deformation as shown in Figure 1-2. The origin of the cylindrical coordinate system is usually set at the center of one side face of the roll. A group of coordinates (θ,r,z) is used to depict the material point of the web. Coordinates z in the cylindrical system should be distinguished from ZD in Cartesian system. Variables involved in solving a web handling problems are usually referred to both systems. For example, E_{MD}, E_θ or E_1 all designate the Young's modulus of the web in MD. E_{ZD}, E_r or E_2 designate the out-of-plane or radial modulus. E_{CMD}, E_z or E_3 designate the CMD Young's modulus. This convention will be inherited through this thesis by default.

1.1.2 Winders

Winders are the equipment responsible for converting the web from a flat state to that of a coil. In industry, several types of winders have been developed to serve specific needs, as shown in Figure 1-3. The center winder (Figure 1-3 (a)) is the simplest and oldest form of winder, which is capable of dealing with many traditional web materials in relatively low speed winding. To meet the challenge raised by modern web processing industry, especially in occasions where high speed winding is demanded and more complex web materials are treated, winders with nip rollers prevail. Nip rollers can be beneficial to winding webs in two main aspects. First, the nip can provide additional winding tension beyond that provided by web line tension alone [3]. This enable the ability to control winding tension at the end of the web line without changing web line tensions, which may be constrained by upstream processing requirements. Second, the nip helps exclude air that would be entrained into the wound rolls and can prevent wound roll defects related with air entrainment [2]. Winders with a single nip roller are categorized into three types, as shown in Figure 1-3 (b), (c), and (d), based upon how torque is input to wind rolls. It is typical that the web will wrap the nip roller π radians before entry to the wound roll to maintain independence between web line tension and nip load; however other wrap angles are witnessed where that independence is lost. The different types of winders that will be considered in this dissertation include:

- Center winder: the roll is completely supported and driven by its core. The core is the structure upon which the roll is wound. It is a tube composed of paper fibers combined with resins, plastic, or in some cases can be composed of metal. Web line tension is established by the motor which provides torque to drive the core.

The internal stresses of the wound roll are only controlled by the web line tension (Figure 1.1(a)).

- Center winder with a nip roller: the roll is still driven by its core, while an additional undriven nip roller is forced against the perimeter of the winding roll. The nip roller can be an effective means of rejecting the air from entraining in the wound roll. The internal stresses in the wound roll are controlled by web line tension and the force of the nip roller (nip load) against the wound roll (Figure 1.1(b)). Nip rollers may be cylindrical metal shells but also may be covered with elastomers. Since elastomers can be nearly incompressible it can increase in velocity in the contact zone. The elastomer will have a wider contact zone for a given nip load compared to a nip roller with a metal surface. This will affect contact pressure, slip in the contact zone and the tension and the tension in the outer layer of the winding roll. We will discuss this in later chapters.
- Surface winder: the configuration of this winder is quite similar to the center winder with a nip roller. However, the drive motor is connected to the nip roller rather than the core inside the wound roll. It is named so because the torque provided to the nip roller drives the surface of the winding roll. Similar to the center winder with a nip roller, the web line tension and the nip load can both affect the stress state inside the wound roll, but the tension developed in the outer layer may be the same or very different (Figure 1.1(c)).
- Center-surface winder: this winder is also called differential torque winder (or hybrid winder) because the core of the wound roll and the nip roller are driven by two independent motors. It can operate over a wider range of web line tension and

nip loads [2]. For this winder the two motor torques and the nip load all affect the pressures and stresses developed in the wound roll (Figure 1.1(d)). This winder can operate similarly to the center winder with a nip or the surface winder depending on how much torque is provided to the core versus the nip. If substantial torque is input at both locations it is possible to wind rolls that are quite different than those produced by other winders.

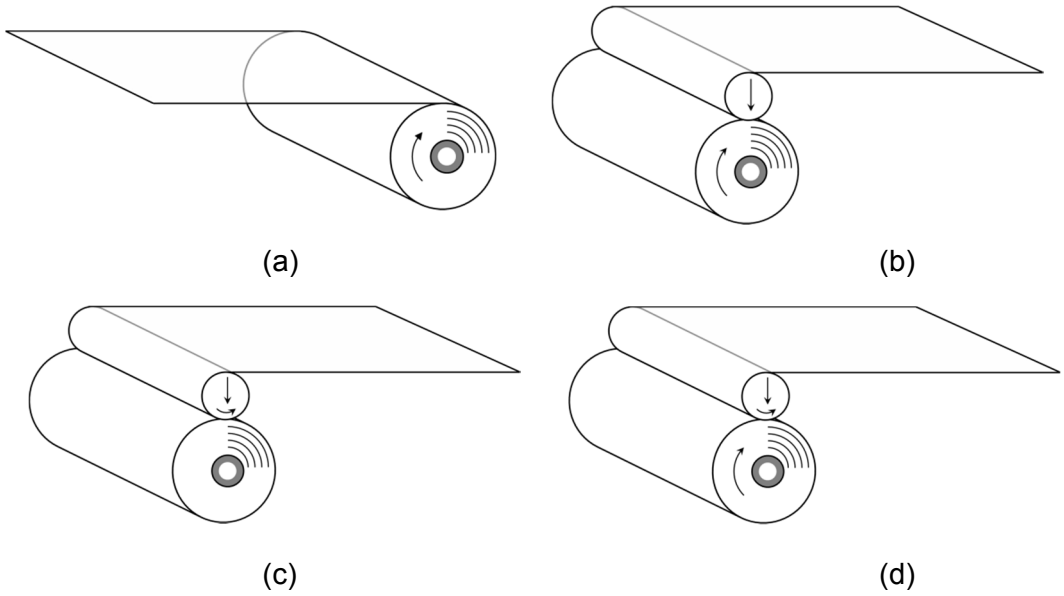

Figure 1-3 Types of winders: (a) center winder, (b) center winder with a nip roller, (c) surface winder, and (d) center-surface winder

For a given web product requiring winding, decisions regarding the best winder to use or purchase is often made by experience of what winder could successfully wind products thought to be similar. Engineers are often forced to make experience based decisions when sciences are not sufficiently developed to help them make quantitative decisions. The existing sciences cannot tell the engineer how a given web will wind on a given winder nor reliably predict the tension which a given winder will induce in the outer layer of the winding roll. This is crucial as the tension in the outer layer of a winding roll

governs the internal stresses [2]. Many roll and web defects are related to the internal stresses in the wound roll. Figure 1-4 shows two typical roll defects: starring and tin canning, which are caused by the buckling of webs in roll due to inappropriate circumferential stress and axial stress respectively. Other defects can result in the nip contact zone where high contact pressures and varied states of stick and slip can occur.

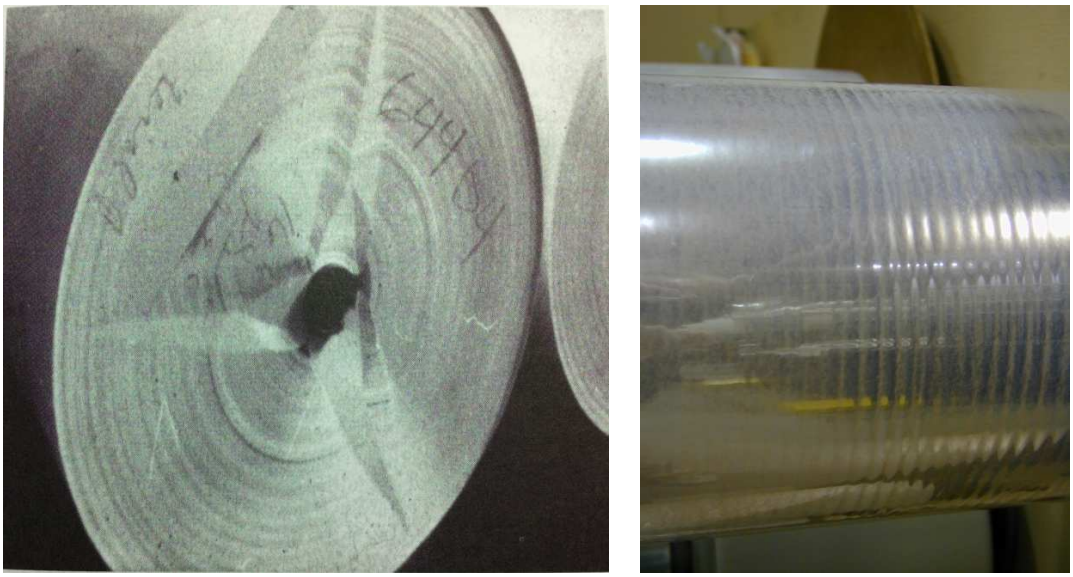

(a) (b)

Figure 1-4 Web and roll defects: (a) starring, (b) tin canning

1.2 Objective and Significance

The objective of this research is to develop a quantitative method for determining the mechanics of tension development in the outer layer of a winding roll impinged by a nip roller. The method developed must be robust such that this tension is reliably determined regardless of winder type, web material type and type of nip roller employed.

A successful development is paramount for helping engineers avoid defects when winding webs and when choosing a winder and winder operating parameters to wind a given web material. This development will hopefully move winding from a field of experiential technology to that of a known science.

Chapter 2. Literature Survey

This chapter consists of three sections. The first section (2.1) briefly reviews the literature that developed in support of the mechanics of winding rolls on center winders. Mechanically center winders are the simplest type of winder (Fig. 1.1(a)) and its configuration in some form exists in all other types of winders. However, the solid mechanics analysis of the rolls wound on a center winder is not so simple. If the tension that a more complex winder induces into the outer layers of a winding roll was known, center wound roll analyses could be extended to other winder types to determine their wound roll stresses. The second section (2.2) reviews the literature that has developed that explore how winders with nip rollers (Fig. 1.1(b), (c), (d)) develop residual stresses that differ from the center winding case. The third section provides a summary of the literature survey and concludes with the objectives of this research study.

2.1 Review of Winding Models

Winding models are the mathematical models that are developed to predict residual stresses (or strains) inside a wound roll. Like a typical solid mechanics problem, wound roll stresses problems are solved through the consideration of four ingredients: geometry, material law, boundary conditions and solution techniques. Winding models can be categorized also based on how those four ingredients are treated, as shown in Figure 2-1. The complexity and details chosen to be considered in the first three ingredients

determine the solution techniques that can be used. Looking back, the history of winding models development seems like a process that the nonlinearity in the problem is gradually unveiled and accounted for. The nonlinearity also comes from those ingredients.

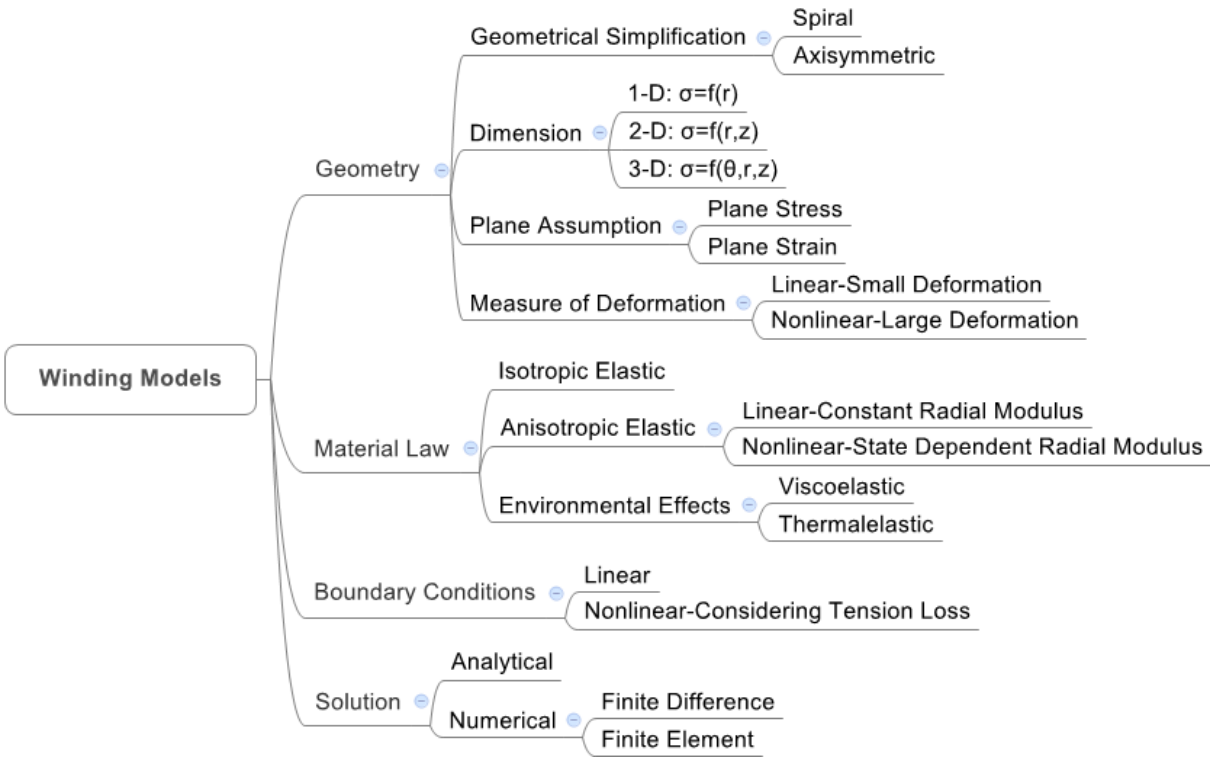

Figure 2-1 Characteristics of winding models

The geometric ingredient of winding models includes geometric simplification, the dimension of the problem being modeled, the assumption of plane stress or plane strain, and the consideration of the scale of deformation. The assumptions of plane stress and plane strain, on one hand, dictate constitutive relations. They have geometric implications as well. Plane stress assumption is being made that the wound roll is relatively narrow in the axial dimension. The surface equilibrium requires that stress components related with the axial dimension on the side faces of rolls to be zero and if the two faces are sufficiently close those stresses components along the whole roll can be assumed negligible. On the contrary, in wide rolls we may assume that any internal section of the

roll is constrained from deforming in the axial direction, which is described as the plane strain assumption. This assumption results in zero axial strain but non-zero stresses in the wound roll.

Geometric simplification regards the level of geometric features of wound roll is going to be modeled. Strictly speaking, the wound roll is a spiral structure. However due to the difficulty in modeling a real spiral and the fact that most webs have a small thickness, most winding models assume a spiral of web associated with one revolution of the roll can be modeled as a cylinder. Early winding researchers Gutterman in 1959 [4] and Catlow et al. in 1962 [5] started to adopt this simplification. An additional benefit of adopting this simplification is it also introduces axial symmetry to the model, and thus greatly reduced the complexity of modeling. This simplification is very effective and has been adopted by researchers for a long period of time, although no careful validation is conducted until recent works of Yanabe et. al. in 2010 [6] and Kandadai et. al. in 2011 [7]. They used finite element method to simulate the winding process where the spiral feature of roll is conserved.

The dimension of the problem defines the number of the spatial coordinates on which the variables of the wound roll depend. If adopting the cylindrical simplification and the hence axial symmetry, the circumferential coordinate θ will be disregarded; the radial and axial position (r, z) are the independent spatial coordinates. If plane stress assumption is further adopted like in earlier models by Gutterman and Catlow et al., the nontrivial stress components are circumferential and radial stress and they only depend on radial position. This kind of model is one dimensional (1-D), where variables are dependent only on the radial position r. Later on as interest was gained in axial stresses which are

created during winding and the defects associated therewith, researchers [8; 9; 10] from 1991 began to model the stress variation with the radial (r) and axial (z) dimensions. These models are two-dimensional (2-D), where variables are dependent on radial and axial positions (*r, z*). The model of finite element simulation of winding process [6] and [7] mentioned earlier is a different kind of 2-D model, where variables are dependent on circumferential and radial positions (θ, r).

The last aspect of the geometry ingredient is the scale of deformation. Earlier models were built on the small deformation theory until Benson in 1995 [11] produced the first model which accounted for large deformation. Small deformation theory assumes that the deformed and undeformed configurations are identical. This is true for stiff webs, however, untrue for some soft web materials, such as nonwovens, which can have large deformation during winding; a large deformation model yields a better prediction of the stresses within the wound roll. Large deformation models are based on continuum theory to depict the motion of body where geometric nonlinearity is accounted for.

The second ingredient of winding models regards the web material that is modeled and the constitutive law used to describe its behavior. The simplest models assumed an isotropic linear elastic material which has an identical modulus in all directions. This might be thought adequate for some thick web materials such as steel. But many web materials have a smaller out-of-plane modulus than their in-plane modulus due to their manufacturing process. For instance when PET webs are manufactured, molecular chain are lying in the plane of web. The web is much stiffer when loading in in-plane than out-of-plane direction. Therefore, Altmann in 1968 [12] produced an anisotropic linear elastic material model to introduce a different value for the ZD modulus. This ZD modulus was

constant during the analysis. Pfeiffer [13] was first to find that the ZD modulus of multiple layers of web in compression is not a constant. He demonstrated the ZD modulus is dependent on ZD strain or stress. Allowing the variation of radial modulus during the analysis introduced nonlinearity to the models. Part of this nonlinearity is due to the geometric nonlinearity of asperities of contact surface between layers subjected to compression. The remainder of the nonlinearity is due to internal material nonlinearity within the web layer when subject to compression. Both sources of this nonlinearity have been accounted for as a material nonlinearity in modeling. As winding models grew to maturity, environmental factors were introduced, where viscoelastic and thermal-elastic properties of the web material began to be modeled.

The third ingredient of winding models is the boundary conditions (BCs). The governing differential equations in winding models are second order and hence require two boundary conditions to determine the particular solution. One is an inner BC at the core surface, which requires knowledge of the core stiffness. The specific inner BC is that the deformation of the outer surface of the core and the inner surface of the first layer of web are equal. The second BC concerns the most recent lap being wound on, which requires knowledge of winding tension in the outer lap and can be used to infer the radial pressure beneath that lap. The outer BC adopted by earlier models is based on the equilibrium of a thin cylinder, which assumes that the radius is constant. For some very compressive materials like newsprint as a new lap is wound on to the roll, the roll layers beneath the outer layer deform radially and achieve equilibrium at a smaller radial position. With elevated winding tension the radial position at which equilibrium is achieved will decrease even further. For this kind of web material, traditional models fail to predict

consistent results with experimental data due to the inaccurate outer BC. Good, et al. [14] reformed a new outer BC which considers the radial deformation and the associated tension losses. The new BC explicitly involves radial strain and the radius of roll, which introduced nonlinearity into the outer boundary condition. Some of the axisymmetric models [15; 16] noted that as a function of web nonuniformity in thickness and length in the CMD that the outer BC was dependent on CMD (z) location and accounted for this in their models.

The last ingredient of winding models to be discussed is the solution technique which is used to solve the governing equations derived in the model. Models by Gutterman, Catlow et al., and Altmann [4; 5; 12] are linear models. They have closed form analytical solutions. It is noted that in Altmann's model [12] although the analytical solution was obtained, due to the complex integration involved, a numerical integration method was used alternatively. Models afterwards involved nonlinearity in one or more aspects of the geometry, material law, or the BC properties. These nonlinear models must be solved by numerical methods. For the 1-D nonlinear model developed by Hakiel [17], a finite difference method was used. The 2-D axisymmetric models [15; 18; 19; 16] which appeared later were solved using the finite element method.

A timeline of corner stones in the history of winding models is shown in Figure 2-2. The literature review will now concentrate on these works.

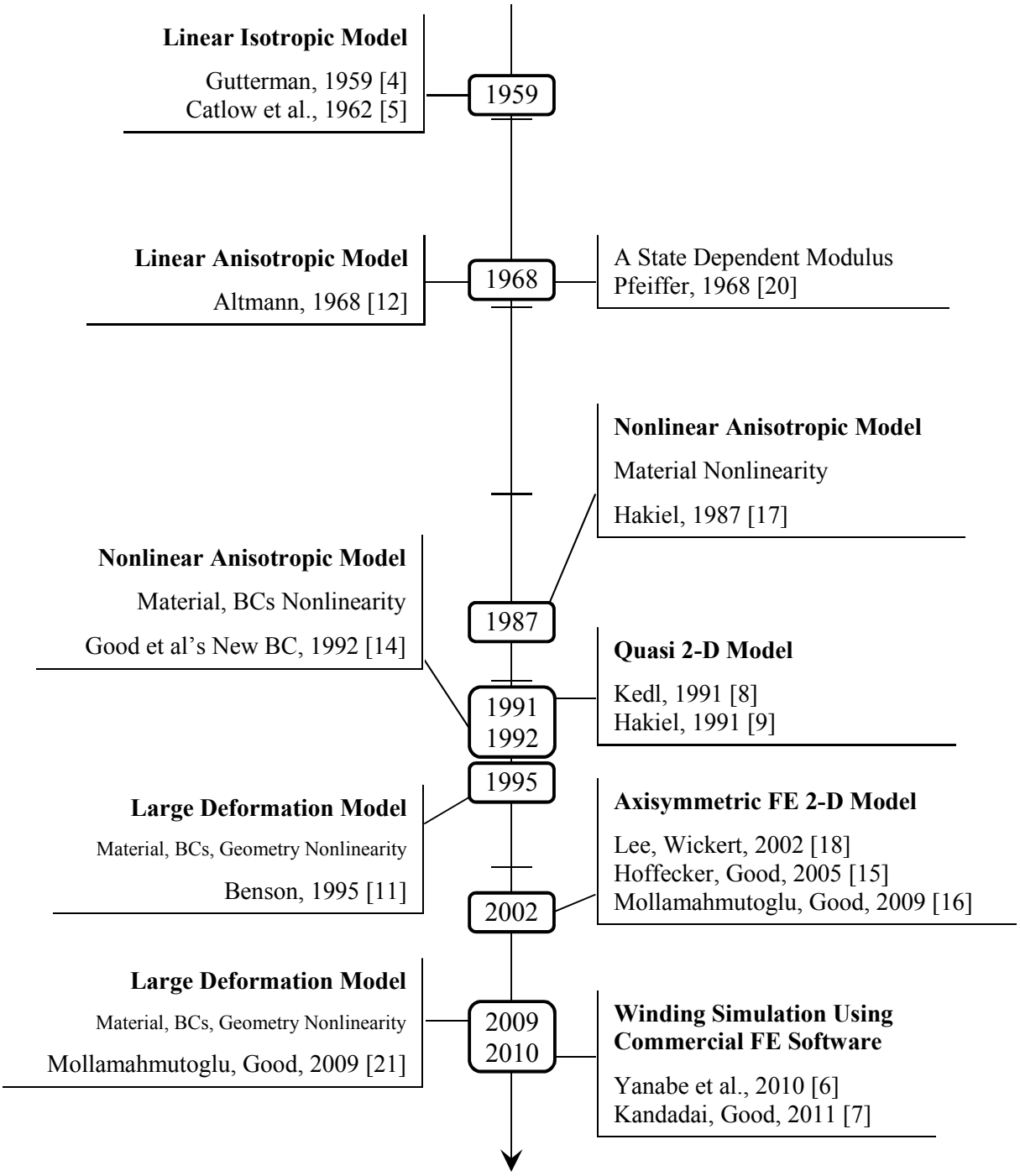

Figure 2-2 Timeline of corner stones in history of winding models

2.1.1 1-D Winding Models

Gutterman and Catlow's Linear Isotropic Model

Gutterman in 1959 [4] and Catlow in 1962 [5] are the forerunners who began modeling the winding problem. They viewed the wound roll as a cylinder under internal and external pressure, as shown in Figure 2-3. The stress distribution of the wound roll was calculated by the superposition of incremental stress generated by adding each lap onto the cylinder. The web was modeled as an isotropic linear elastic material, which might be problematic for most web materials. However, the geometric simplification, the method accreting concentric web layers and summing the incremental stresses to form total stresses was inspired and adopted by many later models. Due to the significance of these models and the similarity with respect to some later models, the derivation in the model is stated in detail, to serve as a foundation for later models.

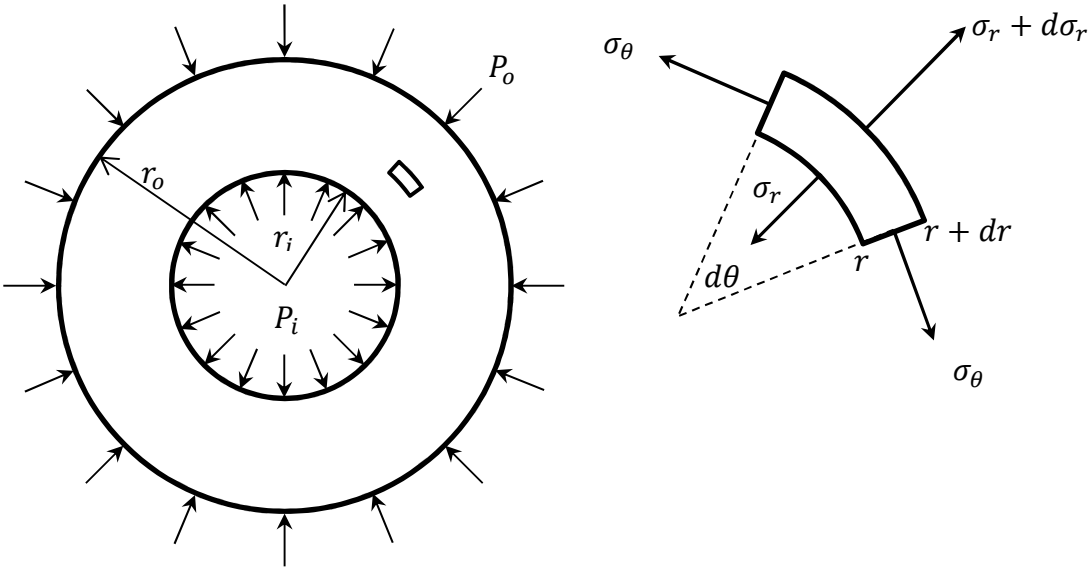

Figure 2-3 Cylinder under internal and external pressure

In Figure 2-3 a small element is shown subject to axisymmetric stresses acting in the $r-\theta$ plane in the absence of body forces. If these stresses are converted to forces acting in a radial direction, an equilibrium expression written in the radial direction can be established. After omitting second order terms this expression becomes:

$$r\frac{d\sigma_r}{dr}+\sigma_r-\sigma_\theta=0 \tag{2.1}$$

The small strain-displacement relationships in a polar coordinate system are:

$$\varepsilon_r=\frac{du}{dr} \tag{2.2.a}$$

$$\varepsilon_\theta=\frac{u}{r} \tag{2.2.b}$$

If expression (2.2.b) is differentiated with respect to radius and combined with (2.2.a), the strain compatibility expression (2.3) results:

$$r\frac{d\varepsilon_\theta}{dr}+\varepsilon_\theta-\varepsilon_r=0 \tag{2.3}$$

These early models adopted the plane stress assumption, and thus the isotropic elastic constitutive equations are:

$$\varepsilon_r=\frac{1}{E}(\sigma_r-\nu\sigma_\theta) \tag{2.4.a}$$

$$\varepsilon_\theta=\frac{1}{E}(\sigma_\theta-\nu\sigma_r) \tag{2.4.b}$$

Equation (2.1), (2.3) and (2.4) can be combined and rearranged to produce the governing equation:

$$\frac{d^2\sigma_r}{dr^2}+\frac{3}{r}\frac{d\sigma_r}{dr}=0 \tag{2.5}$$

The general form of the solution for equation (2.5) is:

$$\sigma_r=C_1+\frac{C_2}{r^2} \tag{2.6}$$

where C_1 and C_2 are two constants. Two boundary conditions are needed to determine the specific solution for the problem. The pressures at inner surface and outer surface are naturally used:

$$\sigma_r|_{r=r_i} = -P_i \tag{2.7.a}$$

$$\sigma_r|_{r=r_o} = -P_o \tag{2.7.b}$$

By inserting (2.7) into (2.6), the specific solution for the radial stress is achieved. By substituting the radial stress into the equilibrium expression (2.1), the circumferential stress is obtained. Now both the radial and circumferential stress is known as a function of radius:

$$\sigma_r = \frac{P_i r_i^2 - P_o r_o^2}{r_o^2 - r_i^2} - \frac{(P_i - P_o) r_i^2 r_o^2}{r_o^2 - r_i^2} \frac{1}{r^2} \tag{2.8.a}$$

$$\sigma_\theta = \frac{P_i r_i^2 - P_o r_o^2}{r_o^2 - r_i^2} + \frac{(P_i - P_o) r_i^2 r_o^2}{r_o^2 - r_i^2} \frac{1}{r^2} \tag{2.8.b}$$

Linear isotropic models use these stress expressions (2.8) in an incremental fashion. These expressions are used to consider the stress change in lap with radius r_l in the wound roll as the k^{th} lap is wound onto the outside of the winding roll:

$$\delta\sigma_r^{l,k} = \frac{P_i^k r_i^2 - P_o^k r_o^2}{r_o^2 - r_i^2} - \frac{\left(P_i^k - P_o^k\right) r_i^2 r_o^2}{r_o^2 - r_i^2} \frac{1}{r_l^2} \tag{2.9.a}$$

$$\delta\sigma_\theta^{l,k} = \frac{P_i^k r_i^2 - P_o^k r_o^2}{r_o^2 - r_i^2} + \frac{\left(P_i^k - P_o^k\right) r_i^2 r_o^2}{r_o^2 - r_i^2} \frac{1}{r_l^2} \tag{2.9.b}$$

The outer BC is determined by considering the equilibrium of the k^{th} lap. Since the tension in the outer k^{th} lap is the winding tension $T_w|_{r=r_k}$, the pressure it applies to the current roll P_o^k can be calculated as:

$$P_o^k = -\frac{T_w|_{r=r_k}}{r_k} h \tag{2.9c}$$

For the inner BC, the calculation of the pressure on the inner surface of the roll is a little bit more complex. First the stiffness of the core E_c is defined in expression (2.10). An assumption here is that no slippage takes place between the first lap of the roll and the core so that the deformation of two is compatible. Equation (2.11) gives an expression [2] for the stiffness of an isotropic core. It is derived based on a similar analysis through (2.1)-(2.8) for the core material, where E_{cm} and ν_c are the modulus and Poisson's ratio of the core material. d_c and t_c are the diameter and the thickness of the core, respectively.

$$E_c = \frac{\sigma_r}{\varepsilon_\theta}\Big|_{r=r_i} = -\frac{P_i^k}{\varepsilon_\theta|_{r=r_i}} \tag{2.10}$$

$$E_c = 2E_{cm}t_c\frac{d_c + t_c}{d_c^2 + 2(1-\nu_c)(d_c t_c + t_c^2)} \tag{2.11}$$

The circumferential strain at the inner surface of the roll can be calculated by (2.12):

$$\varepsilon_\theta|_{r=r_i} = \frac{\sigma_\theta - \nu\sigma_r}{E}\Big|_{r=r_i} \tag{2.12}$$

Combining expressions (2.10), (2.12) and (2.8), yields the inner pressure P_i^k:

$$P_i^k = P_o^k\frac{2r_k^2E_c}{(r_k^2 - r_i^2)(E + \nu E_c) + (r_k^2 + r_i^2)E_c} \tag{2.13}$$

Inserting (2.9) and (2.13) into (2.9a and 2.9b), the incremental stresses resulting from the addition of the k^{th} lap onto the roll are calculated. The final stress distribution in the roll is obtained by the superposition of all the incremental stresses in each layer as the result of all layers that were wound onto the roll outside of that layer:

$$\sigma_r|_{r=r_l} = \sum_{k=l+1}^{n}\delta\sigma_r^{l,k} \tag{2.14.a}$$

$$\sigma_\theta|_{r=r_l} = T_w|_{r=r_l} + \sum_{k=l+1}^{n}\delta\sigma_\theta^{l,k} \tag{2.14.b}$$

Altmann's Linear Anisotropic Model

Altmann in 1968 [12] was first to introduce an anisotropic material law to a winding model. This allowed the tangential modulus E_θ and the radial modulus E_r to differ. The constitutive equations differ from (2.4) and are shown in expressions (2.15), where $\nu_{r\theta}$ and $\nu_{\theta r}$ are the Poisson's ratio that couple a θ direction stress to radial strain and a radial stress to a θ direction strain, respectively.

$$\varepsilon_r = \frac{\sigma_r}{E_r} - \nu_{r\theta}\frac{\sigma_\theta}{E_\theta} \tag{2.15.a}$$

$$\varepsilon_\theta = \frac{\sigma_\theta}{E_\theta} - \nu_{\theta r}\frac{\sigma_r}{E_r} \tag{2.15.b}$$

The development is similar to the previous models. Combining the equilibrium, strain-displacement, and constitutive equations and inserting the two BCs, the incremental stress due to lap with thickness *ds* is expressed in (2.16), where all parameters are defined in (2.17). In this equation, s is the dummy variable of integration from internal radius r to the outside radius R, where s, r, R are nondimensionalized with respect to the core radius r_i.

$$d\sigma_r = -\left(\frac{1+ar^{-2\gamma}}{r^b}\right)\left(\frac{s^b}{1+as^{-2\gamma}}\right)\frac{T_w}{s}ds \tag{2.16.a}$$

$$d\sigma_\theta = -\left(\frac{\alpha+a\beta r^{-2\gamma}}{r^b}\right)\left(\frac{s^b}{1+as^{-2\gamma}}\right)\frac{T_w}{s}ds \tag{2.16.b}$$

$$\begin{aligned}
\epsilon_r &= \frac{E_\theta}{E_r}\\
\epsilon_C &= \frac{E_\theta}{E_c}\\
\mu &= \frac{1}{2}(\nu_{r\theta}+\epsilon_r\nu_{\theta r})\\
\delta &= \frac{1}{2}(\nu_{r\theta}-\epsilon_r\nu_{\theta r})\\
\gamma &= \sqrt{\delta^2+\epsilon_r}\\
\alpha &= \gamma-\delta\\
\beta &= \gamma+\delta
\end{aligned} \tag{2.17}$$

$$a = \frac{\gamma - \mu - \epsilon_r}{\gamma + \mu + \epsilon_r}$$
$$b = 1 - a$$

The final stress distribution of the wound roll is obtained by integrating the incremental stresses:

$$\sigma_r|_{r=r_l} = \int_{r_l}^{R} d\sigma_r \, ds = -\left(\frac{1 + ar^{-2\gamma}}{r^b}\right) \int_{r_l}^{R} \left(\frac{s^b}{1 + as^{-2\gamma}}\right) \frac{T_w}{s} ds \tag{2.18.a}$$

$$\begin{aligned} \sigma_\theta|_{r=r_l} &= T_w|_{r=r_l} + \int_{r_l}^{R} d\sigma_\theta \, ds \\ &= T_w|_{r=r_l} - \left(\frac{\alpha + a\beta r^{-2\gamma}}{r^b}\right) \int_{r_l}^{R} \left(\frac{s^b}{1 + as^{-2\gamma}}\right) \frac{T_w}{s} ds \end{aligned} \tag{2.18.b}$$

A State Dependent Radial Modulus

In earlier studies [12], authors had already acknowledged the nonlinear compression behavior of web in ZD but opted to use a constant modulus in the final solution, probably for the purpose of obtaining a closed form analytical solution. In 1966, Pfeiffer [13] proposed an expression for the ZD modulus based on compression tests of paper, and then modified it to a better form in 1968 [20], which is shown in (2.19). The modulus is the derivative of pressure with respect to the strain as (2.20) shows. This description was later widely accepted by web handling researchers because it identified the compressive material characteristics with only two constants, K_1 and K_2, and is named as Pfeiffer's law. Some authors also expressed the radial modulus in the form of a polynomial equation.

$$P = -\sigma_r = K_1(e^{K_2 \varepsilon_r} - 1) \tag{2.19}$$

$$E_r = \frac{d\sigma_r}{d\varepsilon_r} = \frac{dP}{d|\varepsilon_r|} = K_1 K_2 e^{K_2|\varepsilon_r|} = K_2(P + K_1) \tag{2.20}$$

Hakiel's Nonlinear Anisotropic Model

Hakiel in 1987 [17] created a winding model which allows anisotropy, a state dependent radial modulus and a variable winding tension. The derivation process is similar to the linear isotropic model. With the anisotropic material properties, and considering the incremental stress $\delta\sigma_r$ directly, the governing equation becomes (2.21). It should be noted that E_r is a state dependent variable in this development.

$$\frac{d^2\delta\sigma_r}{dr^2} + \frac{3}{r}\frac{d\delta\sigma_r}{dr} - (\frac{E_\theta}{E_r} - 1)\delta\sigma_r = 0 \tag{2.21}$$

The outer BC is similar to expression (2.9), but it is written in an incremental fashion:

$$\delta\sigma_r|_{r=r_k} = -\frac{T_w|_{r=r_k}}{r_k}h \tag{2.22}$$

The method of incorporating the inner BC is similar to the inner BC (2.13) in the linear isotropic model. In this case a derivative BC is produced that is evaluated at the core each time a new layer is added to the roll:

$$\left.\frac{d\delta\sigma_r}{dr}\right|_{r=r_c} = (\frac{E_\theta}{E_c} - 1 + \nu_{\theta r})\left.\frac{\delta\sigma_r}{r}\right|_{r=r_c} \tag{2.23}$$

Since the governing equation has non-constant coefficients due to the state dependent radial modulus, a central difference approximation (2.24) is used to discretize the governing equation (2.21) and BC (2.22) and (2.23) and results in (2.25). When the $(k+1)^{th}$ lap is being wound on to the roll, (2.25.a) is a set of $k-2$ linear equations with k unknowns with l ranging from 1 to k. Combined with (2.25.b) and (2.25.c), the total number of k equations can be solved to yield the change of stresses at different radial positions caused by adding the $(k+1)^{th}$ lap. The overall stresses distribution is then obtained by the same superposition method that was shown in equation (2.14).

$$\left.\frac{d^2\delta\sigma_r}{dr^2}\right|_{r=r_l} = \frac{\delta\sigma_{r_{l+1}} - 2\delta\sigma_{r_l} + \delta\sigma_{r_{l-1}}}{h^2} \tag{2.24.a}$$

$$\left.\frac{d\delta\sigma_r}{dr}\right|_{r=r_l} = \frac{\delta\sigma_{r_{l+1}} - \delta\sigma_{r_{l-1}}}{2h} \tag{2.24.b}$$

$$\delta\sigma_{r_{l+1}}\left(1 + \frac{3h}{2r_l}\right) + \delta\sigma_{r_l}\left[\frac{h^2}{r_l^2}\left(1 - \frac{E_\theta^2}{E_{r_l}^2}\right) - 2\right] + \delta\sigma_{r_{l-1}}\left(1 - \frac{3h}{r_l}\right) = 0 \tag{2.25.a}$$

$$\delta\sigma_{r_{k+1}} = \frac{T_w|_{r=r_{k+1}}}{r_{k+1}}h \tag{2.25.b}$$

$$\frac{\delta\sigma_{r_2} - \delta\sigma_{r_1}}{h} = \delta\sigma_{r_1}\left(\frac{E_\theta}{E_c} - 1 + \nu_{\theta r}\right) \tag{2.25.c}$$

Good's Modified Nonlinear BC

As stated earlier, for very compressible materials wound at higher winding tensions, the traditional outer BC (2.20) fails to consider the radial deformation of the roll, and yields a value of wound-on-tension that is too high. Good et al. in 1992 [14] reformed the outer BC by considering the radial deformation of the roll:

$$\delta\sigma_r|_{r=r_k} = -\left(T_w|_{r=r_k} + E_\theta\frac{u|_{r=r_k}}{r_k}\right)\frac{h}{r_k} \tag{2.26}$$

This new outer BC involves the radial displacement u which is always negative (the roll always deforms inwardly). Therefore the effective tension is less than the original winding tension T_w, which is also called tension loss. This effect thus produces a smaller pressure at outer surface of the roll. Comparison of experimental data shows that with this BC, the nonlinear anisotropic model predicts consistent results. The cost is that the radial displacement involved in the BC makes it nonlinear. As a new lap comes to the roll, a subroutine which calculates the radial displacement of the current roll is performed first. Then the incremental stresses caused by the new lap with the modified BC are computed.

Benson's Large Deformation Model

Benson in 1995 [11] developed a model to fully account for large deformations in wound rolls. He viewed the radial location of material particles as an unknown and used lap number as the independent variable instead. He also used the stretch ratio as a measure of deformation instead of conventional strains which required a modified form of constitutive equations. The result of Benson's model is consistent with Good's modified outer BC model.

Mollamahmutoglu and Good's Large Deformation Model

Mollamahmutoglu and Good in 2009 [21] conducted a thorough study about large deformation winding models. They used an axisymmetric finite element method to develop two large deformation winding models which are based on two sets of stress and strain measures. The PK1 model they developed employed the first Piloa-Kirchoff stress and a deformation gradient. The second model, called the PK2 model, employed the second Piloa-Kirchoff stress and Green-Lagrange strain. They verified their model with laboratory winding experiments of highly compressible non-woven and bath tissue webs. They also compared the performance of different nonlinear winding models, including Hakiel's model with Good's modified outer BC and Benson's model. The conclusion is some models may perform better for some web materials, but generally speaking all these nonlinear models predict similar results. They also found that Hakiel's model with Good's modified outer BC predicts results as good as other large deformation nonlinear models. The reason is that when a lap is added to the roll, the major deformation occurs in the outer few laps. Both the large deformation nonlinear model and linear small deformation model with the modified outer BC allow the loss of tension in outer layers.

2.1.2 2-D Winding Models

The first 2-D winding models were derived from 1-D models. The web width is parsed into several segments. Each segment is modeled using a 1-D model such as Hakiel's model that was discussed earlier. Web thickness is often nonuniform due to forming and coating processes. The benefit of 2-D winding models is that the effect of nonuniform web thickness on the internal wound roll stresses can be explored. The nonuniform web thickness results in variation in the outer lap radius in the CMD. Since the wound roll must have constant angular velocity, the outer lap radius variation leads to surface velocity variation. Those segments with higher outer lap radius and surface velocity will develop higher outer lap local winding tension levels. The allocation of web tension becomes the key point in these models.

Kedl's 2-D Winding Model

Kedl in 1991 [8] assessed how the web tension varied across the roll width by modeling the deformation of the outer layer of the winding roll as a beam resting on an elastic foundation. He then assumed an identical angular velocity for all segments. Based on Shelton's equation of the continuous transportation of web based on conservation of mass [22], he derived an expression (2.27) for winding tension allocation, where r_i is the radius of ith the segment, V_0 and ε_0 are the velocity and strain upstream of the winder where the web tension is assumed to be uniform in the CMD. Kedl then employed a 1-D winding model developed by Struik [23] to determine the stress distribution in each sector subject to the web tension developed in (2.27). He verified his model using force-sensitive resistors to measure pressure variation across the width of the wound roll at several radial locations.

$$T_{wi} = E_\theta \left[1 - \frac{V_0(1-\varepsilon_0)}{r_i \omega}\right] \tag{2.27}$$

Hakiel's 2-D Winding Model

Hakiel in 1991 [9] developed another algorithm to parse the web tension by introducing the concept of a relaxation radius r_0 for a new outer lap of web to be added to the outside of the wound roll. He then enforced radial displacements due to interference between the outside of the previous layer and the new layer being added. His final web tension expression was:

$$T_{wi} = \frac{E_\theta}{1-\nu^2}\left[\frac{r(i,j) - r_0(i)}{r_0(i)}\right] \tag{2.28}$$

Hakiel then employed his 1-D model which is discussed earlier to calculate the internal stresses for each segment. Later Cole and Hakiel [10] presented an improved model that coupled computed in-roll displacements to a modified version of the expression (2.28). Cole verified his model by measuring strains on the surface of a segmented core which allowed him to infer the core pressure in the wound roll which he could compare in the CMD to model results. He also measured the outer lap radius variation in the CMD using a profilometer which could also be compared to model results.

These pioneer 2-D winding models provided the first means to consider the impact of thickness variation along the CMD and the effects on stresses both incorporated a limiting assumption. The parsing of the roll into segments could not satisfy the compatibility of deformation of a given layer as it passed from one sector to the next.

Lee and Wickert's 2-D Axisymmetric Winding Models

Lee and Wickert [19; 18] created the first real 2-D winding model in 2002. The model employed an axisymmetric finite element method. A layer or group of layers in the

wound roll was represented by a row of quadrilateral elements in the CMD, as shown in Figure 2-4. Stacking rows of elements outward along radial direction resembles wound on layers. The core was modeled by a similar discretization approach. As the core had a general geometry other than cylinders, a commercial finite element package was used to calculate the stiffness of the core. Elements modeling web layers were attached next to the core elements region. Field variables were allowed to vary linearly among an element. Every element can have unique material and geometric properties so that CMD stiffness variations can be modeled. Solution of the problem employed an iterative approach based on Newton-Raphson method. With this new model, they investigated how core stiffness variations affect stress distribution in a wound roll. Lee and Wickert's model relaxed the assumptions made in previous 1-D models in which the roll had uniform core stiffness, winding tension and material properties and guaranteed the compatibility of deformation along the cross width direction which was lacking in earlier 2-D winding models. Their model assumes the width-wise distribution in web tension is known prior to winding and that the shape of the wound roll does not affect this distribution. However, including the effect of width-wise radial profile on winding tension allocation was shown to be important from the work of Kedl, Hakiel, Cole and Spitz [23].

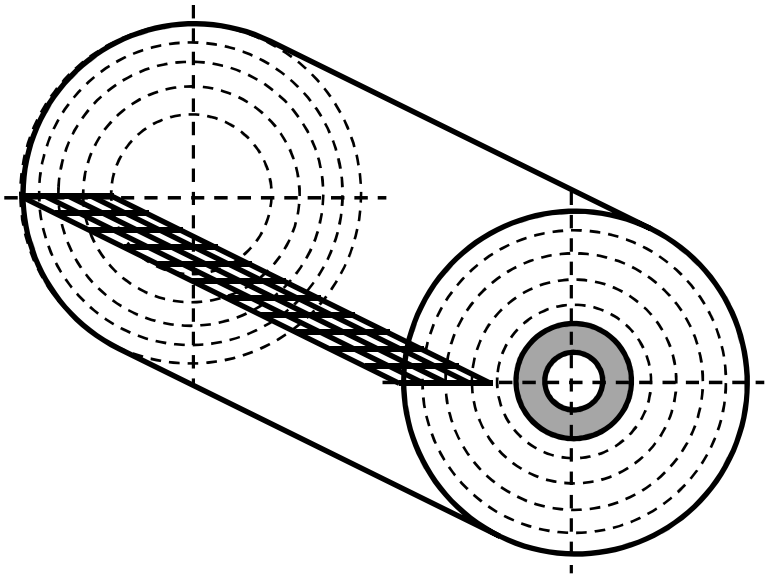

Figure 2-4 2D Axisymmetric winding model

Hoffecker and Good's 2-D Axisymmetric Winding Models

Hoffecker and Good in 2005 [15] developed a model based on the axisymmetric finite element method as well. In their model, the discretization method and BC at inner surface of a wound roll is similar to Lee and Wickert's model. However, they improved the BC at the outer surface of the wound roll. To establish the winding tension variation across the web width, an algorithm similar to that of Kedl (2.27) was used. A Lagrangian method was used to enforce an interference radial constraint between the outer lap and the layer beneath. By this method, the effect of the outer lap radius variation on the winding tension in the CMD was accounted for.

Mollamahmutoglu and Good's 2-D Axisymmetric Winding Models

Mollamahmutoglu and Good in 2009 [16] developed a new axisymmetric winding model based on the pre-stress finite element formation, which incorporated the initial web line

stress of an incoming layer as a source of load for the general roll structure system. The pre-stress axisymmetric model formulation is optimal because only one solution step is required to achieve results where tension loss is considered. If the constraint that the web line stress be equivalent to the average tangential stress in the outer lap is enforced then a three step process is required. Mollamahmutoglu and Good verified their model by comparison of results with the core pressure and outer radius variation measurements.

The significance of these 2-D winding models to the current study is that they were created to deal with web nonuniformity in length and thickness in the MD and CMD directions. These models were developed for the center winding case. The average MD stress in the outer layer may be essentially the uniform stress that would exist in the web upstream of the winder or possibly somewhat less in cases where tension loss is important. Center winding in the geometry shown in Figure 1.1a is not common in the industry where productivity is important for the following reasons:

1. Air Entrainment: At the speeds associated with production winding a hydrodynamic air layer will form between the layers of the winding roll. It is possible for these air layers to become larger than the surface roughness of the web layers. In such cases the web has become airborne and lateral stability of the web is lost which results in telescoping defects in the wound roll. In worst cases this causes the web process line to be shut down and productivity is lost [2].
2. CMD Web Tension Variation: 2-D winding models were discussed earlier where the outer lap radius variation in the CMD was responsible for inducing web tension variation in the CMD per (2.27) or (2.28). Locally the web tension can become large enough that inelastic deformation of the web results. In some cases

the inelastic deformation can result in a tearing failure of the web called a burst [2]. Whether the web tears or not, there has been loss in web quality due to the inelastic deformation.

For these reasons winders of other types such as those shown in Figures 1.1(b), (c) and (d) are employed. These winders employ impinged rollers, called nip rollers, that decrease the entrained air layer and allow winding at much higher speeds than the center winder of Figure 1.1(a). Note in Figures 1.1(b), (c) and (d) that the web first contacts the nip roller. The nip roller will have much less variation in radius than the winding roll. The web tension can be nearly uniform in the CMD as the web contacts the nip roller. Friction between the web and nip roller can reduce or prevent the reallocation of web tension (2.27,2.28) and thus prevent the inelastic web deformation or tearing discussed.

The stresses output by winding models are most affected by the winding tension in the outer layer. For center winding cases such as that shown in Figure 1.1(a) the winding tension is known for cases where web thickness is assumed uniform or nonuniform as already discussed. For the winders in Figures 1.1(b), (c) and (d) the winding tension in the outer layer, called wound-in-tension (WIT) by some wound-on-tension (WOT) by others, is not well known. Thus the residual stresses in rolls wound on such winders that comprise a large portion of the industrial sector is unknown.

2.1.3 2-D Winding Simulations with Commercial FE Software

Yanabe et al.'s Winding Simulation by MARC

Yanabe et al. [6] published the first model in MARC in 2010 to simulate the winding process using commercial FE software. The model was composed of a web and a core,

which are initially fixed together at the leading edge of the web and core surface. A constant angular velocity was applied to the core and a constant tension was applied at the web free end during an implicit static analysis step. Simulations were executed on a 64 node cluster which required approximately 200 hours to complete a winding case where 80 layers were wound on a core. With this model, they were able to investigate the effect of slippage between web layers, the core rigidity and the leading web edge on the wound roll stress distribution. Their claims must be examined carefully. For example, they compared their radial and tangential stresses from a case neglecting slippage to Hakiel's model and showed a similar tendency between two models. But both their simulated radial and tangential stresses are about 30% higher than Hakiel's results. They claimed the reason was that circumferential displacement was neglected in deriving the strain compatibility equation in Hakiel's model, which is not true. The strain compatibility equation in Hakiel's model is same as expression (2.3), which did include the circumferential strain. The actual reason for the discrepancy is that Hakiel's model is built on axisymmetric simplification from beginning to end, which is not able to account for the process of the web bending from a flat state to a spiral state. However this process was exactly modeled and is significant in winding process simulation models like Yanabe's. In their simulations which neglect slippage, no slip is allowed between the outer layer and the layer beneath. The outer lap is subjected to bending as it is laid on to the surface of the winding roll. Since no slip is allowed the bending occurs about an axis at the bottom of the outer lap. The average bending stress in an outer layer is $E_\theta h/(2R_i)$ where h is web thickness, R_i is the current outer lap radius, and E_θ is the circumferential modulus. If this average bending stress is added to the stress created by the winding

tension in Hakiel's model, Yanabe's simulated stresses and Hakiel's results do in fact agree quite well and there is little or no discrepancy.

Kandadai and Good's Explicit FE Model by Abaqus

Kandadai [7] published a winding simulation model with different commercial FE software (Abaqus) and an explicit solution scheme in 2011 (Though Kandadai et al. did not publish their winding simulation model publicly, they began such studies as early as from 2004). The geometric model used in their study is similar to Yanabe's model but employed an explicit solution scheme. The advantage of explicit schemes is that they use a center difference method to predict the solution at the next time increment from the current increment, and do not need to form the stiffness matrix and solve the equation in iteration. This scheme is computationally efficient and does not have the convergence problems involved with implicit solution schemes, which can be problematic for cases with complex contact situations. Kandadai not only studied the center winding but also investigate effect of nip load on the wound-in-tension in the scenario of center winding with nip roller.

2.1.4 Winding Model Summary

The winding models that exist today have reached an apex in development. The most recent developments involve no limiting assumptions except for that of winder type. As such models are applicable to the center winder shown in Figure 1.1(a). These models would be applicable to other winder types (Figs. 1.1(b), (c) and (d)) if the winding tension in the outer layer was known. There is a substantial economic need to be able to

predict the stresses induced in webs by all types of winders to reduce or eliminate web defects that result from these stresses.

2.2 Review of Nip Mechanics during Winding

The effects of nip rollers employed in a winder began to draw researchers' attention as they noticed that the tightness of rolls wound by winders with and without nip rollers is different. This implies a difference in the effective winding tension resulted in these different types of winders. Pfeiffer, in his 1966 paper [13], first described the phenomenon of tension increase due to the nip pressure (nip-induced tension) and coined a new term wound-in tension (WIT). Good concretized Pfeiffer's definition as the tension in the outermost lap of a winding roll and re-coined the term as wound-on-tension (WOT). The term WIT and WOT are essentially identical, though WOT is more commonly adopted today and thus preferred in this document.

One branch of the literature focused on explaining the source of the (WOT) or nip-induced tension (NIT). Pfeiffer [20] developed an experimental test bed in which a nip roller rolls on a flat stack of webs. This is a simplification of the winding case where this slippage would have resulted in changes in circumferential stress in the spiral layers. Good and Wu [24], Arola [28], and Kandadai [29] worked on this simpler case as well, both in rolling nip mechanics tests and simulation of those tests using explicit finite element methods. It was found that the nip roller induces slip between the outer layers. The greatest slippage occurred between the outer layer and the layer beneath. The outer layer advanced in the direction of the rolling nip ahead of the layer beneath. In a winding roll this would result in a tension in the outer layer above and beyond that due just to web

line tension. Jorkama et al. was the first to model the impact of web wrapping the wound roll on the slippage that affects the WOT [31]. Although Jorkama was first to study the impact of the curvilinear web path, his model did not account for the outer layer being integral to the wound roll. Jorkama was first to find the importance of the shear modulus of rigidity on the slippage and hence on WOT. Kandadai [29] was first to simulate the web entering the nip roller and then spiraling into the roll. This was the first time a nipped winder was completely modeled. He too found the shear modulus important in determining the level of WOT.

Another branch of the literature from the 1970s mainly focused on the empirical study of WOT which bred various ways to measure WOT in a winding roll. Rand and Ericsson [25], Pfeiffer [26], and Kandadai [29] developed direct measurement method of measuring WOT which later were found to be interfering methods. Good and Fikes [3] developed an indirect method of measuring the wound-on-tension (WOT) with the aid of winding models. Several web materials were center wound with a nip (Fig. 1.1b) where pressure sensors were wound into the roll. With known web properties a winding model similar to that of Hakiel was used to infer the WOT by iterating the winding tension until the model and test pressures agreed. Based upon this empirical work Good and Fikes deduced the WOT for a center winder with a loaded nip roller was:

$$WOT_{CenterWindingwithNip} = T_w + \frac{\mu_{w/w} N}{h} \tag{2.29}$$

While it appeared this expression worked well for a number of web materials and winding conditions, the limitations of the expression were unknown. Good et al. [32] found that with increased nip loading (N) that the estimate provided by expression (2.29) was too large. At very high nip loads it was found the WOT could become almost

independent of nip load. Using Good and Fikes empirical method for determining WOT for surface winding (Fig. 1.1c) Steves [33] found:

$$WOT_{SurfaceWinding} = \frac{\mu_{w/w} N}{h} \tag{2.30}$$

Both Steves and Good et al. [32] found that at high nip loads (N) the WOT predicted by the expression (2.30) was too high. Again at very high nip loads, similar to center winding with a nip roller, the WOT could become almost independent of nip load for the web that was surface wound.

Good et al. [30] developed a non-contact, non-interfering method to measure the WOT. The method involved differential velocity measurements between a location upstream where tension could be measured and a second point on the wound roll where all slippage was assumed to have ceased between the outer layer and the layer beneath in the winding roll. The change in velocity divided by the upstream velocity formed an estimation of MD strain change between the two measurement sites. When multiplied by Young's modulus and the cross-sectional area of the web this became an estimate in the change in web tension between the upstream site where tension was known and the site on the surface of the winding roll where the WOT had attained its final value. The sum of the upstream measured tension and this change in tension became the estimate of the WOT. The difficulty in applying this method is knowing where slippage has ceased beneath the outer layer. To gain confidence in the results the second velocity measurement must be made at several locations about the circumference of the outer layer to determine where slippage has ceased.

Jiang [34] developed a noninterfering method for measuring the WOT for a polyester web. This web was center wound at several web tensions and nip loads and it was surface

wound at several nip loads. Jiang used a core pressure measurement in conjunction with a winding model to infer the WOT. He also investigated the impact of an elastomeric cover on the nip roller on the inferred WOT level and conducted some differential torque winding tests. These results will be referred to later in this dissertation.

2.3 Detailed Research Objectives

A consistent method for estimating the WOT for center and surface winders of the types shown in Figures 1.1(b), (c) and (d) is needed. The method developed must account for the proportionality witnessed empirically (2.29, 2.30) for low nip loads but also the independence of WOT from nip load at high nip loads. The method must also account for the vast variation in web properties that exist. Whether the web has high or low Young's modulus, shear modulus or friction coefficients may determine the where the transition in WOT between proportional and independent nip load behaviors occurs. The methods pioneered by Kandadai [10] will be further developed to determine if the WOT behaviors witnessed in the laboratory can be captured in simulation. Center winding with an undriven nip roller (Figure 1.1(b)) and surface winding (Figure 1.1(c)) will be explored further. Differential torque winding (Figure 1.1(d)) will be simulated for the first time.

The value of the research is that the methods developed for predicting the WOT will be used with existing winding models to determine the internal residual stresses. Knowledge of those stresses will be used to mitigate web defects and associated economic loss.

Chapter 3. Modeling Pure Center Winding in Abaqus

3.1 Introduction

As reviewed in the previous chapter, almost all winding models whose first mission is to predict wound roll stresses adopt the axisymmetric simplification, disregarding the spiral nature of the roll structure. The underlying assumption is that the spiral geometry does not change the stress distribution much. Specifically, wound roll stresses can only vary with laps (r) or CMD locations (z) of the roll (if the web has thickness variation across the roll width), but have to stay constant within each lap in the same CMD section. Accepting this assumption, each lap of roll can be geometrically modeled as a ring or a cylinder; the dependence of wound roll stresses on the circumferential dimension is removed, which reduces the scale of the problem significantly. Additionally, the axisymmetric simplification also implies that the circumferential friction between adjacent laps within one lap must be ignored; otherwise, circumferential friction would result in changes in the circumferential stress, which contradicts the assumption and brings back the dependence of the stresses on circumferential location. So accepting the assumption introduces a much simplified contact situation between laps: the only effective contact needs to be modeled is the normal contact that handles the radial equilibrium of laps. Those two outcomes benefit the computational implementation: now each layer of roll can be substituted by only one axisymmetric element so the total

number of degrees of freedom of the problem is significantly reduced. Since only the radial equilibrium of laps needs to be considered through the normal contact and the friction is not allowed to appear in circumferential equilibrium, the contact algorithm actually can be bypassed and the nodes of adjacent laps can be treated as shared common nodes at their interface. The radial and circumferential forces directly appear in the nodal equilibrium. This further reduces the difficulty of implementation and the total number of degrees of freedom. This type of winding model calculates the wound roll stresses very efficiently and meets the demand that a common wound roll can easily consists of tens of thousands of laps. Actually, in most cases, adopting axisymmetric simplification may be the only choice if we want to develop a viable model to calculate wound roll stresses that runs in reasonable time.

However it is still worth and important to be fully aware of the validations and limitations of the axisymmetric simplification used in these models. Ignoring the spiral feature may have reasonable physical foundation since the web thickness is usually thin; the radial position of different web particles within each lap has only small difference. The simplified contact situation which ignores the circumferential friction and the following treatment of shared common nodes for nodes of adjacent laps require investigation. On the other hand, if a nip roller is present in the winder, the circumferential friction between web and nip roller, the slip/stick behavior, and the shear deformation of webs in the nip–roll contact zone are critical to determine the wound–on-tension. The simplified contact situation brought by the axisymmetric assumption obviously fails to model the physical condition. Therefore, a kind of model which simulates the winding process and really

winds web laps is imperative for the purpose both to examine the employed assumption and prepare modeling techniques for the wound-on-tension studies.

Winding simulations using finite element software are capable of modeling the real winding process with fewer imposed assumptions. A winder consists of a core and web is built explicitly and virtually. The web is first subjected to web tension and then wound on to the core as the core rotates. The virtually formed roll has the feature of an Archimedean spiral, which is exactly modeled as it is in reality. Quantities like stress and strain are allowed to vary with respect to the radial, circumferential and axial directions. The interaction between adjacent web laps is modeled by contact algorithms: slip between adjacent laps is allowed.

The difficulty of winding simulation mainly lies in handling the expensive computational cost and modeling the web material. While an axisymmetric winding model calculates a roll consisting of hundreds of web laps within seconds, winding spiral simulations of a mere 60 laps can easily costs hundreds of hours of computation with today's common computational resources. Explicitly modeling a web strip into the spiral wound roll form requires a great number of degrees of freedom. Contact interactions in the winding roll introduce severe nonlinearity in boundary conditions. Different numerical methods have their own limitations in dealing with this kind of problem. If an explicit method is used, the very thin thickness of a typical web would limit the stable time increment to a small number, which results in a large computational cost. If an implicit method is used, the severe nonlinearity of the problem may cause convergence difficulty. Besides, the radial behavior between stress and strain in layers of web in a wound roll is well known to be nonlinear and results in a state dependent modulus. The material model that depicts this

behavior is not directly available in any commercial finite element software. To simulate the winding process accurately requires a successful development of the constitutive model. Therefore, how to accurately model the development of wound roll stresses, how different numerical methods perform in producing solutions of these models, and how to make the model run in a reasonable time need exploration.

The pure center winder without nip is the simplest winder type and its configuration in some form exists in all other types of winder. Accurate modeling of this type of winder is the foundation for us to move on modeling other more complex winders and study the wound-on-tension problems. Winding simulations reported in the literature [6; 7] are the only works that employ simulation to model winding processes incorporating the spiral form of the web in the wound roll. While the potential was shown for solving winding problems, a thorough study of solution and modeling methods is in order that was not considered in these sources. In Chapter 2 several 1D pure center winding models were reviewed that have been proven accurate in the laboratory. In this chapter modeling pure center winding problems will be explored using implicit and explicit dynamic finite element modeling. In many cases 1D models will be used to judge the quality of the simulation results.

Both implicit and explicit schemes were tested to determine which scheme is more suitable. In cases where the explicit scheme is used, use of plane stress and plane strain elements were performed. The first simulations employed an assumption of isotropic material properties. Later models included the ability to model orthotropic properties with a state dependent radial modulus. A user material VUMAT subroutine was developed and verified for this purpose. It was found during these early investigations that a

dynamic once round disturbance was introduced in the simulations by the step in radius caused by splicing the web to a winding core. While this is a reality of winding it was not a phenomenon that was to be studied per the research objectives. To eliminate this disturbance, an Archimedean spiral curved core was developed. The spiral core radius increased by one web thickness after one revolution of the core.

3.2 Model Setup

3.2.1 Geometry

Winding simulations reported in the literature [6; 7] and some preliminary 2-D test runs had proven that winding simulations require long computational times. Factors such as element type, mesh size, explicit or implicit solution method can affect the accuracy of results and computational time. A 2-D winding model will be used to quickly test these factors. A 2-D winding model defined in Abaqus is quite similar to the previously discussed 1-D winding model such as Hakiel's [17] in that they are both modeling the axial-orthogonal cut section of the roll. The extra dimension in 2-D model in Abaqus is the circumferential dimension introduced by discarding the axisymmetric simplification and modeling the real winding process. A 2-D model has to adopt either a plane stress or plane strain assumption to depict the web behavior in the CMD dimension. For a wide roll (often the case in industry), web material close to the two ends of the roll approaches a plane stress state since all stresses components associated with the CMD dimension vanishes at the ends. The web in the middle of the roll may approach a *pseudo* plane strain state, as shown in Figure 3-1. Whether a body is in plane stress or plane strain conditions depends on the geometry of the body. Winding presents an interesting case

since the web is thin membrane geometry subject to tension upstream of the winder but becomes integral to a wound roll of nearly cylindrical geometry. Prior to entry of the wound roll the web already has a negative CMD strain due to the MD strain due to web tension and the Poisson effect. Given this web is of adequate width this negative CMD strain may remain constant as the web is wound into the roll. This is why the word *pseudo* was used to describe the plane strain in the wound roll, instead of vanishing it remains constant and negative at the value that existed in the web as it was wound into the roll. An example will be given in Section 3.4.2.

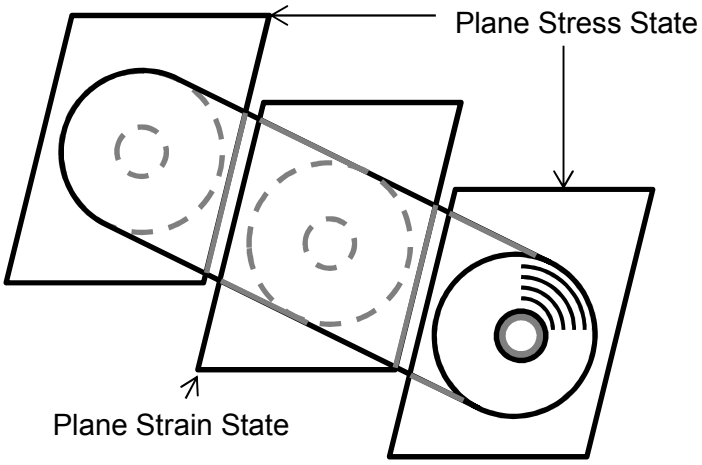

Figure 3-1 Plane assumptions in a wound roll

In the study of pure center winding simulation, we modeled both the end sections and the middle section by setting the element type to plane stress element and plane strain element for the end section and middle section respectively. The geometry of the pure center winder modeled is shown in Figure 3-2. A relatively thick web was chosen since a thick web would result in a larger element size which reduces computational time (this is discussed in detail in Section 3.2.3). The thickness chosen was 0.02". The length of the web is sufficient to produce 16 laps on the core. The core was modeled a perfect circle initially. The detailed geometric parameters are shown in Table 3-2. In later studies, it

was found that the perfectly circular core and the relatively thick web wound formed a small gap between the roll and the core at the end of the first lap. This gap would introduce numerical noise in the stress results due to the incoming web winding over a step in radius in the wound roll. Although this step in radius is realistic and can introduce dynamic disturbances in the web stress this was not a focus of this research. Thus the geometry of the core was altered to an Archimedean spiral form so the gap and the associated dynamic stresses were minimized.

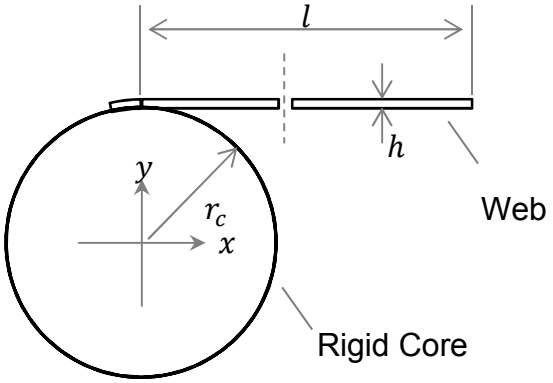

Figure 3-2 Model setup of winding in Abaqus

Table 3-1 Geometry of the model

Web Caliper h	0.02 in
Web Length l / winding laps	200/16 in/laps
Core Radius r_c	1.75 in.

3.2.2 Materials

The web material modeled in this study was given properties that are common for oriented Polyester film. Since the core used in winding experiments is far stiffer than the web material, the core is simplified with a rigid analytical surface in Abaqus. Many webs exhibit elastic anisotropic when subjected to in-plane loading. When webs form a roll or

a stack, the out-of-plane stiffness as compressed in the out-of-plane direction is smaller than their in-plane stiffness and is dependent on the compressing stress. This behavior results from two potential sources either of which can dominate depending on how the web was formed. Webs have surface asperities due to formation. When web surfaces are pressed together, the real area of contact is dependent on the pressure causing the contact and surface asperity deformations. At high contact pressure the real contact area may approach the apparent contact area. Also many webs are formed from fibers and may not be homogenous through their thickness. Internally the material can have voids that can collapse under increased pressure and cause the internal area of contact to increase. The increase of surface and internal area of contact with pressure both contribute to the logarithmic relation between pressure and strain and the state dependent radial modulus observed by Pfeiffer [13]. An easier way to consider these behaviors that most previous winding models have adopted is to treat the combined behaviors as a state dependent material property. While this may seem inappropriate it has led to model developments that can successfully predict wound roll stresses that have been verified through winding tests. The experimental method developed to obtain this combined material property is called the stack test. A stack of web is subjected to increased pressure while strain and pressure is simultaneously recorded. These pressures and strains are used to infer the state dependent radial modulus of elasticity. The levels of strain at the asperity contact surfaces versus the strain internal to the web are unknown. Winding simulations will result in a large number of modeled degrees of freedom without considering the degrees of freedom that would be necessary to model the surface contact. To make these simulations tractable this research will treat the combined out-of-plane behavior as a material property. Web

formation processes often result in producing webs with different in-plane behavior in MD and CMD directions. Therefore, an orthotropic material model would be robust for most web materials. The nonlinear out-of-plane behavior is modeled by changing the out-of-plane parameter in the orthotropic model. This type of material model is not directly available in Abaqus. Abaqus does however allow the use of predefined user subroutines which can be used to update unique element material properties as functions of stresses and strains in those elements. VUMAT is such a subroutine that can be used in Abaqus Explicit solutions while UMAT is a similar subroutine which can be employed in Abaqus Standard Implicit solutions. These subroutines which allow the state dependency of out-of-plane modulus need to be developed. Before directly stepping to the most complex case, simpler isotropic material models will be studied. Formulas (3.1.a, b) show the material isotropic constitutive equations for the web under plane stress and plane strain condition respectively. Table 3-2 shows the specific values that will be used in these trial simulations, values that would be realistic for the in-plane properties of polyester. The *x* and *y* material directions are defined in Fig. 3.2. After winding the *x* direction will become the circumferential θ direction and *y* will become the radial *r* direction in the roll.

$$\begin{Bmatrix}\sigma_{xx}\\ \sigma_{yy}\\ \sigma_{xy}\end{Bmatrix} = \frac{E}{1-\nu^2}\begin{bmatrix}1 & \nu & 0\\ \nu & 1 & 0\\ 0 & 0 & \frac{1-\nu}{2}\end{bmatrix}\begin{Bmatrix}\varepsilon_{xx}\\ \varepsilon_{yy}\\ \varepsilon_{xy}\end{Bmatrix} \quad \text{(3.1.a)}$$

$$\begin{Bmatrix}\sigma_{xx}\\ \sigma_{yy}\\ \sigma_{zz}\\ \sigma_{xy}\end{Bmatrix} = \frac{E}{(1+\nu)(1-2\nu)}\begin{bmatrix}1-\nu & \nu & 0\\ \nu & 1-\nu & 0\\ \nu & \nu & 0\\ 0 & 0 & \frac{1-2\nu}{2}\end{bmatrix}\begin{Bmatrix}\varepsilon_{xx}\\ \varepsilon_{yy}\\ \varepsilon_{xy}\end{Bmatrix} \quad \text{(3.1.b)}$$

Table 3-2 Assumed isotropic material properties of the web

Young's Modulus E	711000 psi
Poisson's Ratio ν	0.3
Density ρ	0.027 lb./in^3

3.2.3 Analysis Types and Solution Techniques

Inertial and dynamic effects are typically insignificant during a proper winding process. Yagoda [27] and Olsen [28] both developed 1D winding models that incorporate inertial effects. Use of such models demonstrates that extreme winding velocities are required to witness inertial effects on the residual winding stresses after the wound roll has finished winding and decelerated to zero rotational velocity. Since these inertial and dynamics effects are known to be insignificant, it is essentially a static or a quasi-static problem. Abaqus has "Static, General" analysis to solve the static problem. If the problem is highly nonlinear that the convergence is of concern, we can use the "Dynamic, Explicit" analysis to solve the equivalent quasi-static problem.

Abaqus has two main solver codes: Abaqus/Standard and Abaqus/Explicit for the different types of analyses. Abaqus/Standard is based on the implicit scheme, specifically the Newton-Raphson method or quasi-Newton method. Linear and nonlinear static problems are mainly solved using this solver. The governing equation solved in a static problem is the equilibrium equation as shown in (3.2), where K is the stiffness, u is the displacements, and R is the external load of the system. Those three terms will have specific matrix and vector form after the finite element procedure is applied to the problem. For nonlinear problems, the stiffness matrix and load vectors do not remain constant as in linear problems but become variables dependent on deformation history.

The tangential stiffness matrix and iteration is required to get a converged solution. For severely nonlinear problems such as the winding problem with complex contact involved, convergence difficulties usually appear. A benefit of the implicit scheme is that the scheme is unconditionally stable, which is a necessary condition to the accuracy of the solution. For static problems if other parameters such as BCs, loading, material, mesh etc. are correctly set and a converged solution is obtained, the solution is consistent with the true solution.

$$Ku = R \tag{3.2}$$

The Abaqus/Explicit solver, on the other hand, is essentially designed for dynamic and transient problems. The governing equation solved is the equation of motion as shown in equation (3.3), which includes the inertial term $M\ddot{u}$ and damping term $C\dot{u}$. Abaqus/Explicit is based upon the implementation of an explicit time integration rule together with the use of diagonal element mass matrices. The equations of motion are integrated using the central difference integration rule. To solve for the displacement at the next time increment$(i + 1)$, the second order time derivative of displacements are solved using (3.5) first, where R is the external load vector and I is the internal force vector. Since the mass matrix is diagonal, its inverse can be obtained effortlessly by inverse of the diagonal elements. Then expressions (3.4) are used to solve for the displacements. Initial values are needed to initiate the solution. Details can found in [29]. From the solution procedure, the displacement solution at the next time increment is obtained directly from the solution from previous increments, no iteration is needed. Also, the tangential stiffness matrix is not formed for the structure. In this way, the explicit scheme can be very efficient and does not have any convergence difficulty as the implicit

scheme has. The limitation is that the explicit scheme is only conditionally stable. A conservative estimation of the stable increment can be given by equations (3.6), where l_{min} is the smallest element dimension, c_d is the dilatational wave speed of the material which can be estimated by (3.6.b) for an isotropic elastic material. In most cases, the time increment in an explicit model must be very small to achieve stable results. Since inertial effects are present in an explicit solution, the loading rates should be controlled cautiously when solving quasi-static problems. Otherwise, the quasi-static condition will not be satisfied and the deformation due to impact and stress wave propagation can dominate and the simulation results will diverge from the static solution.

$$M\ddot{u} + C\dot{u} + Ku = R \tag{3.3}$$

$$\dot{u}^{(i+\frac{1}{2})} = \dot{u}^{(i-\frac{1}{2})} + \frac{\Delta t^{(i+1)} + \Delta t^{(i)}}{2}\ddot{u}^{(i)} \tag{3.4.a}$$

$$u^{(i+1)} = u^{(i)} + \Delta t^{(i+1)}\dot{u}^{(i+\frac{1}{2})} \tag{3.4.b}$$

$$\ddot{u}^{(i)} = M^{-1}(R^{(i)} - I^{(i)}) \tag{3.5}$$

$$\Delta t_s = \frac{l_{min}}{c_d} \tag{3.6.a}$$

$$c_d = \sqrt{\frac{E}{\rho}} \tag{3.6.b}$$

Based on the traits of two solution schemes, the implicit scheme seems more matched to the characteristics of the problem. However, the complex contact in winding process causes severe convergence difficulty. If the implicit scheme is used, a stabilization algorithm has to be introduced to assist convergence. Even when using these stabilization algorithms winding simulations using the implicit scheme attempted in this study sometimes terminate in the middle of the solution process. The explicit scheme was found most robust in tests. Since the explicit schemes include inertial and dynamic effects, when solving quasi-static problems, loads and velocities have to be applied gradually to guarantee a nearly steady process. Also noise may appear in the results of explicit

simulations. This can be the result of dynamic effects or to round-off errors that occur due to the very large numbers of computations that are required to simulate a winding event of time duration t with a very small time increment Δt required to achieve stable results.

3.2.4 Boundary Conditions, Loadings, and Interactions

To start a center winder in reality, the incoming layer is first fastened to the core and secondly tensioned. Then the winder begins to rotate with web layers winding in a spiral fashion on the core. To mimic the actual center winding condition, the loading procedure is divided into two steps: pretension and winding, as shown in Figure 3-3. In the pretension Step-1, the leading end of the incoming web layer is fastened to the core in a small area, while the core has all degree of freedoms (DOFs) restrained. The lower end point on the right end surface of the web is restrained on its vertical (y) DOF such that only horizontal (x) displacement is allowed. A constant winding tension T_w is prescribed at the right end surface of the web and is maintained during the whole analysis. In the Step-2, winding, core's rotational DOF about z axis is released and an angular velocity ω is assigned to the core. All other loads and BCs are inherited from the previous step. The values of winding tension and angular velocity used in the simulation are shown in Table 3-3.

Table 3-3 Loading conditions

Tension T_w	100, 500, 800, 1000, 1200, 1600 psi
Angular Velocity ω	2π rad/s
COF μ	0.3

The contacts in a wound roll can be divided into two parts based on the material involved in a contact. First is the web to core contact between the web and the rigid core, which is modeled by a penalty contact pair algorithm. Second is the web to web contact between the bottom surface of the current lap and the top surface of the previous lap contacting as the web is wound. This part of the contact is also modeled by a penalty self-contact algorithm.

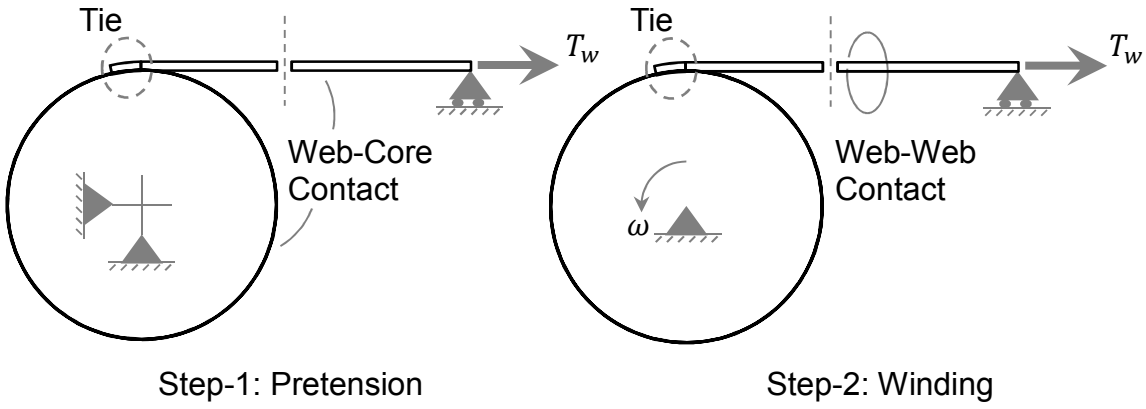

Figure 3-3 BCs, loadings and steps

A Coulomb friction model is employed that relates the maximum allowable frictional (shear) stress across an interface to the contact pressure between the contacting bodies. In the basic form of the Coulomb friction model, two contacting surfaces can react shear stresses up to a certain magnitude across their interface prior to slipping relative to one another, in a state is known as stick. This is schematically represented in Figure 3-4. The Coulomb friction model defines this critical shear stress (τ_{crit}) as the stress at which sliding of the surfaces starts as a fraction of the contact pressure (p(x)) between the surfaces per expression (3.7).

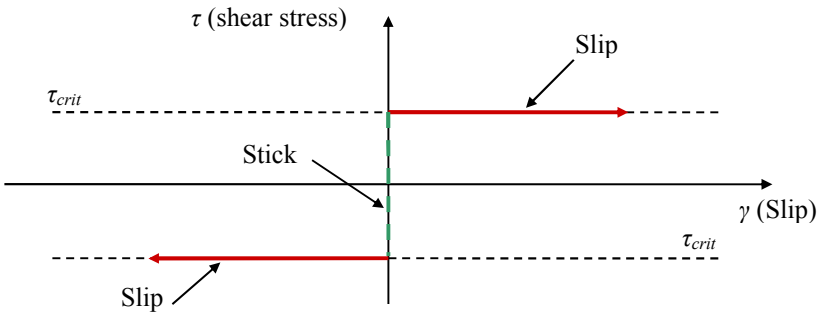

Figure 3-4 Coulomb's friction model

$$\tau_{crit} = \mu p(x) \Rightarrow \text{slip}$$
$$\tau_{crit} < \mu p(x) \Rightarrow \text{stick} \qquad (3.7)$$

The stick/slip calculations determine when a point in a contact region moves from stick to slip or from slip to stick. This friction law is basic and is sometimes criticized due for the critical shear stress being independent of the magnitude of the slip velocity (V) shown in Figure 3-4. This friction model was used exclusively in these simulations. The coefficient of friction for all contacts was selected to be 0.3.

3.2.5 Elements and Mesh

Abaqus has a family of quadrilateral elements for modeling the plane problems. Second order 8-node elements are not suitable if the problem involves contact interaction. Four-node isoparamatric elements were used. If quadrilateral elements are used which fully integrate for stiffness a numerical deficiency called "shear locking" occurs. This causes the elements to be very stiff if subject to bending and thus affects the accuracy. Therefore quadrilateral elements using first order reduced integration were used. In Abaqus this element type is CPS4R for plane stress problems and CPE4R for plane strain problems. Reduced integration elements eliminate the "shear locking" effect. However they may

introduce another numerical deficiency, the hourglass mode, where the element is free to deform without consuming any energy. This deformation pattern may easily propagate through the whole mesh region and can have large effects on accuracy. The solution to this problem is to use a finer mesh and multiple elements through the thickness when in bending or to introduce a numerical hourglass control mechanism. Therefore, a study of mesh convergence is necessary in the problem to determine the proper mesh.

As discussed earlier, first order reduced integration plane stress elements CPS4R and plane strain elements CPE4R are chosen in this study. To test the mesh convergence, a smaller winding model, winding only one lap of web, was developed. The same geometry, material, boundary conditions, loadings and contact that were discussed in last section were used except that only one winding lap is modeled to the problem scale. In order to exclude dynamic issues generated by the explicit scheme, Abaqus/Standard was used for both Step-1: Pretension and Step-2: Winding. The implicit code can handle one lap of winding without convergence concerns since the contact condition is simpler. To accurately approximate the circular arc deformed geometry of a web wound onto a roll, the MD length of the elements was set to 0.05 in. The number of elements throughout the thickness of the web determines the accuracy of the stresses that are computed. Therefore, the mesh convergence in ZD is tested. Table 3-4 shows 4 different types of mesh with 1 to 4 layers of elements throughout the web thickness, respectively.

Table 3-4 Element size in mesh convergence test

Mesh Type	Element Size (in)
Mesh-0.05X1	0.05X0.02
Mesh-0.05X2	0.05X0.01
Mesh-0.05X3	0.05X0.0067
Mesh-0.05X4	0.05X0.005

It was found that while tangential stress was not affected much by the number of layers of elements throughout the web thickness, the radial pressure was very sensitive to that number. On the other hand, equilibrium analysis of the lap provides a closed form solution to calculate radial pressure shown in expression (2.9c). Therefore radial pressure is selected as the criterion to evaluate the performance of the meshes in Table 3-4. In this study, the radial pressure is obtained by harvesting the radial stress at the bottom nodes of the web. Since the radial stress value is negative for the web is under a radial compressive state, the absolute value of the radial stress is taken as the radial pressure value. Figure 3-5 shows the results of the mesh convergence study. The closed form solution of the radial pressure, 9.14 psi, is calculated by the formula (2.9c) with the winding tension of 800 psi, radius of 1.75 in. and web thickness of 0.02 in. The red line in Figure 3-5 shows the closed form solution. The results indicate that as the number of layers of element throughout the web thickness increases from 1 to 4, the radial pressure values approach the closed form solution. It is obvious that the mesh with only 1 layer of elements throughout the thickness direction cannot provide enough accuracy. The mesh with 2 to 4 layers of elements yields close results compared well with the closed form solution. Specifically, the results from 3 layers of elements and 4 layers of elements cases have very little difference, which indicates a convergence is obtained. However, to save computational time without losing much accuracy, the Mesh-0.05x2 is selected as the mesh used for the current study. Mesh-0.05x3 will be used in the study of winding involving nip rollers since the greater stress gradient in these cases requires more refined mesh to guarantee the accuracy.

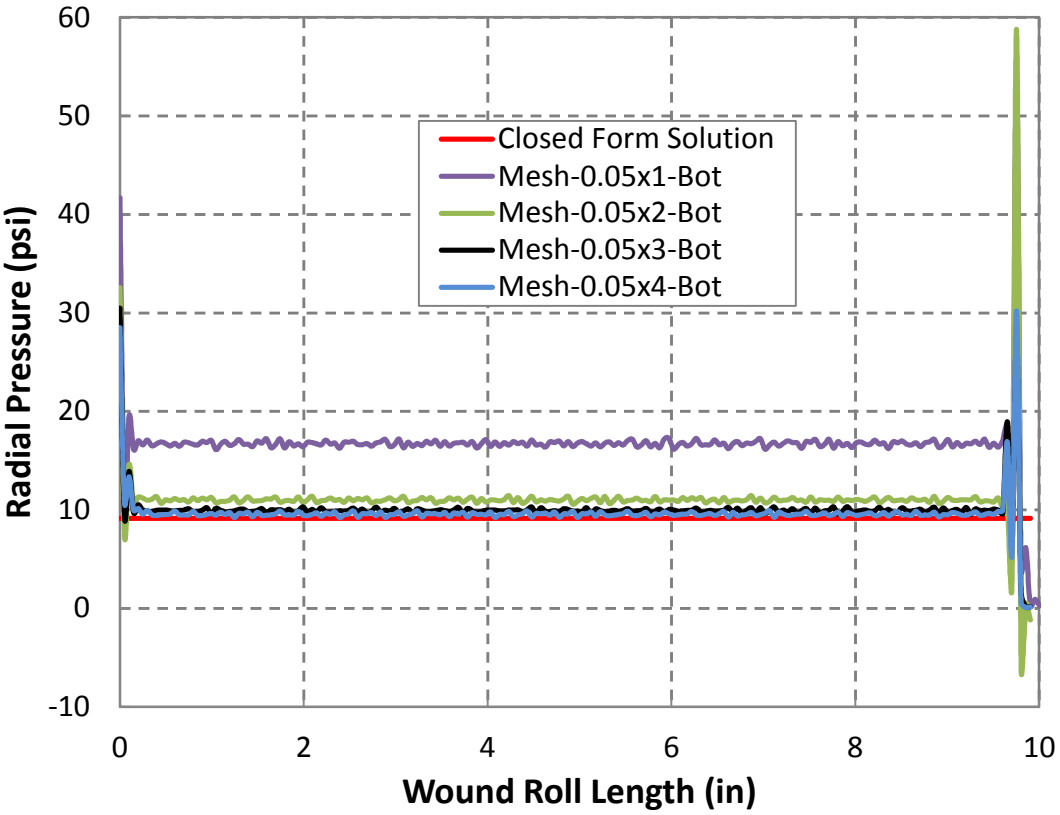

Figure 3-5 Convergence of radial pressure in mesh convergence study

3.3 Advanced Modeling Issues

The previous section describes the basic winding model setup in Abaqus. To get an accurate solution at a reasonable computational time, some parameters and procedures should be tested. In this section, different mesh sizes will be studied to guarantee the mesh convergence. Loading steps will be adjusted to increase the efficiency of computation. The implementation of nonlinear state dependent radial modulus will be discussed.

3.3.1 Decreasing Computational Cost

To have an approximate estimate of the computational cost, the stable increment is calculated with a magnitude of 10^{-8} s using equation (3.6), if the original material density is used. One run using the original density was attempted and the computational time was extremely large and unacceptable. One of the techniques for accelerating the simulation solution is use of a mass scaling factor. Using equation (3.6), if the web density is artificially increased n times, the stable increment will be decreased by a factor of the square root of n and therefore the total computational time will be reduced correspondingly. In this study, a mass scale factor of 300 is used to reduce the stable increment to a magnitude of 10^{-6} s. This mass scale factor was tested to ensure no dynamic behavior was influencing the output results.

Another technique to decrease the simulation solution time is to increase the loading rate, which specifically means to initiate loads such as winding tension and angular velocity in a shorter duration and use a greater winding velocity. Dynamic effects limit the extent that loading rates can be increased. A typical recommendation of the duration of loading is 10 times of the 1^{st} natural period of the response of structure subject to the same loading. The 1^{st} natural frequency or period of the structure is also depending on the density of the structure. Remaining other conditions, a greater density produces a longer 1^{st} natural period of the structure, which means the loadings need to be applied in a longer duration to maintain the quasi-static condition. We just used the mass scaling to increase the stable time increment to reduce the computational cost in the winding step. However, the artificial-increased density would require a longer loading period, which may counteract some of the reduced cost by the mass scaling. Figure 3-5 shows the

tensile stress developed in the mass-scaled web after the pretension step by using different time durations to initiate the winding tension. The stress wave propagation dominates the problem if the duration is set too short. In this case, the steady state is achieved only when the duration is set above 6s, which takes 2~3 hours to compute. A similar problem occurs in applying the winding velocity. Other commercial FE packages like LS-DYNA provide a method called dynamic relaxation to initiate loadings with low computational time and maintain a steady state load. But Abaqus lacks this capacity. We also tried to turn on the mass scaling only in the winding step not in the pretension step. It also requires large amount of computation. In this study, a solution was developed by first conducting a static analysis using Abaqus/Standard for the pretension step. Then in a second step the results from the static analysis were imported into the winding step, which conducted a dynamic Abaqus/Explicit analysis. After the static analysis for pretension, the entire model is in an equilibrium state. The resultant stress/strain file is imported in predefined fields for the explicit analysis. In the initial state of the winding step, an angular velocity is assigned to the core and a corresponding linear velocity is assigned to the web to initiate the movement of the core and web. Following the initial step, the winding tension and angular velocity were applied instantaneously to maintain the equilibrium from the previous step. This method saves much of the computational time used to initiate loads and velocity stably in explicit (this saves about 10 hours of computational time). It also helps to calculate stresses more accurately during the first several laps.

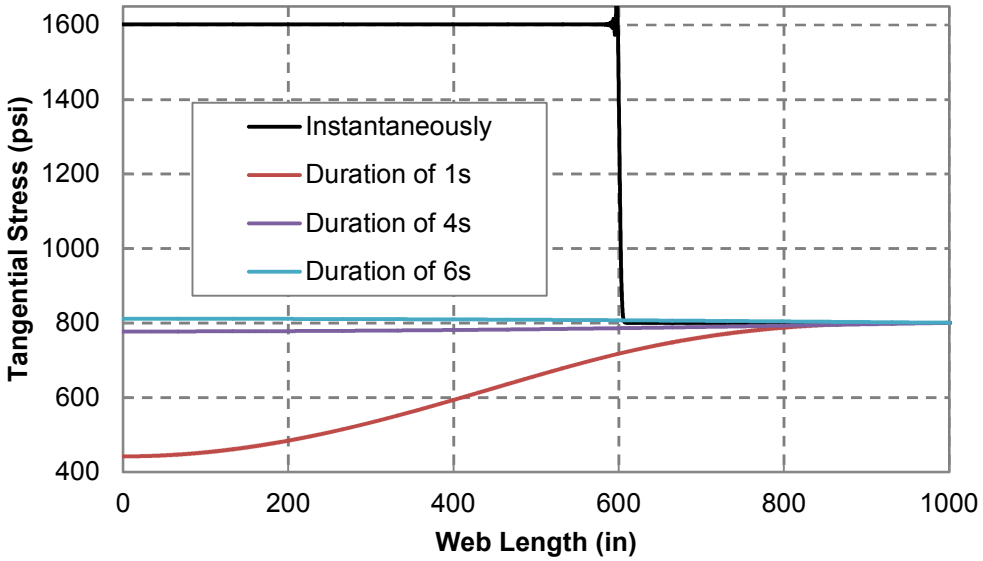

Figure 3-6 Effects of loading rates

3.3.2 Implementation of a State-dependent Radial Modulus

As discussed earlier, most web materials are anisotropic and have a state dependent radial modulus varying with radial strain or pressure. Such anisotropic material properties coupled with the state dependency are not available in any commercial FE package. To implement the material model, a user-defined material is developed using VUMAT subroutine. Kandadai [7] first started development of the state dependent radial modulus for 2-D plane strain elements in Abaqus using VUMAT in 2006. However, due to the computation capacity and modeling techniques at that time, large computational times were required to simulate winding using VUMAT subroutines. Thus Kandadai opted to set the radial modulus to a fixed but low value compared to the in-plane modulus. He could estimate this by using a 1D winding model to predict an average contact pressure in the wound roll and thus an average radial modulus from expression (2.20). In this study,

the subroutine originated from Kandadai's work will be completed, verified, applied to winding simulations, and extended to 2-D plane stress elements.

To develop a subroutine as general as possible that can be applied to most web materials, the web is assumed to be fully orthotropic. The constitutive equation for general orthotropic material is shown in equation (3.7).

$$\begin{Bmatrix}\sigma_{xx}\\ \sigma_{yy}\\ \sigma_{zz}\\ \sigma_{yz}\\ \sigma_{zx}\\ \sigma_{xy}\end{Bmatrix} \tag{3.7.a}$$

$$= \begin{bmatrix} E_x(1-\nu_{yz}\nu_{zy})\Delta & E_x(\nu_{yz}+\nu_{zx}\nu_{yz})\Delta & E_x(\nu_{zx}+\nu_{yx}\nu_{zy})\Delta & 0 & 0 & 0 \\ & E_y(1-\nu_{zx}\nu_{xz})\Delta & E_y(\nu_{zy}+\nu_{zx}\nu_{xy})\Delta & 0 & 0 & 0 \\ & & E_z(1-\nu_{xy}\nu_{yx})\Delta & 0 & 0 & 0 \\ & & & 2G_{yz} & 0 & 0 \\ & sym & & & 2G_{zx} & 0 \\ & & & & & 2G_{xy} \end{bmatrix} \begin{Bmatrix}\varepsilon_{xx}\\ \varepsilon_{yy}\\ \varepsilon_{zz}\\ \varepsilon_{yz}\\ \varepsilon_{zx}\\ \varepsilon_{xy}\end{Bmatrix} \tag{3.7.a}$$

$$\frac{E_x}{\nu_{xy}} = \frac{E_y}{\nu_{yx}}, \quad \frac{E_x}{\nu_{xy}} = \frac{E_y}{\nu_{yx}}, \quad \frac{E_x}{\nu_{xy}} = \frac{E_y}{\nu_{yx}} \tag{3.7.b}$$

$$\Delta = \frac{1}{1-\nu_{xy}\nu_{yx}-\nu_{yz}\nu_{zy}-\nu_{zx}\nu_{xz}-2\nu_{xy}\nu_{yz}\nu_{zx}} \tag{3.7.c}$$

In plane strain problems, any strain components related with the z direction are assumed to be zero. Equation (3.7.a) simplifies to (3.8.a) when written in an incremental form.

$$\begin{Bmatrix}\delta\sigma_{xx}\\ \delta\sigma_{yy}\\ \delta\sigma_{zz}\\ \delta\sigma_{xy}\end{Bmatrix} = \begin{bmatrix} E_x(1-\nu_{yz}\nu_{zy})\Delta & E_x(\nu_{yx}+\nu_{zx}\nu_{yz})\Delta & 0 \\ E_x(\nu_{yx}+\nu_{zx}\nu_{yz})\Delta & E_y(1-\nu_{zx}\nu_{xz})\Delta & 0 \\ E_x(\nu_{zx}+\nu_{yx}\nu_{zy})\Delta & E_y(\nu_{zy}+\nu_{zx}\nu_{xy})\Delta & 0 \\ 0 & 0 & 2G_{xy} \end{bmatrix} \begin{Bmatrix}\delta\varepsilon_{xx}\\ \delta\varepsilon_{yy}\\ \delta\varepsilon_{xy}\end{Bmatrix} \tag{3.8.a}$$

$$\frac{E_x}{\nu_{xy}} = \frac{E_y}{\nu_{yx}}, \quad \frac{E_x}{\nu_{xy}} = \frac{E_y}{\nu_{yx}}, \quad \frac{E_x}{\nu_{xy}} = \frac{E_y}{\nu_{yx}} \tag{3.8.b}$$

$$\Delta = \frac{1}{1-\nu_{xy}\nu_{yx}-\nu_{yz}\nu_{zy}-\nu_{zx}\nu_{xz}-2\nu_{xy}\nu_{yz}\nu_{zx}} \tag{3.8.c}$$

In explicit codes, nonlinear problems are solved incrementally. At the beginning of a new increment, the displacement increments are solved by equation (3.4) as discussed earlier.

Then strain increments are calculated by strain-displacement matrix. Following this, stress increments are calculated by constitutive matrix for simple material models. If a VUMAT subroutine is used in the model, the strain increments are transferred into the VUMAT subroutine. The stress increments are calculated inside the subroutine based upon the user-defined constitutive equations and the input strain increments.

To implement the state dependent radial modulus, Pfeiffer's expression (2.20) is coded to update the radial modulus E_y based on the current radial strain, as shown in (3.9.a). The Maxwell's relations that relate the Young's modulus and Poisson's ratio for both principal axes are assumed to be satisfied in this material model. Two minor Poisson's ratio involving radial (2) direction are dependent on radial modulus and are calculated by equations (3.9.b)

$$E_y = K_1 K_2 e^{K_2|\varepsilon_y|} \tag{3.9.a}$$

$$\nu_{yx} = \frac{E_y}{E_x}\nu_{xy}\,, \quad \nu_{zy} = \frac{E_z}{E_y}\nu_{yz} \tag{3.9.b}$$

Then E_y, ν_{yx} and ν_{zy} are substituted into equation (3.8.a) to calculate the incremental stress for this increment. To verify the user-defined material subroutine, one CPE4R element is compressed with a vertical prescribed displacement of 0.1 in. The BCs of the four nodes of the element are shown in Figure 3-7.a. Material properties used in this model is from a kind of polyester web material as shown in Table 3-5. Specifically, Pfeiffer's constants $K_1,\ K_2$ have values of 0.5 psi and 120 which were determined using stack compression tests. These material properties will also be used in the winding simulations incorporated with orthotropic state dependent properties. Absolute values of vertical resultant stress shown in Figure 3-7.b indicates that the elemental stress conforms to Pfeiffer's formula.

Table 3-5 Orthotropic state dependent material properties

Young's Modulus	$E_x = E_z = 711000\ psi$
Shear Modulus	$G_{xy} = 355000\ psi$
Poisson's Ratio	$\nu_{xy} = \nu_{yz} = 0.01\ ,\ \ \nu_{xz} = 0.3$
Density	$\rho\ = 0.027$ lb./in3
Pfeiffer's Constants	$K_1 = 0.5\ psi\ ,\ \ K_2 = 120$

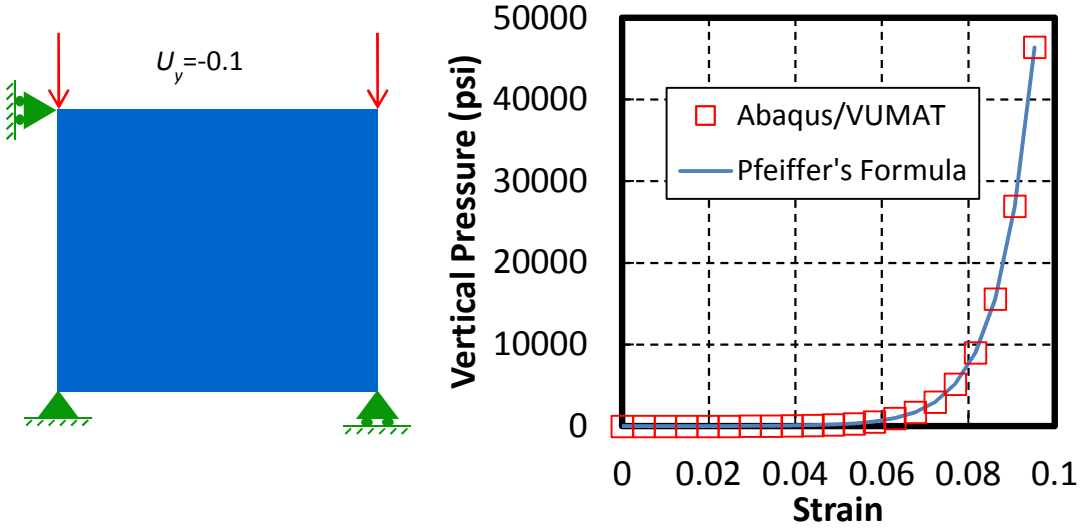

(a) One element model (b) Comparison with Pfeiffer's formula

Figure 3-7 Verification of VUMAT subroutine

Similar procedures are used to develop a VUMAT subroutine to implement the state-dependent radial modulus for plane stress elements CPS4R. In plane stress problems, all stress components involving subscripts of z are assumed to be zero. Equation (3.7.a) simplifies to equation (3.10.a). The normal strain increment $\delta\varepsilon_{zz}$ is related to other two normal strains by equating normal stress increment $\delta\sigma_{zz}$ to zero as shown in (3.10.d). Equations (3.10.a-d) and equations (3.9.a, b) are both coded in the VUMAT subroutine to solve for the stress increments.

$$\begin{Bmatrix} \delta\square_{\square\square} \\ \delta\square_{\square\square} \\ \delta\square_{\square\square} \end{Bmatrix} = \begin{bmatrix} E_x(1-\nu_{yz}\nu_{zy})\Delta & E_x(\nu_{yx}+\nu_{zx}\nu_{yz})\Delta & E_x(\nu_{zx}+\nu_{yx}\nu_{zy})\Delta & 0 \\ E_x(\nu_{yx}+\nu_{zx}\nu_{yz})\Delta & E_y(1-\nu_{xz}\nu_{zx})\Delta & E_y(\nu_{zy}+\nu_{zx}\nu_{xy})\Delta & 0 \\ 0 & 0 & 0 & 2\square_{\square\square} \end{bmatrix} \begin{Bmatrix} \delta\square_{\square\square} \\ \delta\square_{\square\square} \\ \delta\square_{\square\square} \\ \delta\square_{\square\square} \end{Bmatrix} \quad (3.10.a)$$

$$\frac{\square_{\square}}{\square_{\square\square}} = \frac{\square_{\square}}{\square_{\square\square}}, \quad \frac{\square_{\square}}{\square_{\square\square}} = \frac{\square_{\square}}{\square_{\square\square}}, \quad \frac{\square_{\square}}{\square_{\square\square}} = \frac{\square_{\square}}{\square_{\square\square}} \quad (3.10.b)$$

$$\Delta = \frac{1}{1-\nu_{xy}\nu_{yx}-\nu_{yz}\nu_{zy}-\nu_{zx}\nu_{xz}-2\nu_{xy}\nu_{yz}\nu_{zx}} \quad (3.10.c)$$

$$\square\square_{\square\square} = -\frac{\square_{\square}(\nu_{zx}+\nu_{yx}\nu_{zy})\square\square_{\square\square} + E_y(\nu_{zy}+\nu_{zx}\nu_{xy})\delta\square_{\square\square}}{E_z(1-\nu_{yz}\nu_{zy})} \quad (3.10.d)$$

3.4 Results and Discussion

2-D winding processes of isotropic and anisotropic web materials were modeled using the modeling methods and techniques discussed in the previous section. Winding simulations of isotropic web materials using plane stress and plane strain assumptions were conducted.

3.4.1 Winding Simulation of Isotropic Web

Explicit Isotropic Winding

Explicit 2-D winding simulation of an isotropic web material under the plane stress assumption was conducted first. The web modeled is 200 in long which corresponds to 16 laps on the 1.75 in rigid core. The winding tension was set at 800 psi. Mesh-0.05x2 from Table 3-4 was used to discretize the web such that there were 2 layers of elements

and 3 rows of nodes through web thickness. Absolute values of stress S22 (σ_r) from the Abaqus output file were harvested from the 3 rows of nodes to indicate the radial pressure. It is found that radial pressures harvested from 3 rows of nodes for the same circumferential position are almost identical. Therefore, only the radial pressure of the middle nodal row was reported. Figure 3-8 shows the radial pressure as a function of MD location at the end of the winding step. The MD location is essentially the *x* coordinate in Figure 3.2. After winding is complete the linear coordinate has become a curvilinear spiral. MD locations from 0 to ~10.6" comprise the first layer of web wound onto the core. MD locations from ~178.8 to 191.7" comprise the sixteenth layer wound onto the roll. MD locations in the web greater than 191.7" are part of a small portion of the web that was not wound onto the roll at the close of the simulation. The radial pressure oscillates about a mean value with 16 obvious peaks. The oscillation is caused by the essence of the explicit scheme. The peaks are the stress concentration generated by the contact of bottom surface of the web to the starting edge of the first lap. As the roll grows, the magnitude of the peak dissipates. The curve between two peaks is the radial stress distribution of one lap. The complete curve shows that the radial pressure is highest at core and near zero at the outer lap.

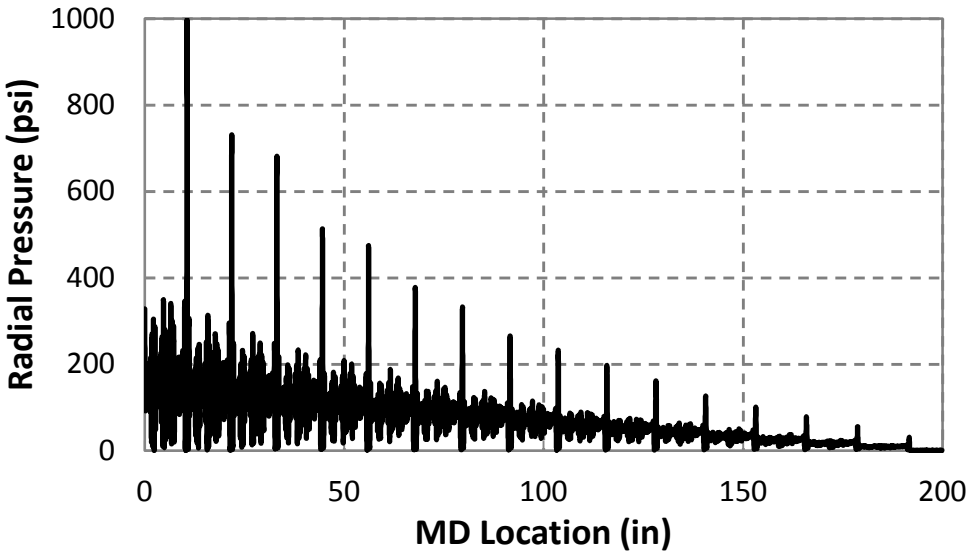

Figure 3-8 Radial pressure for T=800 psi by Abaqus/Explicit

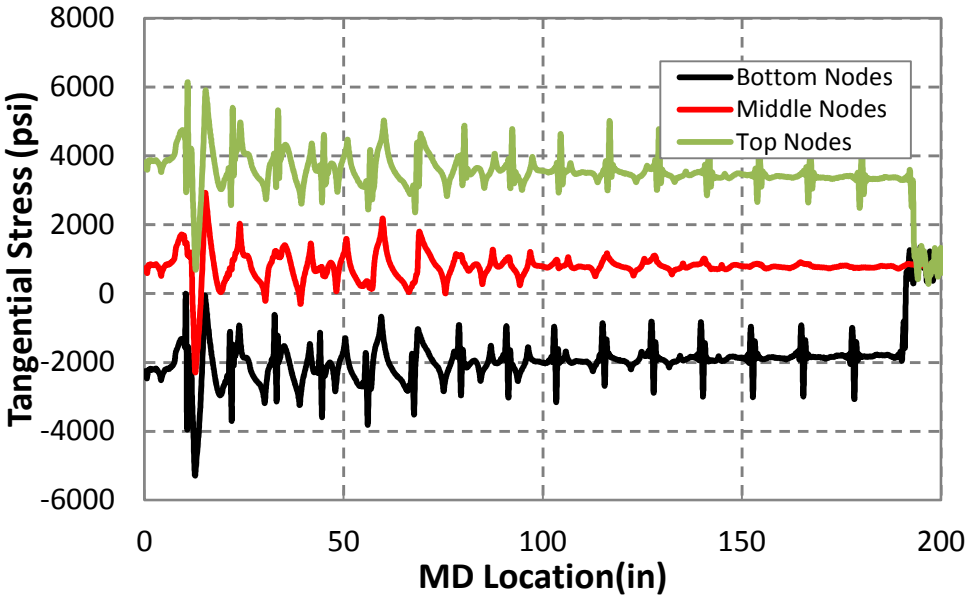

Figure 3-9 Tangential Stress for T=800 psi by Abaqus/Explicit

Figure 3-9 shows the tangential stress in the roll as a function of MD location. Stress values S11 (σ_θ) are harvested on the 3 rows of nodes. Unlike the consistency of radial pressures on different nodal rows, the tangential stress varies largely between different nodal rows due to the significant bending stresses. Bending stress is related with web thickness and curvature. Due to the fact that solution time in explicit schemes is inversely

proportional to the least characteristic dimension of the element as we discussed earlier, it is difficult to simulate a very thin web material using an explicit scheme for it will result in a very large solution time. The web thickness and radius of the core chosen in the current study produce a significant bending stress at the top and bottom surface of the web in the wound roll. The top nodes are in a tensile state while bottom nodes are in compression. The stress curves shown in Figure 3-9 indicate the total stress consisted of bending stress and membrane stress. Similar stress peaks exit at the top and bottom nodal rows of the wound roll. In the free spans shown at the right end of the 3 curves, the tangential stress from all 3 nodal rows meets each other, approximately equal to the winding tension applied. Figure 3-10 shows the tangential stress of the middle nodes and the average values of tangential stress of top nodes and bottom nodes. It is found that the curve of average tangential stress is exact overlapped on the curve of middle nodes, which indicates that the middle nodes are on the neutral axis of bending. Tangential stresses harvested from the middle nodes have only the membrane stress component. When comparing the tangential stress from Abaqus with 1-D winding models, the tangential stress (σ_θ) is only harvested from the middle nodes.

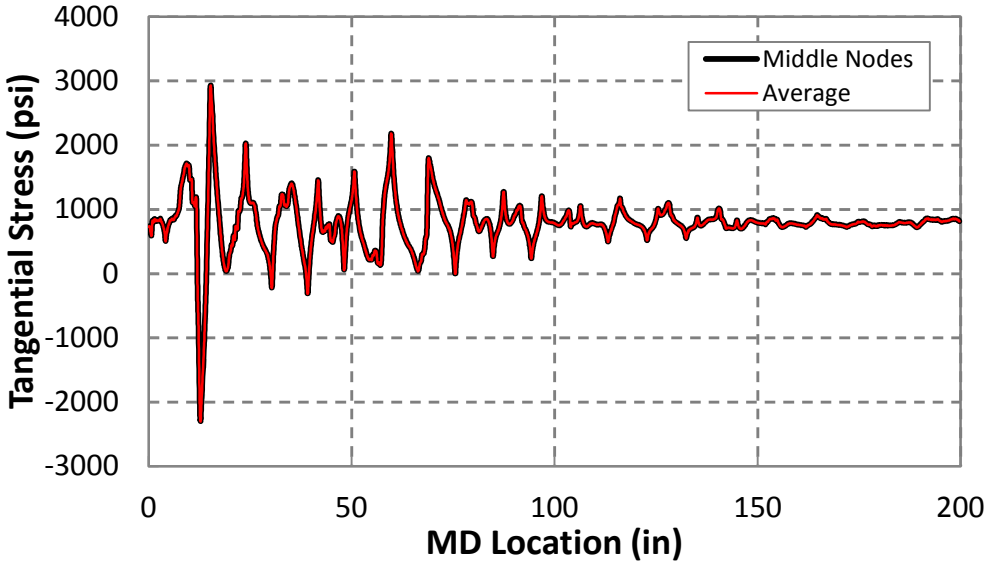

Figure 3-10 Tangential membrane stress component for T=800 psi by Abaqus/Explicit

The wound roll stresses from Abaqus are compared to the results from Winder 6.2. Winder 6.2 is a 1-D winding code developed by Ron Markum using Excel and VBA. The program is based on the Hakiel's model, which also incorporates the plane stress assumption. Thus, a consistent comparison can be made. To make the comparison, stresses that vary with MD location from Abaqus are transferred to be a function of wound roll radius. The transformation is made by calculating the average value of stress data shown in Figure 3-8 and Figure 3-10 on each lap separately. Figure 3-11 and Figure 3-12 show the radial pressure and tangential stress comparison between Abaqus and Winder 6.2 after transformation. The radial pressure from Abaqus compares very well with Hakiel's model except a slight disagreement at the area close to the core. This disagreement was found to be due to the starting edge of the web. As discussed in the previous modeling section, the starting edge of the web is tied to the core with kinematic contraints. In the beginning period of winding process, the web material is gradually feeding in contact with the core. After about one lap of web material wound onto the core,

the bottom surface of the web comes to get in contact with the top tip of the starting edge of the web, which causes a sudden change of radius of the lap. This sudden change of radius coupled with the contact between a surface and a tip generate severe stress concentration in the web layers adjacent to the starting edge. The stress concentration is severe in that area for the first several laps of web and dissipates as the roll winds alleviating the change of radius, as shown in Figure 3-13. The counterpart, Hakiel's model, assumes that each lap in a wound roll is a perfect circular hoop such that the spiral nature and radial discontinuity at the area of starting edge is are not modeled. That is the reason for that the radial pressure from Winder 6.2 is smoother and that the difference between two curves is maximum at the core and fades out gradually.

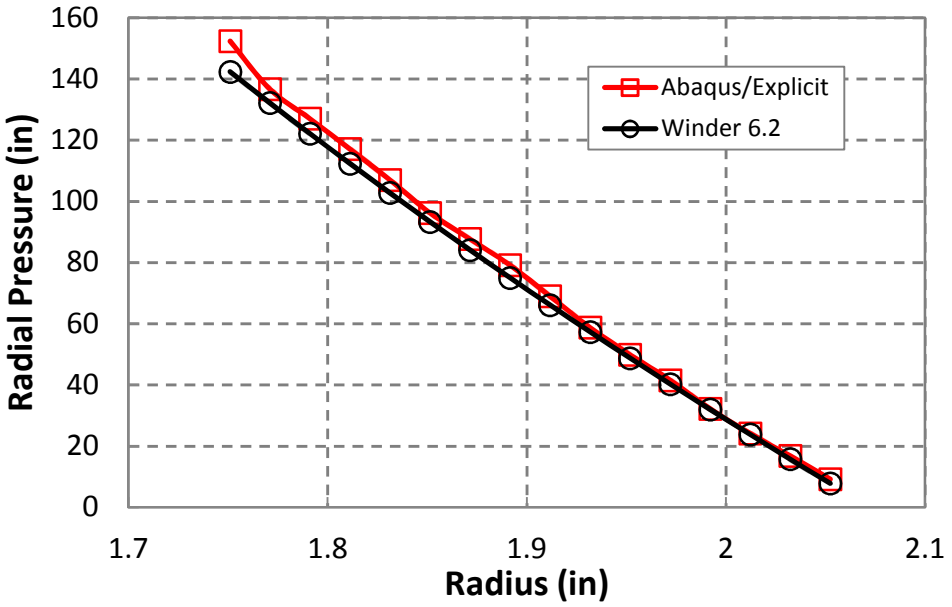

Figure 3-11 Comparison of radial pressure between Abaqus/Explicit and Winder 6.2

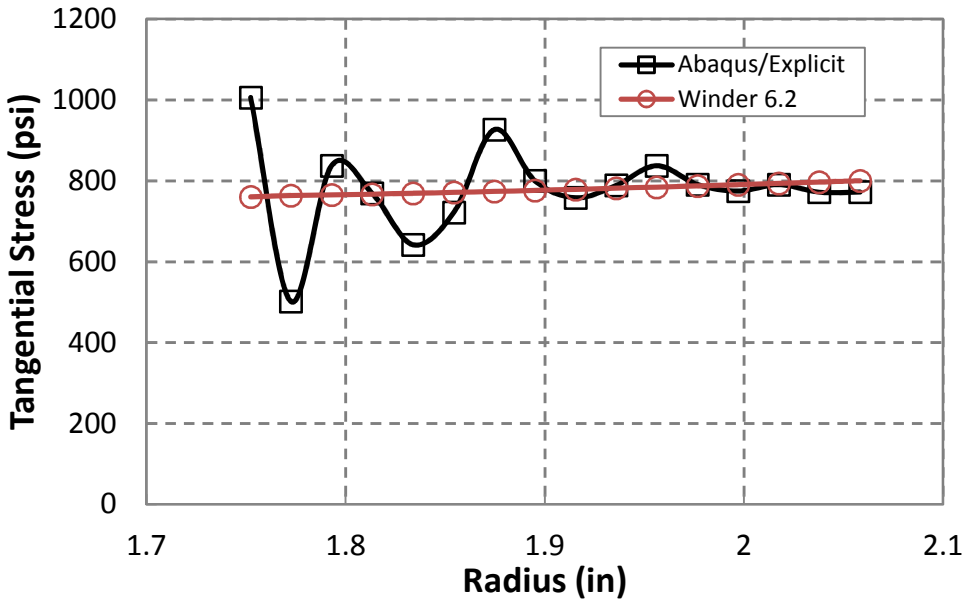

Figure 3-12 Comparison of tangential stress between Abaqus/Explicit and Winder 6.2

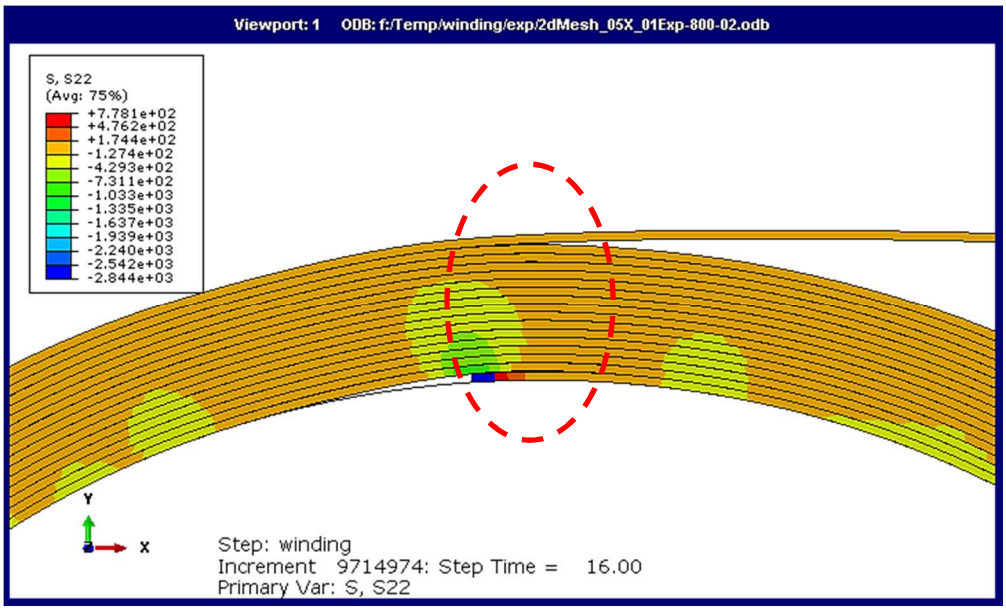

Figure 3-13 Radial pressure concentration at the starting edge of the web

Figure 3-12 shows the comparison of the tangential stress between Abaqus/Explicit and Winder 6.2. It is seen that the average tangential stress compared to Hakiel's model is noisier than the comparison of the radial pressure. The tangential stress from Abaqus oscillates about the stress predicted by Hakiel's model. The magnitude of the oscillation

decreases with increased wound roll radius. The tangential stress in outer laps is close to the winding tension applied.

Explicit Isotropic Winding with Different Winding Tensions

Similar results are seen at different winding tensions as shown in Figure 3-14 and Figure 3-15. As might be expected, higher winding tensions produce greater pressure in the wound roll.

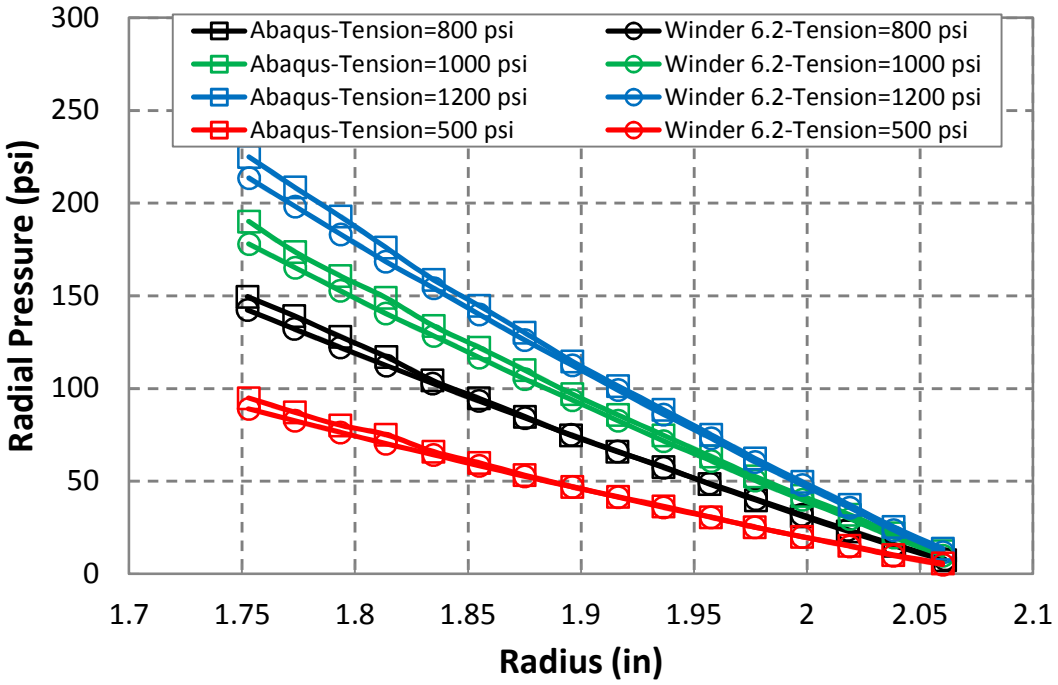

Figure 3-14 Radial pressure vs. radius for different winding tensions

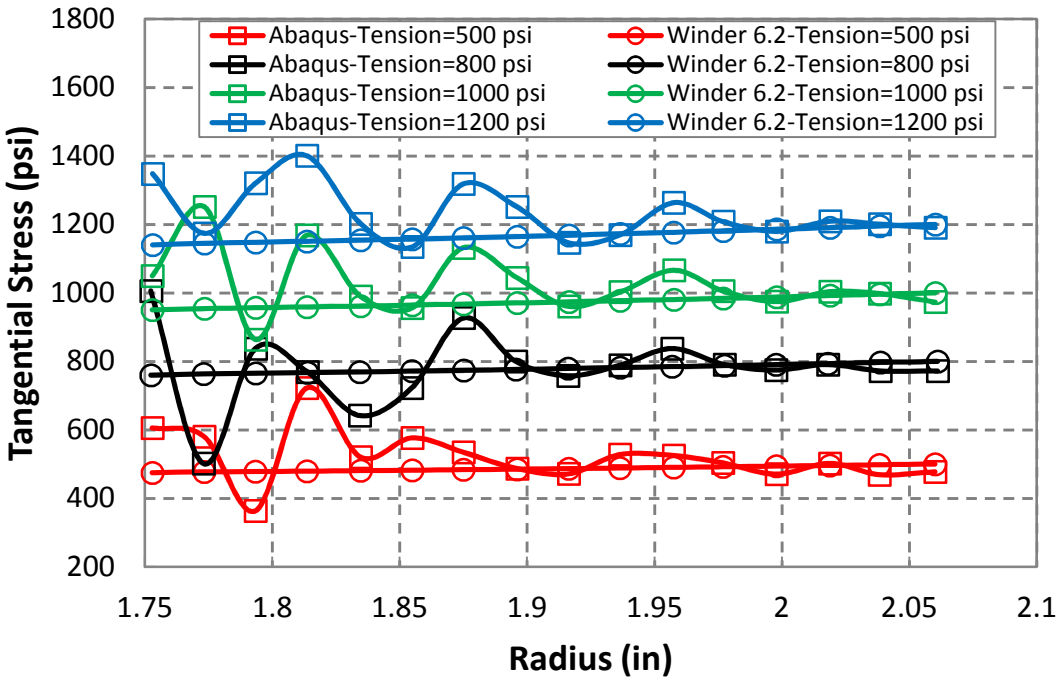

Figure 3-15 Tangential stress vs. radius for different winding tensions

Implicit Isotropic Winding

To determine the performance of an implicit scheme in winding simulations, a "Static, General" analysis which employs the implicit scheme using the Abaqus/Standard solver was conducted to model the same configuration of the winding process. Due to the difficulty to achieving convergence in implicit scheme, the solving process diverges in the middle of the process where only 11 full laps are wound on the core. Figure 3-16 shows the radial pressure as a function of wound roll length. A web with a length of 130 in. has been wound on to the core forming the wound roll of 11 laps, while, the rest of the web (about 70 in. long) remains in the free span. The radial pressure reaches a maximum of 100 psi in the lap closest to the core, decreases as the wound roll length increases, and drops to zero in the free span. To clearly compare the performance of the implicit and explicit schemes, the output file of the winding simulation modeled by explicit scheme in

the previous section is also post processed after the *11th* lap is wound on. The results are also plotted in Figure 3-16. It was found that radial pressure from the implicit run also has peaks in the same circumferential areas of each lap where the web contacts with the starting edge. The decreasing trend of these peaks' magnitude as the roll winds also exists as it did in the explicit simulation, which is caused by the identical mechanism. Comparing the two curves, it is found that the implicit solution has far less oscillation than the explicit solution. It not only has a lower magnitude in peaks, but also in the pressure noise is reduced between peaks. That is fundamental to the explicit scheme since dynamic effects are modeled. A similar phenomenon also exists and is enlarged in the tangential stress distribution of the roll, as shown in Figure 3-17. It can be seen that the tangential stress from the implicit solution is smooth and very close to the winding tension of 800 psi in the whole range of wound roll length with only a small oscillation in first 3 laps. The explicit solution oscillates severely in the web close to the core, stabilizes as the wound roll length increases, and reaches the values of 800 psi in the free span. Figure 3-18 and Figure 3-19 show the comparison of radial pressure and tangential stress between two solution schemes and the Winder 6.2. The radial pressures from three solutions compare well to each other. Elimination of dynamic effects causes the implicit solution to match the Winder 6.2 results better than the explicit solution, especially at the core. This trend is even more obvious in the tangential stress distribution. Therefore, from the essence of the problem as well as the comparison of the results, it appears that the implicit scheme produces better results than the explicit scheme. However, the difficulty in achieving a converged solution using implicit limits the application in winding simulation at this stage. By many attempts using different mesh sizes and stabilization

factors, the most number of wound laps achieved currently using the implicit scheme is 11. The solution diverged and the simulation terminated. More exploration will be required to wind more laps in implicit simulations.

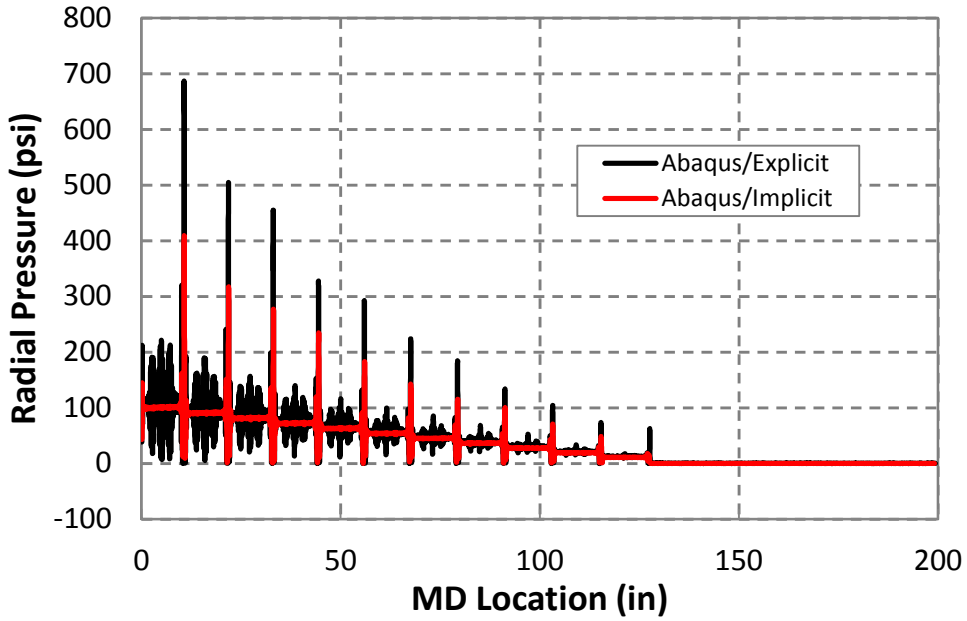

Figure 3-16 Comparision of radial pressure using explicit and implicit schemes

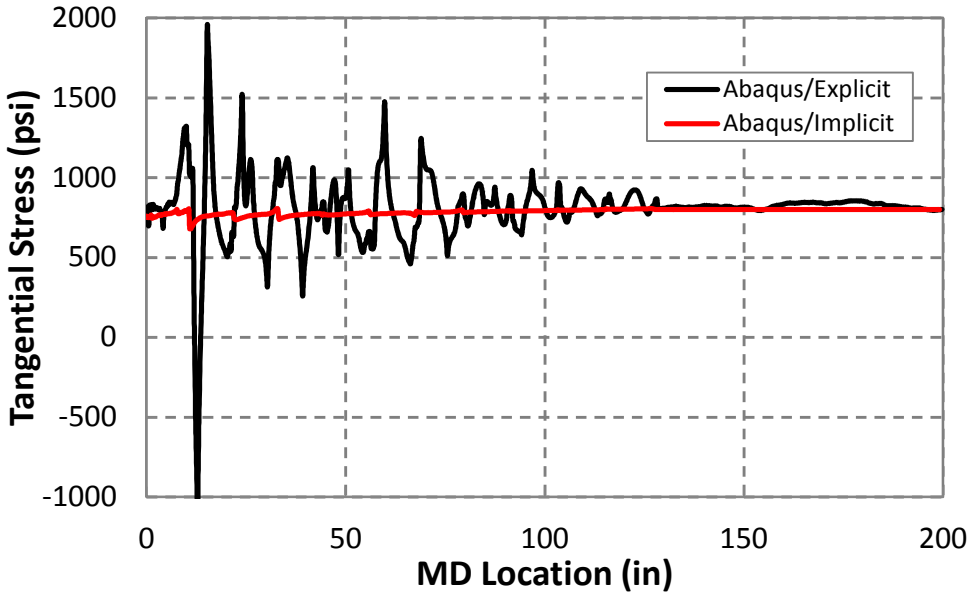

Figure 3-17 Comparison of tangential stress using explicit and implicit schemes

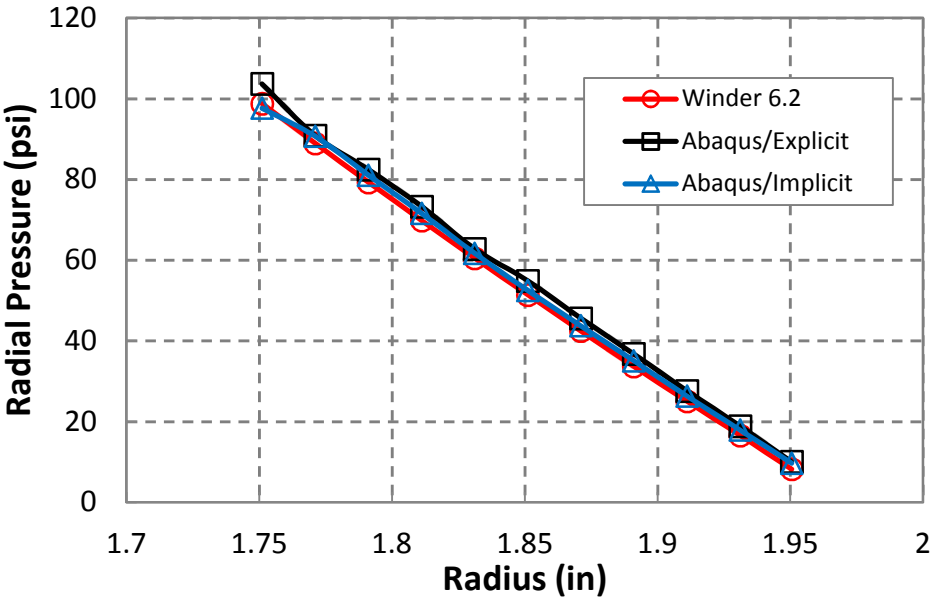

Figure 3-18 Comparison of radial pressure using Abaqus/Implicit, Abaqus/Explicit, and Winder 6.2

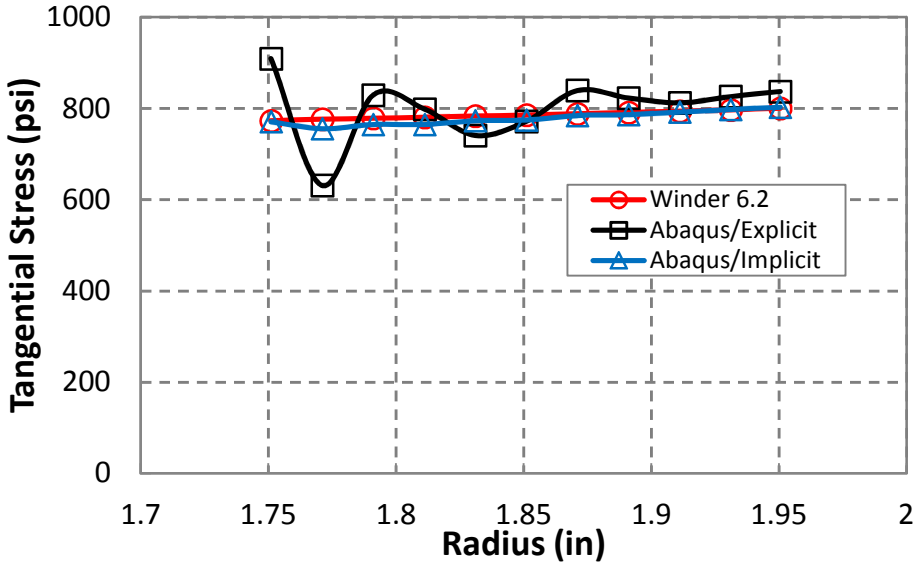

Figure 3-19 Comparison of tangential stress using Abaqus/Implicit, Abaqus/Explicit, and Winder 6.2

3.4.2 Explicit Winding Simulations Incorporating Orthotropic State Dependent Properties

Currently the ability to incorporate state dependent properties in a subroutine appears to work only in the explicit solution method. Thus winding simulations of orthotropic webs with state dependent properties must be conducted using explicit. These simulations were conducted using the setup parameters shown in Table 3-6.

Table 3-6 Model parameters of winding simulations with orthotropic state dependent web material

Web Caliper h	0.02 in
Web Length l / winding laps	200/16 in/laps
Core Radius r_c	1.75 in.
Young's Modulus	$E_1 = E_3 = 711000\ psi$
Shear Modulus	$G_{12} = 355000\ psi$
Poisson's Ratio	$\nu_{12} = \nu_{23} = 0.01\,,\ \ \nu_{13} = 0.3$
Density ρ	0.027 lb./in^3
Pfeiffer's Constants	$K_1 = 0.5\ psi\,,\ \ K_2 = 120$
Tension T_w	800 psi
Angular Velocity ω	2π rad/s
COF μ	0.3

As discussed in 3.3.2, the VUMAT subroutine developed to implement the state dependent radial modulus is dependent on the plane assumptions. For the plane stress assumption, the plane stress elements CPS4R are used. Figure 3-20 and Figure 3-21 show the comparisons of radial pressure and tangential stress using Abaqus/Explicit with the VUMAT subroutine and Winder 6.2. It is found that after considering of the state dependent radial modulus, the trend of the radial pressure and tangential stress curves are different from those with constant isotropic material properties. In the results of winding constant isotropic material web, the radial pressure and tangential stress seem in a linear relationship with wound roll radius. The trends become nonlinear after considering the state dependency. The nonlinear trend in the tangential stress result is more obvious that

the curve changes to U shape. It is also found that the results from using Abaqus/Explicit with the VUMAT subroutine compares well with the Winder 6.2.

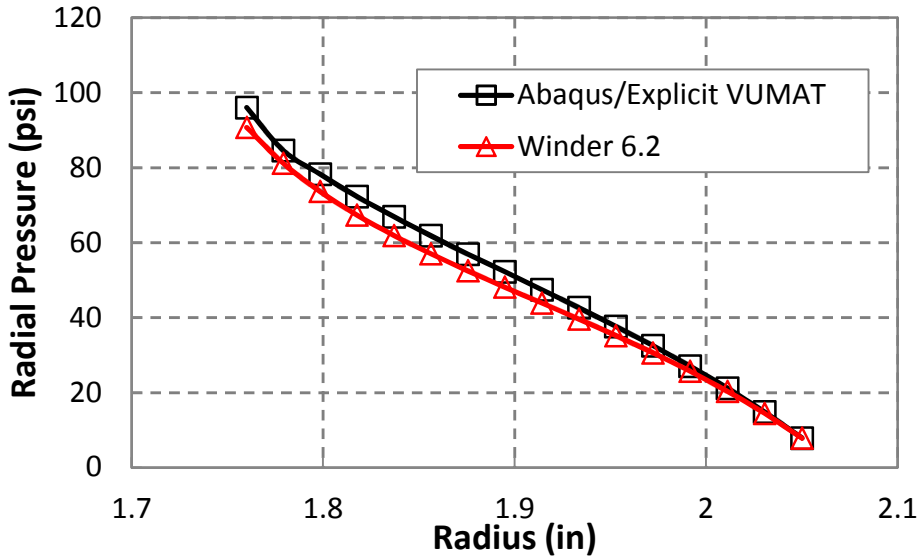

Figure 3-20 Comparison of radial pressure using Abaqus/Explicit with VUMAT and Winder 6.2 under plane stress assumption

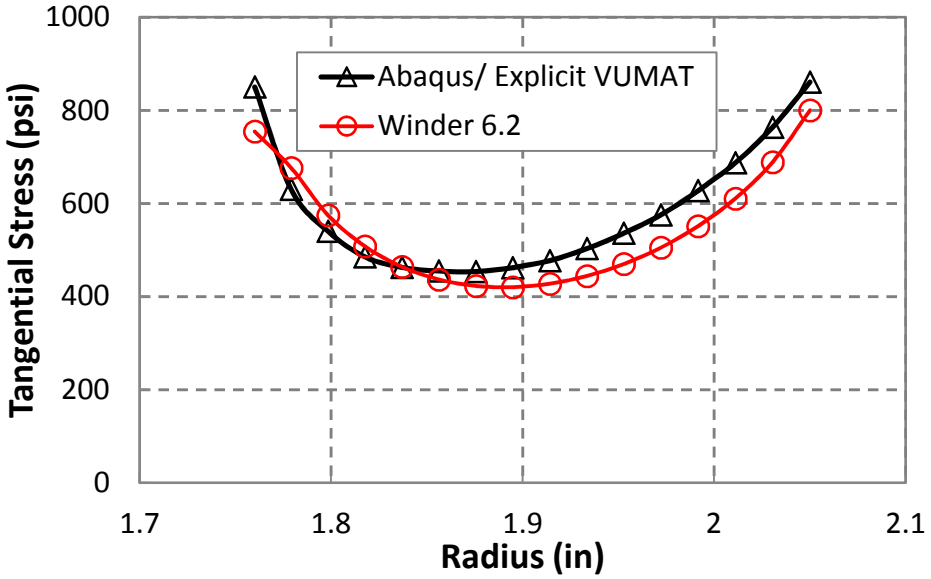

Figure 3-21 Comparison of tangential stress using Abaqus/Explicit with VUMAT and winder 6.2 under plane stress assumption

The second implementation of the state dependent radial modulus is based on the plane strain assumption. Plane strain elements CPE4R were used. Winding simulations which invoke the plane strain assumption provide an additional output, the axial stress distribution inside the roll. The results will be true only if the webs are in a real plane strain state. The assumption of plane strain infers that z direction (CMD) deformations and strains vanish. In reality the web upstream of the winder is in a plane stress state. This means the web has already contracted in the z dimension due to web tension and the Poisson effect prior to entry to the winder. The web on the winder can exist in a pseudo plane strain behavior where the negative CMD strain in the web upstream of the winder remains constant in all layers in the wound roll. Thus it might be said that all *changes* in z deformation and associated strains vanish in the wound roll in this *pseudo* plane strain condition. Winder 6.3b is a 1-D axisymmetric winding code based on this pseudo plane strain assumption to model this situation. The results using Abaqus/Explicit scheme will be compared with Winder 6.3b. Abaqus cannot directly simulate the reality of the web entering the winder in this case. The web elements in Figure 3.2 are either identified as having plane strain or plane stress behaviors prior to the beginning of the simulation. If plane strain is chosen, the web never contracts in the z direction after tension is applied but prior to the rotation of the core. Figure 3-22 and Figure 3-23 show that the radial pressure and tangential stress using Abaqus/Explicit with VUMAT compare well with Winder 6.3b. Figure 3-24 shows the comparison of axial stress using Abaqus/Explicit with VUMAT and Winder 6.3b appear to be offset by a constant value. It is also evident that the axial stress using Abaqus/Explicit is positive inside the wound roll. This is due to the pseudo plane strain state that Winder 6.3b accounts for *not* being accounted for in

Abaqus. The Abaqus axial stresses can however be corrected. The axial stress caused by constraint of the Poisson contraction upstream of the winder due to web tension can be approximated by equation (3.11):

$$\sigma_{zz} \approx \nu_{xz} E_z \frac{T_w}{E_x} = 0.3 \times 800 = 240\ psi \tag{3.11}$$

To correct the axial stresses output by Abaqus, the axial stress calculated by equation (3.11) is subtracted from the total axial stress to produce the real axial stress due to winding, shown as the red line in Figure 3-24. It can be seen that the corrected axial stress due to winding using Abaqus/Explicit compares well with Winder 6.3b. Note that the axial stress tends toward zero at the outside of the wound roll. This is compatible with the zero CMD stress that would be expected in the web upstream of the winder.

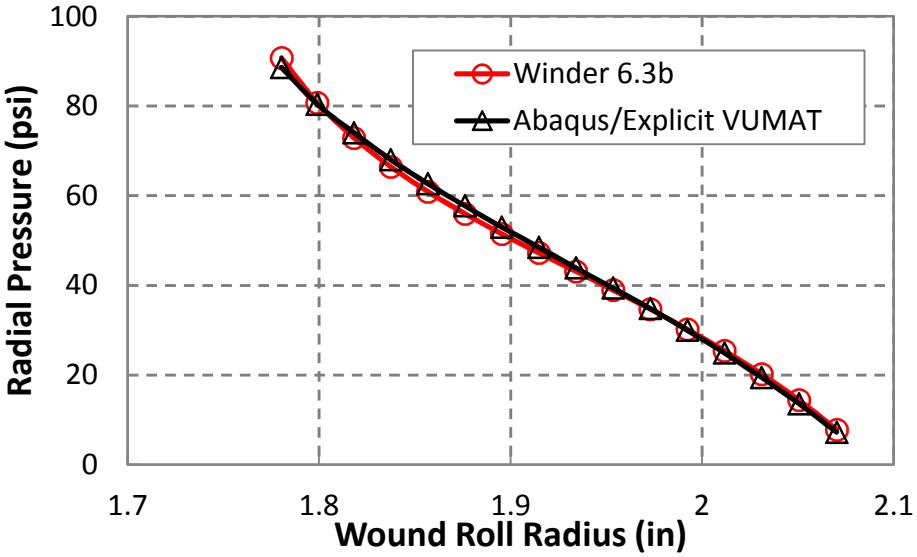

Figure 3-22 Comparison of radial pressure using Abaqus/Explicit with VUMAT and Winder 6.3b under the plane strain assumption

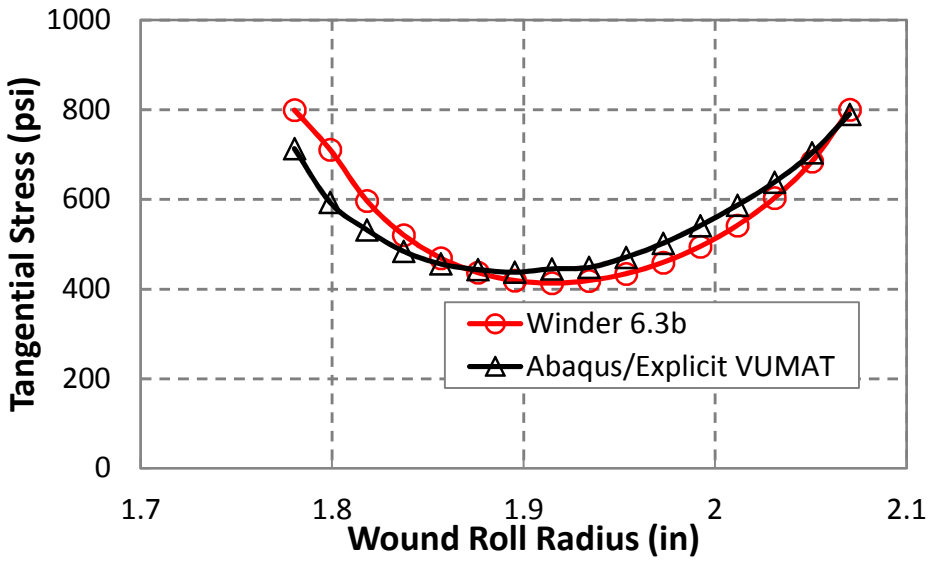

Figure 3-23 Comparison of tangential stress using Abaqus/Explicit with VUMAT and Winder 6.3b under the plane strain assumption

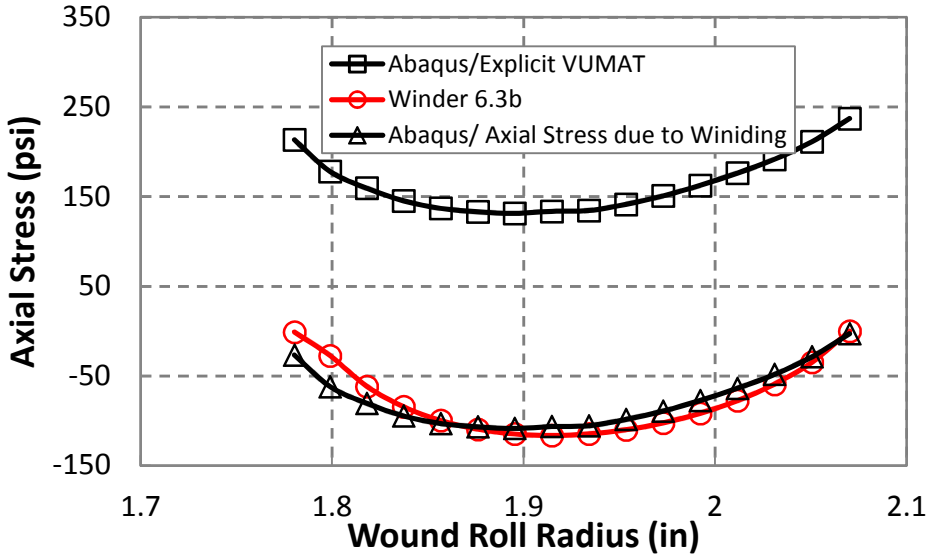

Figure 3-24 Comparison of axial stress using Abaqus/Explicit with VUMAT and Winder 6.3b under the plane strain assumption

3.4.3 Comparison of Running Time and Accuracy

The computational time required to simulate 11 layers being wound onto a roll is shown in Figure 3.25. ASC and CC denote Archimedean Spiral Core and Concentric Core,

respectively. All simulations produced pressures that agree well with 1D winding models. Use of the Archimedean Spiral Core produced tangential stresses that agreed much better with 1D winding models. Use of the Archimedean Spiral Core significantly increased the solution time when the implicit method was used. Use of 2nd order finite elements allowed only in the implicit method also substantially increased the solution time. Major limitations of the implicit method were the divergence of the solution after winding 11 layers and the inability to model the state dependent radial modulus. It is unclear if these limitations can be resolved. The Explicit method using the Archimedean Spiral Core provides the shortest solution times combined with reasonable stress accuracy and allowing state dependent properties.

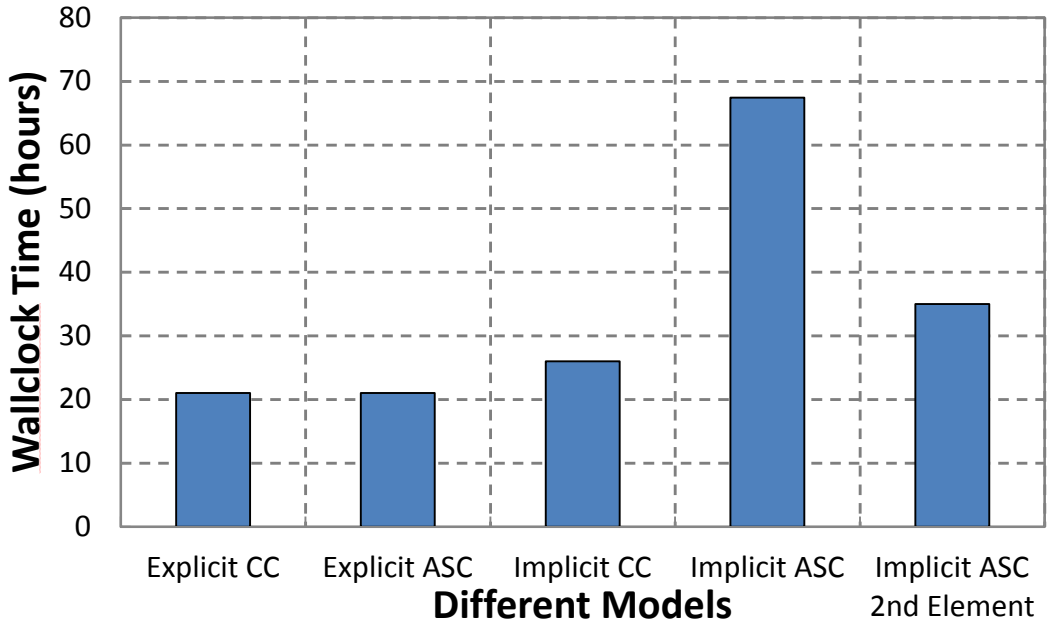

Figure 3.25 Comparison of computational cost

3.5 Summary

The 2D pure center winding process was simulated in Abaqus. The purpose is to find the best way to model the winding problems and deal with nonlinearity of radial stress versus strain exhibited by the roll of web materials. Both explicit and implicit numerical schemes were tested. It is found that the implicit method generates smooth results while explicit method generates noisy stress results. The lap average values of radial stress from two methods are close to each other and match the results of axisymmetric winding models (Winder 6.2 & 6.3) very well. The dynamic effects in the explicit method and the gap between web and the circular core affect the accuracy of circumferential stress. The implicit method and use of a spiral core to eliminate the gap helps to reduce the noise and produce accurate circumferential stresses. However, the computational cost of implicit method is higher than explicit method. The main finds are listed below:

1. The best modeling practices were found to efficiently simulate the pure center winding problem with Abaqus and those practices can be extended to model other more complex winding problems.
2. The model was verified by the axisymmetric winding model Winder 6.2 & 6.3. The gap between the spiral model and the axisymmetric model is filled
3. The Explicit method has the least computational cost. With the use of a spiral core the wound roll stresses can be calculated accurately. The Explicit method will be the preferred method for the next study of wound-on-tension problems which involve nip rollers in Chapter 4.

4. A VUMAT subroutine was successfully developed to model the state dependent radial modulus of winding rolls and results were verified. The ability to model the state dependent properties is important.

Chapter 4. Modeling Winding with Nip Rollers in Abaqus

4.1 Introduction

In the previous chapter, a finite element method was refined to model the pure center winding process. By working with this simplest form of winder, it was proven that the explicit finite element method can be successfully used to simulate the winding process and the resulting wound roll stresses agreed with simpler axisymmetric winding models. Experience was gained regarding proper modeling techniques to minimize the computational cost. The accuracy and performance of different solution methods was assessed. It was found that the explicit method is a better choice in handling the nonlinearity and complexity of the winding problems without sacrificing the accuracy of the solution. Even though the pure center winder is mechanically the simplest winder it is less desirable in industry due to its productivity. Winders with nip rollers can achieve greater productivity due to their ability to wind at higher speeds while preventing air from entraining into the wound roll. Balanced with this enhanced productivity is the lack of understanding regarding how the tension in the outer layer, called the Wound-On-Tension (WOT), is affected by the contact mechanics of the nip roller. In nipped winders, the WOT becomes the most critical parameter that governs the wound rolls stresses during and after formation. In this chapter, the explicit finite element method will be used with all the modeling techniques gained from the previous chapter to model winders with

a single nip roller. In this chapter the simplest case of such winders will be addressed. If the torque required to wind the roll is provided to the core this is a center winder with a nip roller, shown in Figure 1.1(b). If the torque required to wind the roll is provided to the nip roller this is a surface winder, shown in Figure 1.1(c). These two winders are very prevalent in industry and understanding how they develop WOT is of great importance due to the impact on wound roll residual stresses. Wound rolls in industry can be comprised of several thousand layers and the intention is not to use explicit simulation to model the entire winding process. The intention is provide the ability to assess the WOT at several wound roll radius locations which can then be used in conjunction with a 1D winding model to assess the winding residual stresses in the wound roll comprised of thousands of layers. How these winders differ in producing WOT and how this WOT is affected by winding and web material properties will be explored.

4.2 Development of Explicit Finite Element Winding Models of Winding with Nip Rollers

The explicit finite element simulation method was previously described in Section 3.2.3 and will not be repeated here. The web, nip roller and a core, as shown in Figure 4.1 were modeled in Abaqus/Explicit. The web material modeled in this study was an oriented Polyester film 254 μm (0.01 in.) in thickness. It will be assumed that the nip roller and the core are far stiffer than the web material and that the deformation of these rollers is insignificant compared with that of web. Thus the nip roller and the core are modeled with rigid analytical surfaces in Abaqus to save computational cost. Based on the consideration of solution accuracy (by eliminating numerical deficiencies such as shear

locking and hour glassing) and computational cost, a mesh consisting of four-node quadrilateral reduced integration plane strain elements (CPE4R in Abaqus) with the size of 0.635×0.085 mm (0.025×0.003 in.) was used in this study. Three such elements were used through the thickness of the web to capture bending effects.

As a winding operation starts, the incoming layer is first fastened to the core and tensioned. Second, the nip roller approaches the incoming layer on the core and is impinged at a given nip load. Third, the winder begins to rotate with web layers winding in a spiral fashion on the core. To model the center winding condition, the loading procedure in Abaqus/Explicit was also divided into three steps: pretension, nip loading and winding, as shown in Figure 4.1. In the pretension step shown in Figure 4.1 (a), the leading end of the incoming web layer is tied to the core in a small area, while the core and nip roller are restrained. The lower end point on the right end surface of the web is restrained on its vertical (y) DOF such that only horizontal (x) displacement is allowed. A constant winding tension T_w is prescribed at the right end surface of the web and is maintained during the simulation. In the nip loading step shown in Figure 4.1 (b), the y DOF of nip roller is released. Then a vertical downward concentrated force representing the nip load N was applied at the central reference node of the nip roller and was maintained during the simulation. All other loads and BCs are inherited from the previous step. In the winding step shown in Figure 4.1 (c), the rotation of the core about the z axis is released and an angular velocity ω is assigned to the core. The other loads and BCs remain identical. Modeling surface winding was very similar except the angular velocity in Figure 4.1 (c) was now input to the nip roller and core/wound roll was free to rotate.

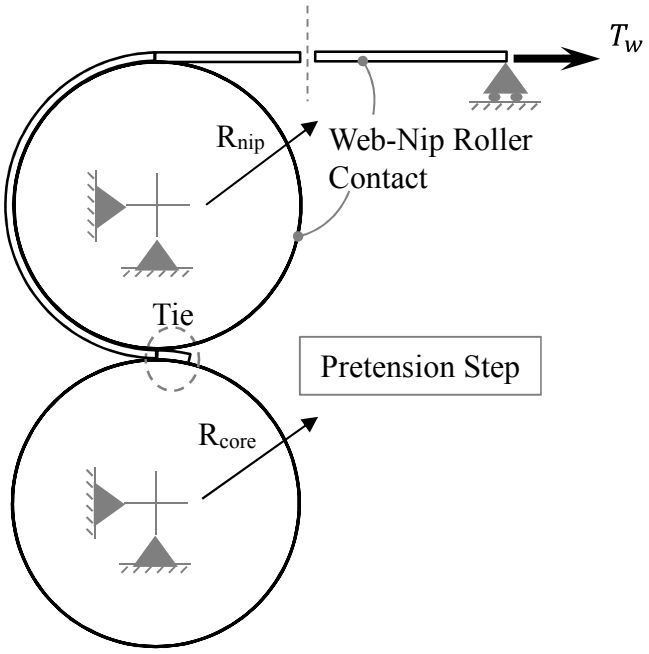
T_w
R_{nip}
Web-Nip Roller Contact
Tie
Pretension Step
R_{core}

(a)

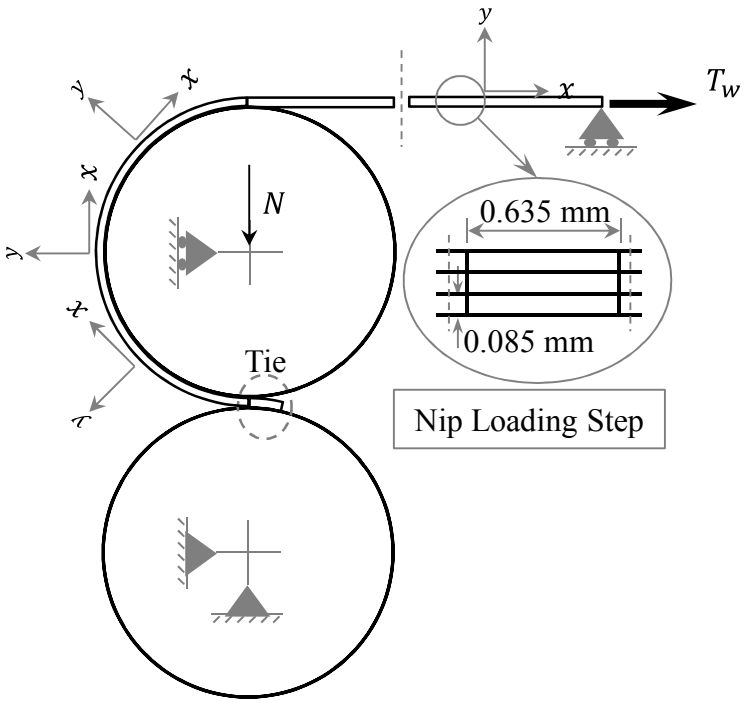
y
x
T_w
N
0.635 mm
0.085 mm
Tie
Nip Loading Step

(b)

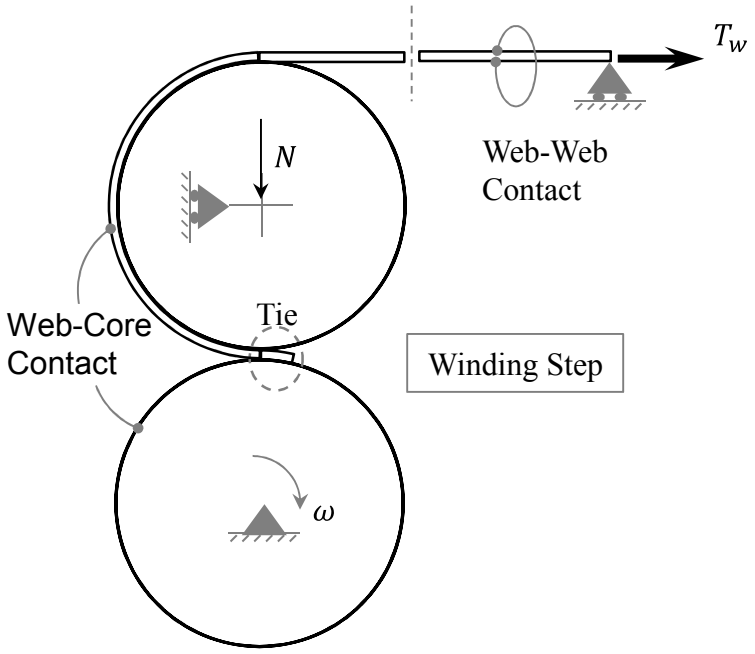

(c)

Figure 4-1 Modeling steps for center winding using explicit analysis

In Figure 4.1 the potential for surface interaction is shown between the web and the nip, the web upon the core and self-contact of the web winding upon itself. One of the challenges in modeling a winding process using an explicit FE method is to accurately model the surface interactions. This is accomplished by modeling the contact pairs using a kinematic predictor-corrector contact algorithm [15] to strictly enforce the contact constraints that allows for no nodal penetrations. The friction between all contacting surfaces is modeled using Coulomb's friction law with a constant coefficient of friction as was discussed in Section 3.2.4.

As stated before, the explicit method is conditionally stable. Due to low density and the thinness of typical web materials, the stable time increment Δt is usually very small which makes the solution computationally very expensive. Two techniques can be used to accelerate the solution process: increasing loading rates and mass scaling. The former

technique artificially reduces the time duration of physical events to reduce the overall simulation time. The latter artificially increases the mass of the entire or partial structure to increase the stable time increment Δt. In this study, both techniques were adopted. First the time durations for applying web tension, nip loads and angular velocity of core were reduced. To overcome the potential noise in solution generated by increasing loading rate, a smooth amplitude function is used to apply these loading in their respective steps to prevent sudden changes in acceleration. Second, a mass scaling factor of 300 is used for the web material, which increases the stable time increment to an order of magnitude around 10^{-6} s. By using these techniques, the solution time for single winding case is around 15 hours on an Intel Xeon 3.07 GHz workstation.

4.3 Center vs. Surface Winding for Constant Orthotropic Web with High MD Modulus

The first focus will be for high modulus materials that would encompass many grades of paper and some plastic films such as polyester. The web modeled is 254 μm (0.01 in.) thick and the width is 15.24 cm (6 in.). In these simulations the radius of the nip (R_{nip}) and the core (R_{core}) were 5.08 (2 in.) and 4.29 cm (1.7 in.), respectively. The friction coefficient between web layers, between the web and the nip and between the web and the core were all set at 0.3. The 1, 2 and 3 material property directions are related to the machine direction (MD), cross machine direction (CMD) and the radial z direction (ZD) in Figure 4.2.

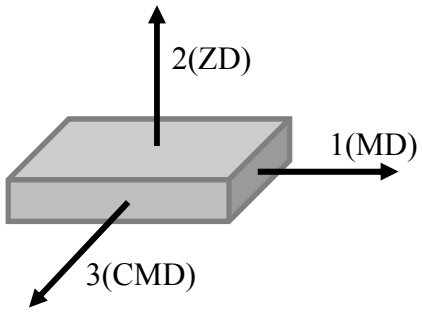

Figure 4-2 Identification of material property directions

Assumptions of plane strain and constant orthotropic web properties were made initially. The orthotropic material properties needed for plane strain analyses in the 1-2 plane are shown in the constitutive expressions (4.1) relating strain $\{\varepsilon\}$ to stress $\{\sigma\}$:

$$\begin{Bmatrix} \varepsilon_{11} \\ \varepsilon_{22} \\ \varepsilon_{33} \\ \gamma_{12} \end{Bmatrix} = \begin{bmatrix} 1/E_1 & -\nu_{21}/E_2 & -\nu_{31}/E_3 & 0 \\ -\nu_{12}/E_1 & 1/E_2 & -\nu_{32}/E_3 & 0 \\ -\nu_{13}/E_1 & -\nu_{23}/E_2 & 1/E_3 & 0 \\ 0 & 0 & 0 & 1/G_{12} \end{bmatrix} \begin{Bmatrix} \sigma_{11} \\ \sigma_{22} \\ \sigma_{33} \\ \tau_{12} \end{Bmatrix} \tag{4.1}$$

Using the Maxwell-Betti reciprocity theorem it can be proven that there must be symmetry in the constitutive relations shown in expression (4.1):

$$\nu_{12}/E_1 = \nu_{21}/E_2 \quad \nu_{13}/E_1 = \nu_{31}/E_3 \quad \nu_{23}/E_2 = \nu_{32}/E_3 \tag{4.2}$$

This effectively reduces the number of material properties to be input to seven. The properties used in this investigation are shown in Table 4.1:

Table 4-1 Constant orthotropic properties for high in-plane modulus simulations

E_1	E_2	E_3	ν_{12}	ν_{13}	ν_{23}	G_{12}
4.89 GPa	47.2 MPa	5.10 GPa	0.3	0.36	0.01	16.3 MPa

These properties will be discussed thoroughly later in a section devoted to properties. As discussed earlier the radial modulus E_2 is state dependent on pressure, expression (2.20) for instance. To speed the computations an average value of E_2 was selected for the range of nip loads studied. The constant value of G_{12} came from an approximation made originally by St. Venant [16]. Later these constant values will be allowed to vary.

Results will be examined first for a low nip load where slippage is prevalent in the contact zone. Then results will be examined for a high nip load where stick behavior now exists in the contact zone. This section will conclude with a discussion of the resulting WOT that was computed for a range of nip loads and web line tensions.

4.3.1 Low Nip Load Behavior

The web line tension for the web entering the winder (T_w) was set at 2.07 MPa (300 psi) and the nip load was 26.3 N/cm (15 lb/in) for the simulations that produced the following results. The web machine direction (MD) stresses are considered first in Figure 4.3. These stresses were determined by averaging the MD stresses through the thickness of the web. The stresses in Figure 4.3 are shown at the conclusion of the winding simulation where the entire web modeled is now in the form of a spiral in the wound roll. The results are presented versus a curvilinear MD coordinate. The origin of this coordinate system is near the entry of the nip contact zone. A negative MD coordinate refers to web material prior to or in contact with the nip roller. Note that at the left side of the chart an MD membrane stress of 2.07 MPa (300 psi) is seen for the web that did not contact the nip

roll for both center and surface winding, which is the level of web line tension stress which was set.

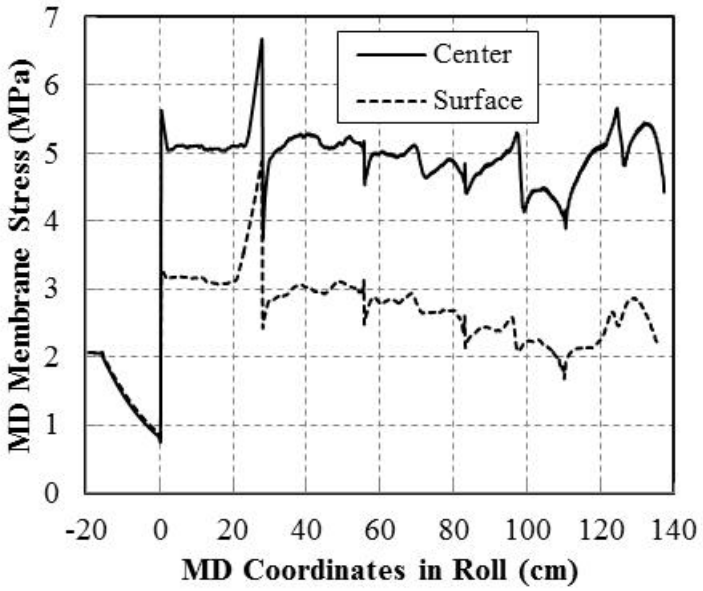

Figure 4-3 Machine direction membrane stress in the web, N=26.3 N/cm (15 lb/in)

The objective is to study the WOT in the outer layer and the results for MD coordinates in the range of -20 to 20 cm (-7.9 to 7.9 in.) are of most interest. The spike in MD stress at 27 cm is of consequence and will be discussed later. The positions of the spikes at 27, 56, 80 and 109 cm (10.6, 22, 31.5, and 42.9 in.) would have fallen on a radius of the wound roll beneath the nip roller at the completion of the simulation.

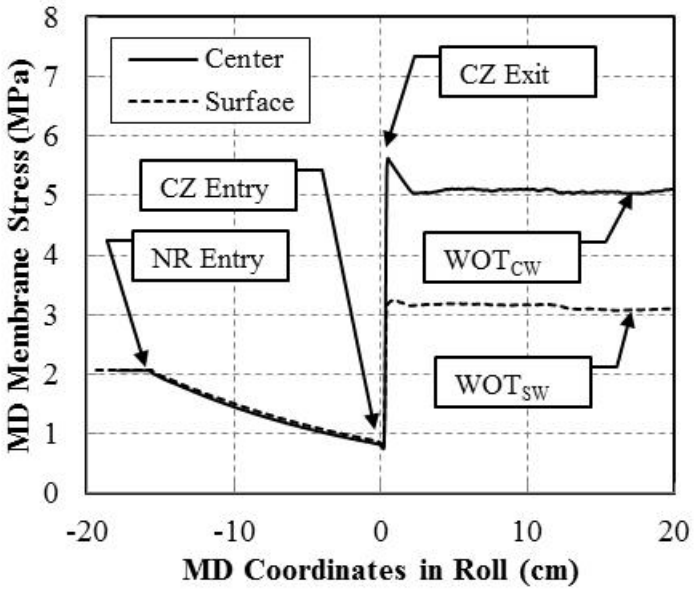

Figure 4-4 MD membrane stresses and the WOT, T_w=2.07 MPa (300 psi), N=26.3 N/cm (15 lb/in)

In Figure 4.4 the MD membrane stresses are shown for a smaller range of the abscissa from Figure 4.3. Prior to entry of the nip roller the free web is shown to exhibit the set level of web line tension (T_w=2.07 MPa=300 psi). As the web transits the surface of the nip roller the MD membrane stresses exponentially decay as a result of slippage. Using the capstan slippage expression the MD stress prior to the entry of the nip contact zone should be:

$$T_{entry,contact\ zone} = \frac{T_w}{e^{\mu\theta}} = \frac{2.07}{e^{0.3\pi}} = 0.81\,MPa \tag{4.3}$$

where θ is the angle of wrap and μ is the friction coefficient. This is very near the computed value of stress for both center and surface winding seen at the entry of the nip contact zone in Figure 4.4. Large increases in membrane stress are witnessed in the nip contact zone. After exiting the nip contact zone only modest changes in MD stress occur

and the final value of WOT is witnessed. Note that the WOT for center winding is nearly 2 MPa (291 psi) larger than for surface winding, which is equal to the web line tension of 2.07 MPa (300 psi).

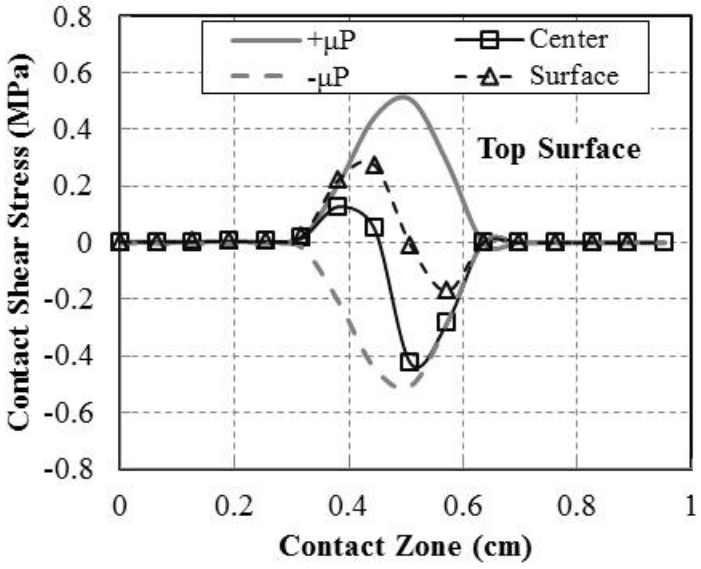

(a)

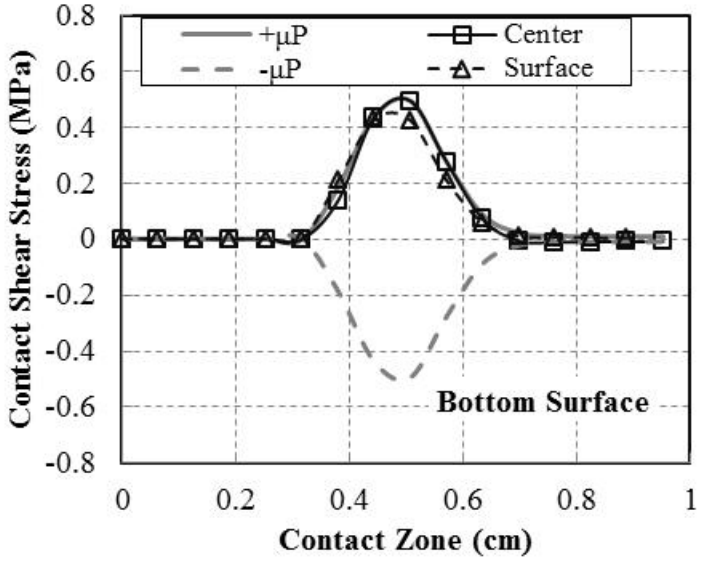

(b)

Figure 4-5 Contact shear stresses on the top web surface (a) and the bottom web surface (b) in the contact zone, T_w=2.07 MPa (300 psi), N=26.3 N/cm (15 lb/in)

The largest changes in MD stress which affected the final WOT values in both center and surface winding occurred in the nip contact zone as shown in Figure 4.4. To examine what caused these changes the contact shear stresses are shown in Figure 4.5 superimposed on the envelopes of the critical levels of Coulomb shear stress required to induce slippage (τ_{crit}). Note the contact shear stresses never exceed the critical shear stresses. When the contact shear stress reaches the critical shear stress slippage will result. In cases where the contact shear stress is less than the critical value stick behavior will result. Slip is occurring through the entire contact zone on the lower surface for both center and surface winding as shown in Figure 4.5 (b). The lower surface is in contact with the previous layer that was wound onto the roll. The behavior on the upper surface (Fig. 4.5 (a)) however is markedly different with slip occurring near the entry and exit but separated by a zone of stick. It is also evident that the contact shear stresses differ between center and surface winding on the upper surface. The upper web surface is in direct contact with the surface of the nip roller. Equilibrium can be established for the web in the contact zone if the contact shear stresses are integrated on the upper and lower surfaces as shown in Figure 4.6.

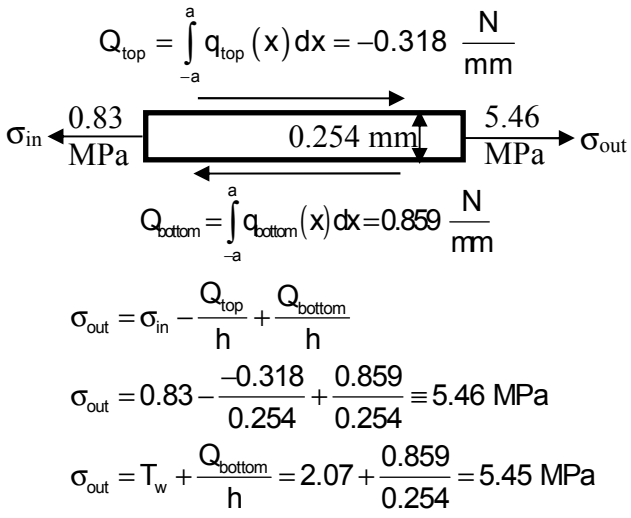

(a) Center Winding

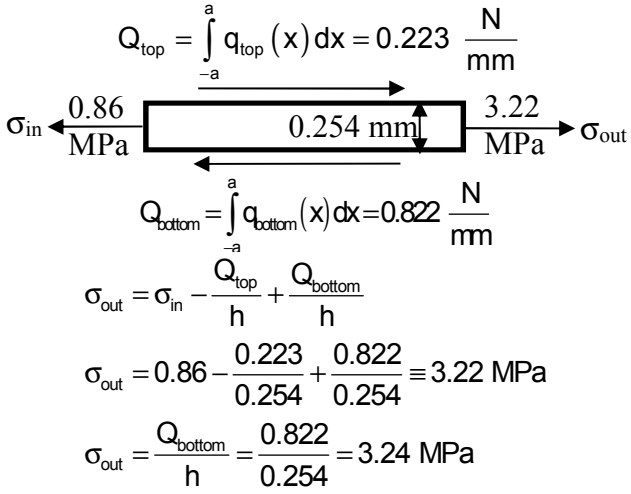

(b) Surface Winding

Figure 4-6 Equilibrium of web in contact zone, T_w=2.07 MPa (300 psi), N=26.3 N/cm (15 lb/in)

Now the difference between center and surface winding becomes quantifiable. The major difference is the sign and magnitude of the shear traction on the upper surface of the web in the contact zone. It is this difference which is responsible for the majority of the 2.24 MPa difference in σ_{out}, which is approximately the value of the web line tension T_w of

2.07 MPa (300 psi). This is consistent with what the empirically derived expressions (2.29) and (2.30) forecast as the difference in WOT between center and surface winding. Why this difference occurs is difficult to understand when considering how similar the values of σ_{in} were for both center and surface winding as demonstrated in Figures 4.44 and 4.6. If equilibrium is considered on another scale, as shown in Figure 4.7, this difference can be explained.

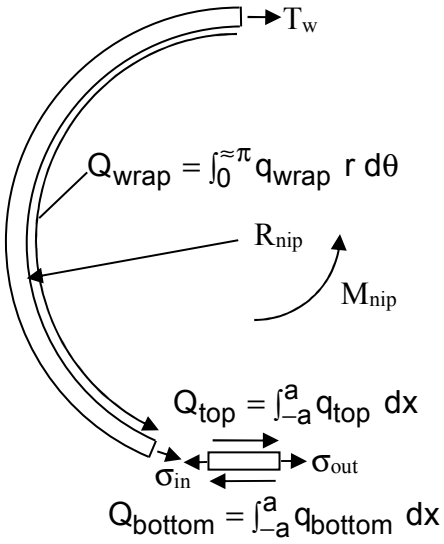

Figure 4-7 Equilibrium of the web on the nip roller and in the contact zone

The first focus is equilibrium of the web on the surface of the nip roller prior to the nip contact zone:

$$\sigma_{in} = T_w - \frac{Q_{wrap}}{h} \tag{4.4}$$

Equilibrium must also be sustained for the web in the contact zone:

$$\sigma_{out} = \sigma_{in} - \frac{Q_{top}}{h} + \frac{Q_{bottom}}{h} \tag{4.5}$$

For center winding, the torque applied to the nip (M_{nip}) is zero. The applied surface tractions acting on the nip roller must be in equilibrium:

$$Q_{top}R_{nip} + Q_{wrap}R_{nip} = 0 = M_{nip} \tag{4.6}$$

For center winding the MD stress at the exit to the contact zone is found by inserting expressions (4.4) and (4.6) into (4.5):

$$\sigma_{out} = \sigma_{in} - \frac{Q_{top}}{h} + \frac{Q_{bottom}}{h} = \left(T_w - \frac{Q_{wrap}}{h}\right) - \frac{-Q_{wrap}}{h} + \frac{Q_{bottom}}{h} = T_w + \frac{Q_{bottom}}{h} \tag{4.7}$$

For surface winding, a torque (M_{nip}) must be applied to wind the roll. The torque will be approximately the web line tension, in units of force, multiplied by the radius of the nip (R_{nip}). Again the applied surface tractions acting on the nip roller must be in equilibrium with the applied torque:

$$Q_{top}R_{nip} + Q_{wrap}R_{nip} = M_{nip} = T_w R_{nip} h \tag{4.8}$$

For surface winding the MD stress at the exit to the contact zone is found by inserting expressions (4.4) and (4.8) into (4.5):

$$\sigma_{out} = \sigma_{in} - \frac{Q_{top}}{h} + \frac{Q_{bottom}}{h} = \left(T_w - \frac{Q_{wrap}}{h}\right) - \left(\frac{T_w h - Q_{wrap}}{h}\right) + \frac{Q_{bottom}}{h} = \frac{Q_{bottom}}{h} \tag{4.9}$$

Comparison of expressions (4.7) and (4.9) shows that the MD stress at the exit of the contact zone is higher by a value of the web tensile stress (T_w) for center winding than in surface winding. Results from expressions (4.7) and (4.9) are shown in Figures 4.6 (a)

and 4.6 (b) which compare quite well with the MD stress at the exit of the contact zone (σ_{out}) computed by Abaqus. Expressions (4.7) and (4.9) become expressions (2.29) and (2.30) only when the lower contact surface is void of stick behavior and for cases where there is little change in the membrane stress after the web exits the nip contact zone, then σ_{out} approaches the WOT.

4.3.2 High Nip Load Behavior

The web line tension for the web entering the winder (T_w) remained at 2.07 MPa (300 psi) and the nip load was increased to 109.5 N/cm (62.5 lb/in) for the simulations that produced the following results. The MD membrane stresses are shown in Figure 4.8 for web just entering the nip roller, wrapping the nip roller, passing through the nip contact zone and exiting to become the outer layer in the winding roll.

There is some similarity of the stresses presented in Figure 4.8 with those shown in Figure 4.4 but the nip load increasing over four times has caused some differences. The WOT has increased significantly for both center and surface winding cases. Note how the MD stresses continue to increase after the web exits the contact zone. The peak values that correspond to the WOT occur almost 10 cm beyond the exit of the nip contact zone.

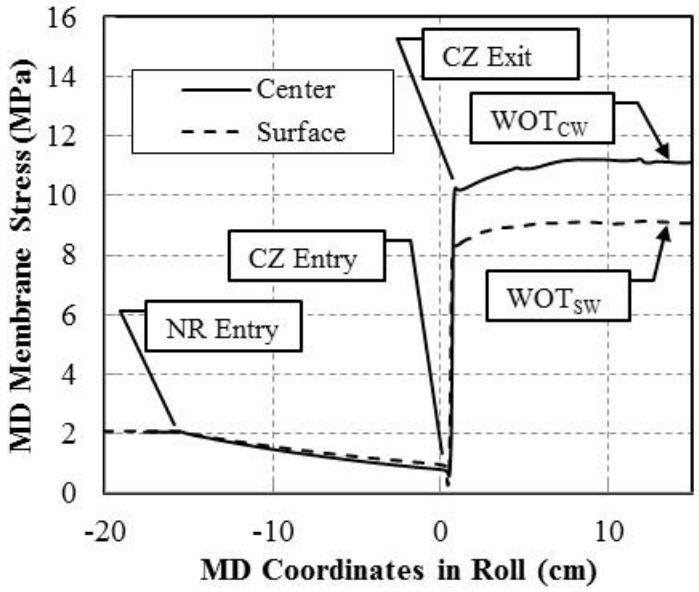

Figure 4-8 MD membrane stresses and the WOT, T_w=2.07 MPa (300 psi), N=109.5 N/cm (62.5 lb/in)

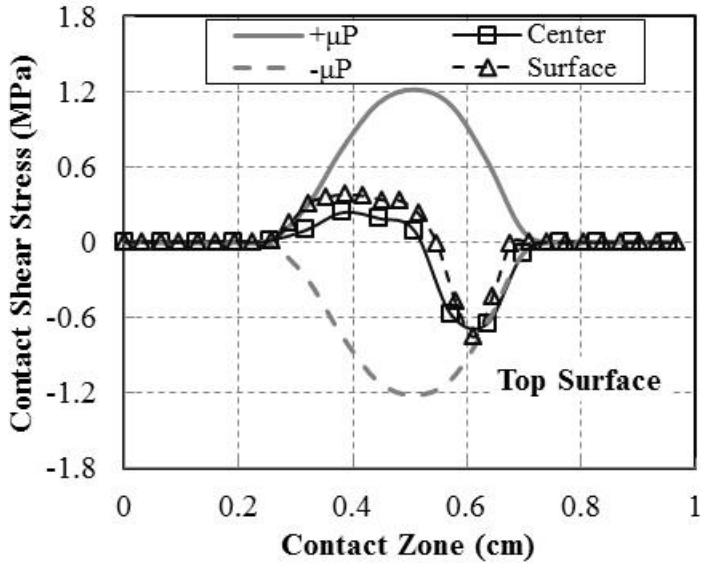

(a)

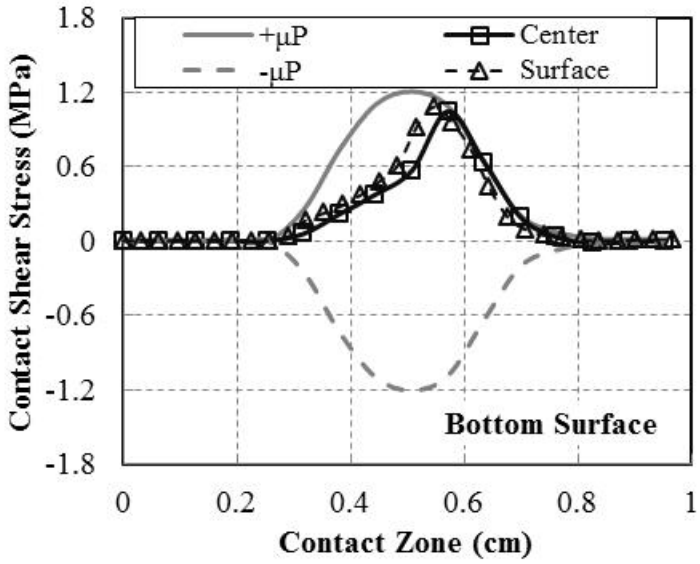

(b)

Figure 4-9 Contact shear stresses on the top web surface (a) and the bottom web surface (b) in the contact zone, T_w=2.07 MPa (300 psi), N=109.5 N/cm (62.5 lb/in)

The contact shear stresses are shown in Figure 4.9 which can be compared to the lower nip load results in Figure 4.5. With the higher nip load larger contact pressures are developed. The contact shear stresses in Figure 4.9 are considerably larger than those in Figure 4.5. Note that a large zone of stick behavior occurs on the bottom surface in Figure 4.9 (b) whereas in Figure 4.5 (b) the lower surface is exhibiting slip throughout the contact zone.

The equilibrium of the web in the contact zone is shown in Figure 4.10. Note the surface tractions on the lower surface are comparable for center and surface winding but much larger than those shown in Figure 4.6 for a lower nip load. As in Figure 4.6 the largest difference is in the magnitude and change in sign of the surface tractions on the upper surface. Note that expressions (4.7) and (4.9) produce values for the MD stress at the exit to the contact zone (σ_{out}) that are comparable to those computed directly by Abaqus.

$$Q_{top} = \int_{-a}^{a} q_{top}(x)\,dx = -0.421\ \frac{N}{mm}$$

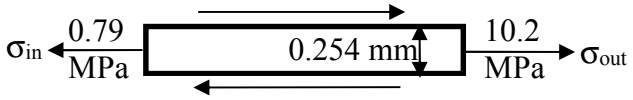

$$Q_{bottom} = \int_{-a}^{a} q_{bottom}(x)\,dx = 1.970\ \frac{N}{mm}$$

$$\sigma_{out} = \sigma_{in} - \frac{Q_{top}}{h} + \frac{Q_{bottom}}{h}$$

$$\sigma_{out} = 0.79 - \frac{-0.421}{0.254} + \frac{1.97}{0.254} \equiv 10.2\ \text{MPa}$$

$$\sigma_{out} = T_w + \frac{Q_{bottom}}{h} = 2.07 + \frac{1.97}{0.254} = 9.8\ \text{MPa}$$

(a) Center Winding with nip

$$Q_{top} = \int_{-a}^{a} q_{top}(x)\,dx = 0.270\ \frac{N}{mm}$$

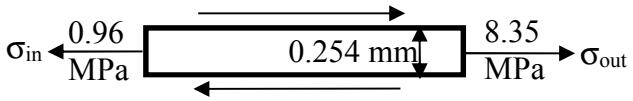

$$Q_{bottom} = \int_{-a}^{a} q_{bottom}(x)\,dx = 2.149\ \frac{N}{mm}$$

$$\sigma_{out} = \sigma_{in} - \frac{Q_{top}}{h} + \frac{Q_{bottom}}{h}$$

$$\sigma_{out} = 0.96 - \frac{0.270}{0.254} + \frac{2.149}{0.254} \equiv 8.35\ \text{MPa}$$

$$\sigma_{out} = \frac{Q_{bottom}}{h} = \frac{2.149}{0.254} = 8.46\ \text{MPa}$$

(b) Surface Winding

Figure 4-10 Equilibrium of web in contact zone, T_w=2.07 MPa (300 psi), N=109.5 N/cm (62.5 lb/in)

4.3.3 The Impact of Nip Loads, Web Line Tension and Nip Diameter on WOT

In the preceding sections the MD stresses at the exit of the contact zones (σ_{out}) have been studied. For low nip loads the stress at the exit of the contact zone may be very close to the WOT as shown in Figure 4.4. For a high nip load the highest MD stress and hence the WOT occurred after exiting the contact zone as shown in Figure 4.8. The WOT for several nip load levels are shown in Figure 4.11 in units of load per unit width. This is obtained by taking the product of the WOT in units of stress times the web thickness h. Results are shown for web line tensions of 2.07 MPa (300 psi) or 5.25 N/cm (3 lb/in) and 6.89 MPa (1000 psi) or 17.5 N/cm (10 lb/in).

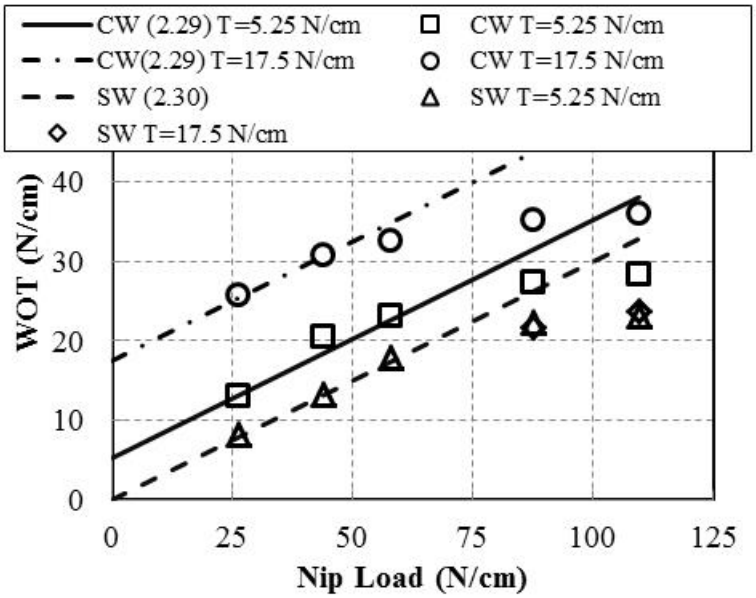

Figure 4-11 The WOT for center (CW) and surface (SW) winding per expressions (2.29) and (2.30) and from Abaqus/Explicit (discrete data) for a high in-plane modulus web

With WOT and nip load in like units the results of the Abaqus/Explicit computations can be compared directly to the WOT expressions (2.29) and (2.30) that were empirically

derived. At lower nip load levels the slope of the center and surface winding results are very close to 0.3, the friction coefficient used in these analyses. The agreement between expressions (2.29) and (2.30) and the Abaqus results is quite good at low nip loads. The stick behavior on the lower surface of the contact zone causes the Abaqus results to be lower than predicted by expressions (2.29) and (2.30) at higher nip loads. Note that web tension has a negligible effect on WOT when surface winding which agrees in form with expressions (2.30) and (4.9). Web line tension is shown to affect the WOT in center winding in Figure 4.11. Use of expressions (2.29) or (4.7) would predict a constant WOT difference of 12.25 N/cm between the WOT developed at web line tensions of 5.25 and 17.5 N/cm. From Abaqus the difference in WOT begins at 12.75 N/cm at a nip load of 26.3 N/cm and decreases to a difference of 7.7 N/cm at a nip load of 109.5 N/cm. The Q_{top} and Q_{bottom} terms that entered the discussion of equilibrium in expression (4.5) were integral in deriving expressions (4.7) and (4.9). The Q_{top} and Q_{bottom} terms may have a dependency on the winding tension (T_w). Although this dependency is small here for surface winding (Figure 4.11) it is significant for center winding. The trends in WOT seen in Figure 4.11 are very similar to those witnessed by Hartwig [32] for center winding and Steves [33] for surface winding.

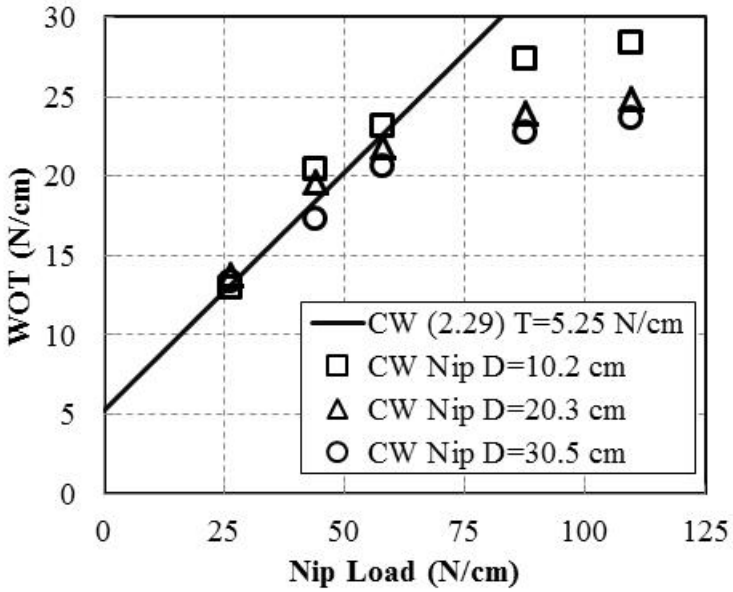

Figure 4-12 Effect of nip diameter on WOT for center winding per expressions (2.29) and Abaqus/Explicit (discrete data)

The explicit model was then altered to study the impact of nip diameter on WOT. The results show that smaller diameter nips produce greater WOT at high nip loads while at low nip loads the WOT produced becomes less dependent on nip load. The 20.3 and 30.5 cm (8 and 12 in.) diameter nips produced nearly the same WOT, thus the effect diminishes with increased nip diameter. This trend was witnessed by Pfeiffer [27].

4.4 Center vs Surface Winding for Constant Orthotropic Web with Low MD Modulus

The impact of a low in-plane modulus on WOT will be shown to be significant. Additional explicit analyses were conducted where all properties remained the same per Table 4-1 except the MD and CMD modulus as shown in Table 4.2. This modulus is

similar to what might be expected for a tissue, non-woven or a low density polyethylene web.

Table 4-2 Table Constant orthotropic properties for low in-plane modulus simulations

E_1	E_2	E_3	ν_{12}	ν_{13}	ν_{23}	G_{12}
138 MPa	47.2 MPa	138 MPa	0.3	0.3	0.01	16.3 MPa

The MD membrane stresses in the vicinity of the nip contact zone are shown in Figure 4.13 for two web line tensions and a nip load of 87.6 N/cm. These can be compared to the MD membrane stresses for high in-plane modulus webs in Figure 4.4. One apparent difference is that prior to the nip contact zone entry the MD membrane stress is essentially that of web line tension (T_w). Thus the impact of slippage of the web that wrapped the nip roller that was witnessed for high in-plane modulus webs in Figure 4.4 is much reduced for the low in-plane modulus web in Figure 4.13. After the exit of the contact zone the MD membrane stresses become very uniform and the final value of the WOT is attained shortly after the web exits the contact zone. Also note that for the two surface winding results shown that the MD membrane stress and hence the WOT is now affected by web line tension. Thus very different behaviors are witnessed for the low in-plane modulus webs than were previously witnessed for the high in-plane modulus webs.

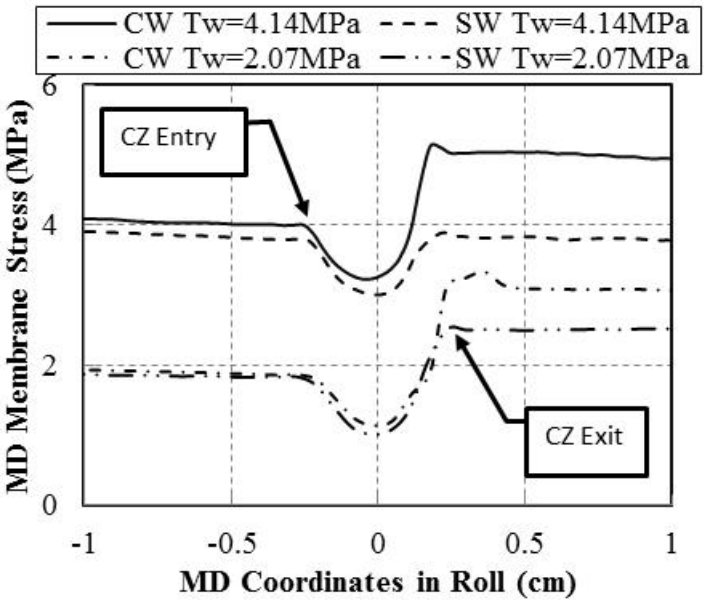

Figure 4-13 MD membrane stresses and the WOT for a low modulus web, N=87.6 N/cm (50 lbs/in)

The majority of the difference witnessed is due to the slip behavior in the contact zone. This can be examined in Figure 4.14 for both center and surface winding cases for a web line tension T_w of 4.14 MPa (600 psi) and a nip load of 87.6 N/cm (50 lbs/in). Note that large zones of stick behavior are witnessed by the web on both the top and bottom surfaces. If this slippage is compared to that for the high in-plane modulus webs that were presented in Figures 4.5 and 4.9 it can be noted that the stick behaviors witnessed in Figures 4.14 (a) and (b) are occurring over a larger portion of the contact zone than even for the high modulus results shown in Figure 4.9. The difference is that these zones of stick behavior become established at much lower nip loads for the low in-plane modulus webs.

The effects of this stick behavior on the WOT are shown in Figure 4.15. The WOT for several nip load levels are shown in Figure 4.15 in units of load per unit width. This is obtained by taking the product of the WOT in units of stress times the web thickness h.

Results are shown for web line tensions of 2.07 MPa (300 psi) or 5.25 N/cm (3 lbs/in) and 4.14 MPa (600 psi) or 10.5 N/cm (6 lbs/in). Note that for center winding that the Abaqus results bare little comparison to expression (2.29) except at the smallest nip load. The WOT appears to be almost independent of nip load for the center winding cases. For surface winding there is some dependency on nip load which would compare with expression (2.30) at the lowest nip loads. At higher nip loads the dependency on nip load declines and now the WOT appears to be affected by web line tension (compare results for T=5.25 N/cm (3 lbs/in) and 10.5 N/cm (6 lbs/in)) which is not a behavior that is consistent with expression (2.30).

As shown in Figure 4.13 the MD membrane stress at the exit of the contact zone (σ_{out}) is close to the final value of the WOT in the outer layer of the winding roll. If the equilibrium expressions (4.7) and (4.9) generated earlier are recast in units of load per unit width by multiplying by the web thickness (h):

$$WOT_{CW} \approx \sigma_{out} h = T_w h + Q_{bottom} = T + Q_{bottom} \quad (4.10)$$

$$WOT_{SW} \approx \sigma_{out} h = Q_{bottom} \quad (4.11)$$

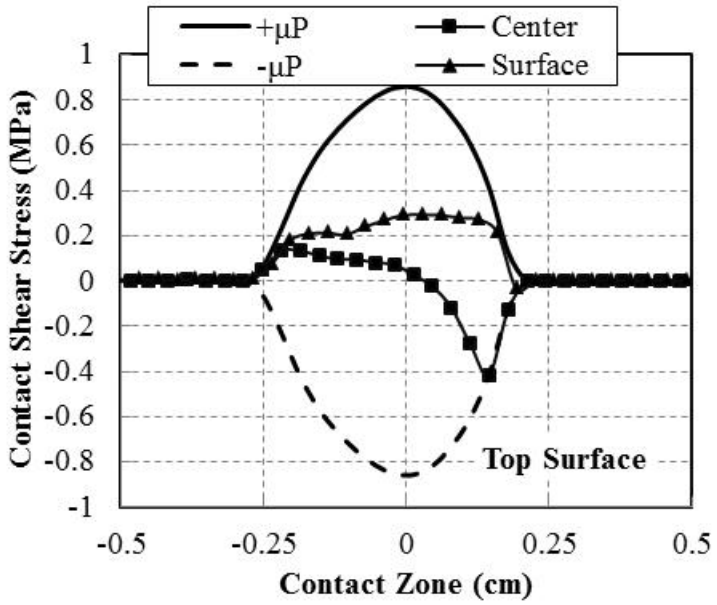

(a)

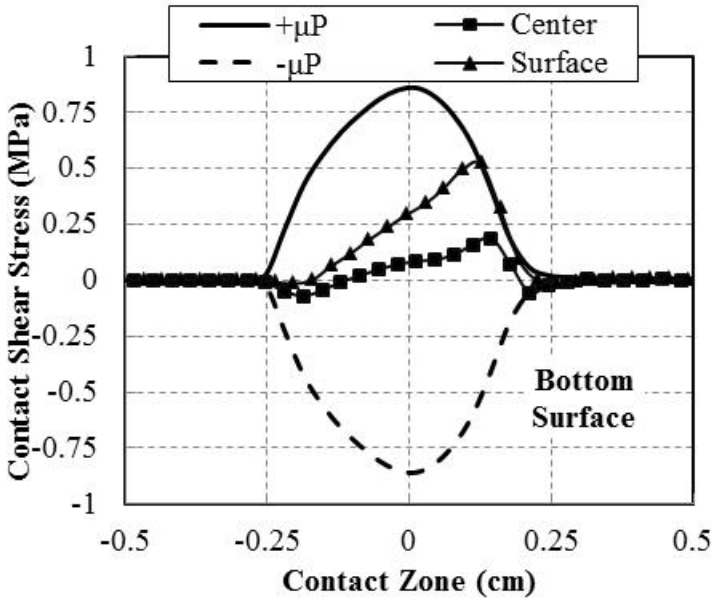

(b)

Figure 4-14 Contact shear stresses for a low in-plane modulus web on the top web surface (a) and the bottom web surface (b) in the contact zone, T_w=4.14 MPa (600 psi), N=87.6 N/cm (50 lbs/in)

In Figure 4.16 (a) comparison of the estimate of the WOT for center winding (4.10) is compared with the final value of WOT extracted from MD membrane stress data. To form this comparison required that the contact shear stresses (such as those shown in

Figure 4.14 (b)) be integrated over the bottom surface of the web in the contact zone to obtain Q_{bottom} for use in expression (4.10). Observe that over the range of nip load in Figure 4.16 that Q_{bottom} is not large and does not vary much with respect to nip load. For the two winding tensions shown the WOT is affected more by web line tension than by nip load. The nip load did however have to be sufficient to cause stick behavior over the majority of the nip contact zone.

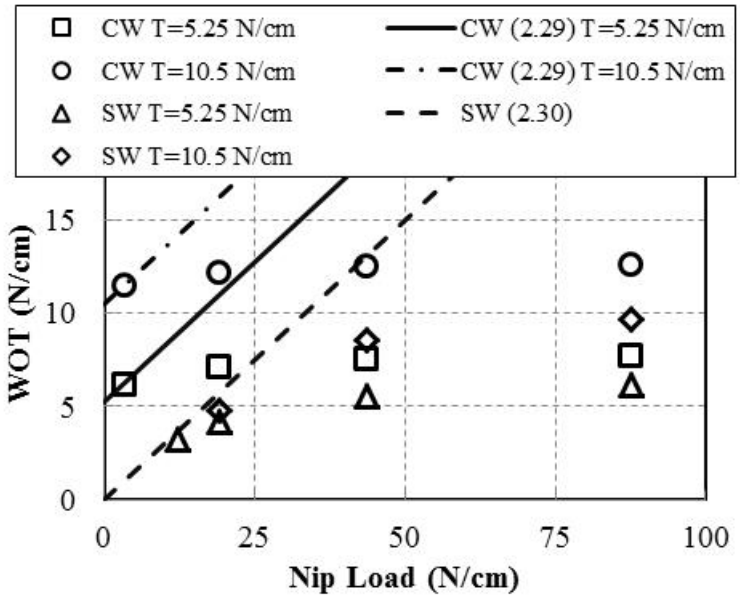

Figure 4-15 WOT for center (CW) and surface (SW) winding per expressions (2.29) and (2.30) and from Abaqus/Explicit (discrete data) for a low in-plane modulus web

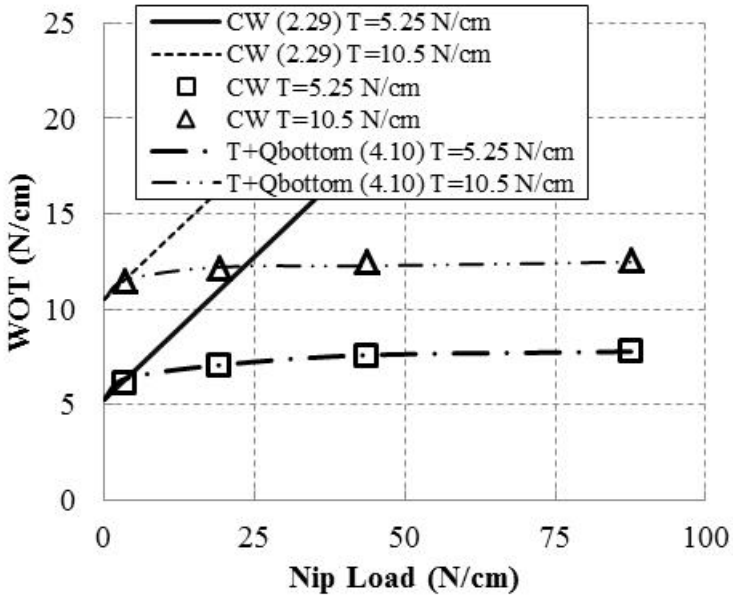

Figure 4-16 WOT for center winding (CW) per expressions (2.29) and (4.10) and from Abaqus/Explicit (discrete data) for a low in-plane modulus web

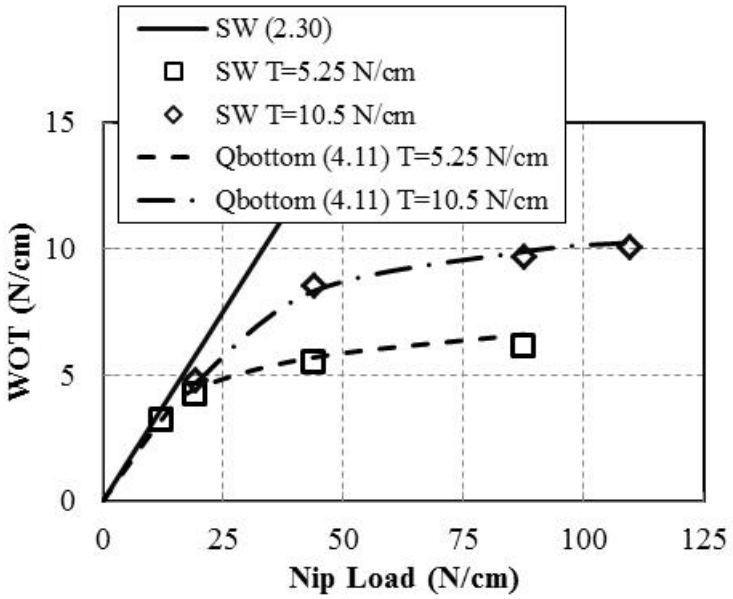

Figure 4-17 WOT for surface winding (SW) per expressions (2.30) and (4.11) and from Abaqus/Explicit (discrete data) for a low in-plane modulus web

In Figure 4.17 a comparison of the estimate of the WOT for surface winding (4.11) is compared with the final value of WOT extracted from MD membrane stress data. Note at

lower nip loads the WOT behavior becomes similar to that given by expression (2.30). Again the results that show the WOT is affected by web line tension (T_w) are not consistent with expression (2.30) which does not account for stick behavior. Through expression (4.11) it is apparent that the WOT is influenced by web line tension (T_w) but by affecting Q_{bottom}.

Expressions (4.10) and (4.11) are approximations for the final value of the WOT. The expressions through equilibrium should exactly predict the web line tension at the exit of the contact zone. While simplistic in form expressions (4.10) and (4.11) both rely upon knowledge of Q_{bottom}. To determine Q_{bottom} requires the contact mechanics analyses which in this case were performed using Abaqus/Explicit. The explicit analyses also determine if there will be additional slippage between the outer layer and the layer beneath after the exit of the nip contact zone which will affect the final value of the WOT.

4.5 Complete Characterization of Web Material Properties

It has been well documented that some orthotropic web properties are constant for many webs, the MD and CMD modulus for example. Other properties are not well documented. Some properties are well known to be state dependent. This section describes the complete characterization of web material properties.

4.5.1 Characterization of High Modulus Polyester Web

The purpose of this section is to fully document the properties of the 254 μm (0.01 in.) polyester web. These properties will be used in explicit simulations and then compared to

test data in a following section. Seven material constants will be needed to fully define an orthotropic web material undergoing plane strain analysis.

The in-plane moduli for the polyester web were measured using procedures consistent with ASTM D882-12 [17]. The machine direction (E_1) and cross-machine direction (E_3) modulus of the film were measured at 4895 MPa and 5102 MPa, respectively. To determine the modulus in the z or radial direction (E_2) compression tests were conducted on a 2.54 cm (1 in.) high stack of web coupons that were cut into 15.2×15.2 cm (6×6 in.) squares. The experimental pressure-strain behavior along with Pfeiffer curve fit (2.19) is shown in Figure 28. A least squared error routine was used to provide the best possible fit of Pfeiffer's expression (2.19) to the test data. The least error resulted when K_1 and K_2 were 3.45 KPa and 120, respectively. Note K_2 is dimensionless. With K_1 and K_2 determined the z direction modulus could be formed (2.20):

$$E_2 = 120\left(P + 0.00345\right)\ \text{MPa} \tag{4.12}$$

where P is the contact pressure in units of MPa.

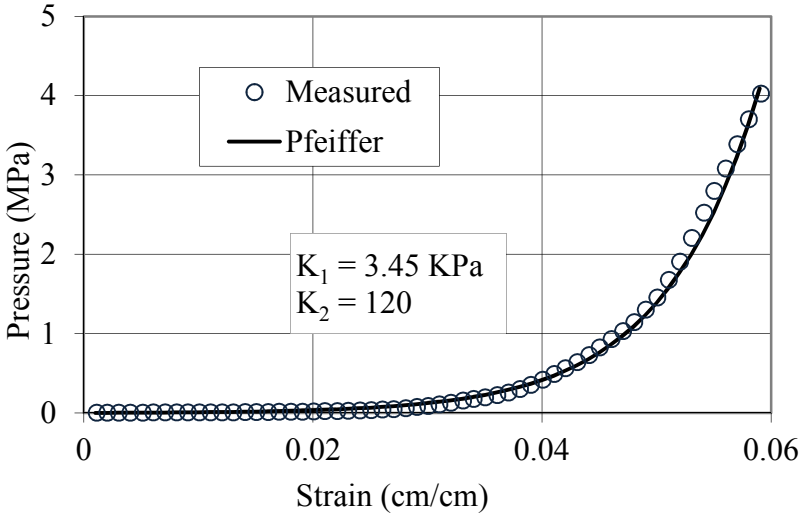

Figure 4-18 E_2 stack compression test

A value of the in-plane Poisson ration ν_{13} was taken at 0.36, consistent with tests conducted using ASTM D638-10 [35, 36]. The Poisson ratios ν_{12} and ν_{32} were not evident in the literature and a test was devised to determine the values. A web was subjected to a tensile strain in the machine direction (ε_1) in a material testing system as shown in Figure 4.19.

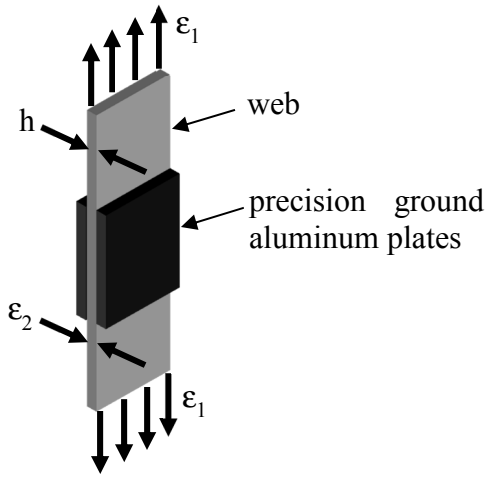

Figure 4-19 Test setup for measurement of Poisson's ratio

The strain was measured in the z or 2 direction by measuring the change in capacitance between the two precision ground aluminum plates shown. The plates were held in contact with the web with light clamping pressure. For a parallel plate capacitor the capacitance is:

$$C = \frac{\varepsilon_o k A}{h} \qquad (4.13)$$

where ε_o is the permittivity of space ($8.854*10^{-12}$ F/m), k is the dielectric of polyester (taken as 3 [37] for polyester), A is the area of the aluminum plates and h is the separation of the plates and is also the deformed web thickness. Expression (4.13) can be

rearranged to infer the web thickness (h) which will decrease as the strain in the machine direction strain increases. The strain in the z or 2 direction can then be inferred from the measured changes in capacitance:

$$\varepsilon_2 = \frac{h_1 - h_0}{h_0} = \frac{C_1 - C_0}{C_0} \quad (4.14)$$

where h_0 and h_1 are the unstrained web thickness and the deformed web thickness at an MD strain (ε_1) level. C_0 and C_1 are the capacitances measured when the web was unstrained and then strained in the MD at level ε_1, respectively.

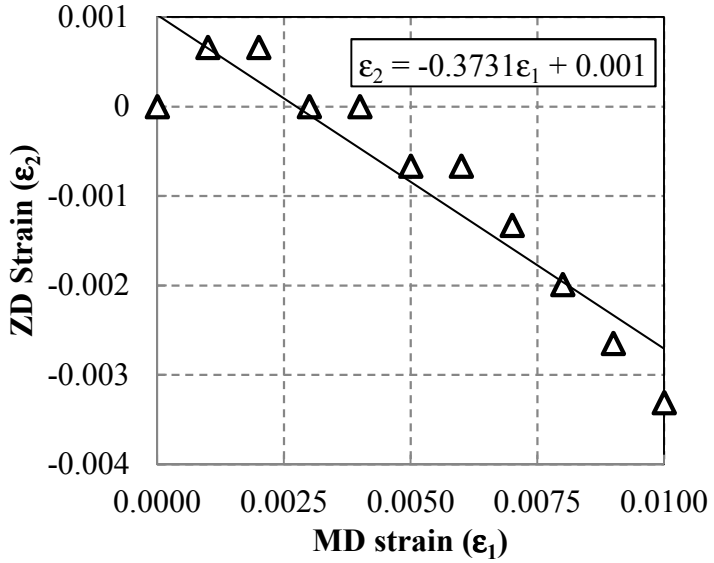

Figure 4-20 Strain data used to discern ν_{12}

The results of such a test are shown in Figure 4.20. The slope is reasonably constant considering the friction that is involved in the test. For a web subject to uniaxial stress in the MD, ν_{12} can be determined from the slope:

$$\nu_{12} = -\frac{\varepsilon_2}{\varepsilon_1} = 0.37 \quad (4.15)$$

This is essentially equal to the in-plane value (ν_{13}) of 0.36 taken from the literature.

We have seen that the radial behavior of the web is nonlinear. However, we preferred to use the linear orthotropic elastic model as a framework and relaxed some constants in the linear model to be state dependent. Therefore, the Maxwell relation (4.2) from linear orthotropic model is assumed to hold still. So the minor Passion's ratio ν_{21} can be inferred by E_1, E_2, and ν_{12} according to (4.2). Since E_2 is state dependent, ν_{21} is also state dependent. ν_{32} was also taken as 0.37 due to the similar MD and CMD properties of web. The minor Poisson's ratio ν_{23} is also inferred by (4.2).

The shear modulus G_{12} was also needed. The shear modulus of thick board grades of paper were studied by Stenberg [38]. The apparatus used measured a value of the shear modulus for a single board sheet. With the radial modulus E_2 known to be dependent on pressure (4.12) was it possible that the shear modulus was as well? To explore such behavior required the ability to set and control the pressure at varied levels in a stack of web coupons while investigating the shear modulus. A study ensued in which a stack of web was subjected to set levels of pressure by a material testing system. An electromagnetic shaker harmonically oscillated a steel platen which subjected the web stacks in compression to an oscillatory shear as shown in Figure 4.21. The frequency of oscillation input to the shaker was varied slowly until an accelerometer (shown) on the opposite side of the platen produced peak output. When this peak was found it was known that the system composed of the web stacks and the steel platen were oscillating at the first natural frequency in shear. This natural frequency is related to the shear modulus. Thus measurement of the natural frequency allowed the inference of the shear modulus.

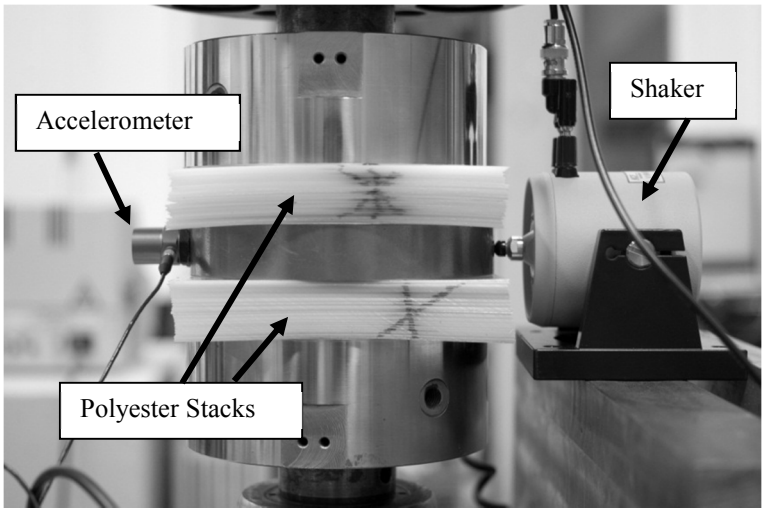

Figure 4-21 Test setup for investigation of G_{12} as a function of stack pressure

This setup can be modeled as a single degree of freedom dynamic system:

$$G_{12} = \frac{2\pi^2 f_n^2 H}{A}\left(M + \frac{2}{3}m\right) \quad (4.16)$$

where f_n is the natural frequency (hz), H is the height of each web stack and A is the area of the stack, M is the mass of the platen and m is the mass of each of the web stacks, which are assumed identical. Results for the polyester web are shown in Figure 4.22.

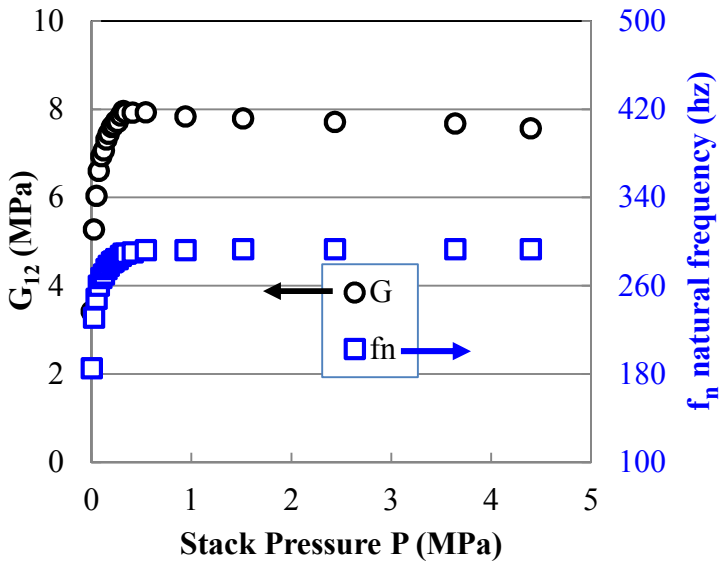

Figure 4-22 Shear modulus G_{12} inferred from natural frequency

Thus the shear modulus is shown to be highly dependent on stack pressure when stack pressure is low but becomes nearly constant at high stack pressure. Although not required for plane strain analyses the shear modulus G_{32} was also determined using this method. For the polyester web G_{12} and G_{32} were essentially equivalent, whether this is true for other webs is currently unknown.

All of the material parameters required for the plane strain analysis of a polyester web have been determined and are shown in Table 4.3. The moduli of elasticity, the shear modulus and the contact pressure P all have units of MPa. Any properties that are state dependent on pressure require the pressure to be input in units of MPa.

Table 4-3 Characterization of a 254 μm PET web (P in MPa)

E_1 (MPa)	E_2 (MPa)	E_3 (MPa)
4895	120(P+0.00345)	5102
ν_{13}	ν_{12}	ν_{32}

0.36	0.37	0.37
ν_{31}	ν_{21}	ν_{23}
0.38	$9.07*10^{-3}$(P+.00345)	$8.7*10^{-3}$(P+.00345)
	G_{12},P<0.23 (MPa)	G_{12},P>0.23 (MPa)
	15.54P+4.81	7.8

4.5.2 Characterization of Low Modulus SMS Nonwoven Web

Chapter 4.3 and 4.4 show that high modulus and low modulus web exhibit different behavior on the nip roller and in the nip contact zone. We also would like to study if the Abaqus model would work for real low modulus webs. Nonwovens comprise a large group of low modulus webs; therefore, we choose to use a nonwoven web for our study. This specific kind of nonwoven is called SMS nonwoven, kindly sponsored by Kimberly-Clark. It consists of two layers of spunbond fabric with one layer of meltblown nonwoven. We need to measure the geometry, material properties, and coefficient of friction of nonwoven as it contacts with itself and nip roller surfaces.

A Mitutoyo dial indicator shown in Figure 4-23 was used to measure the thickness of the nonwoven web. We took 20 measurements for a single layer of web and 10 measurements for multiple layers of web. The measurements were taken at different circumferential locations of web that were cut from different radius in a wound roll.

Figure 4-23 A Mitutoyo dial indicator laying on SMS nonwoven

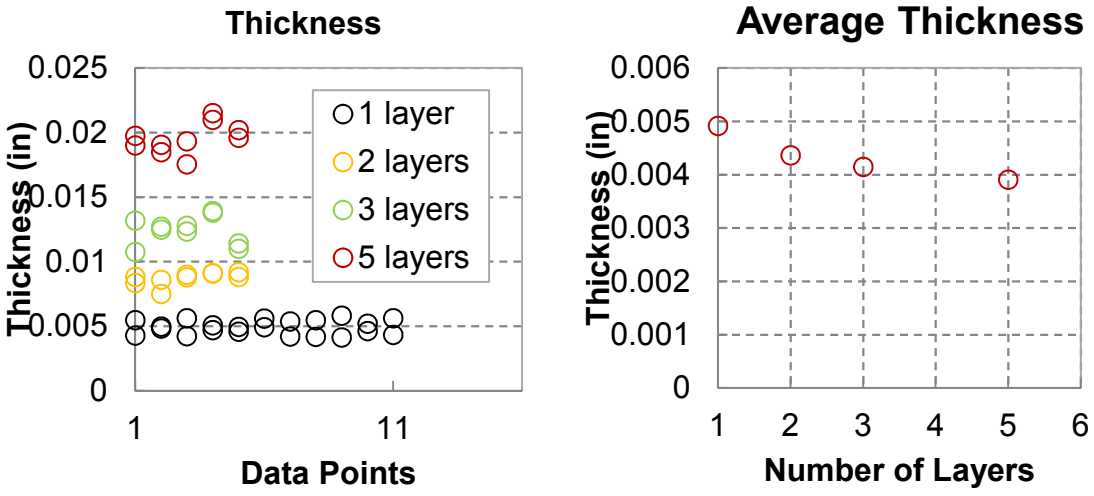

Figure 4-24 (a) Thickness measurement of 1, 2, 3, 5 layers of web, (b) average thickness obtained from different number of layers measurement

Figure 4-24 (a) shows the thickness of single, two, three, and five layers. (b) shows the average thickness obtained from different number of layers measurement. The average thickness tends to decrease from 0.005" to 0.004" as the number of layer in the measurement increases. This is due to the surface compliance and pressure applied by the

tip of the indicator. In the Abaqus model, we will use the average thickness of 20 single layer measurements.

Since MD modulus of nonwovens is much lower than that of PET webs, usually in a magnitude of thousand to ten thousands psi, only few pounds of force is needed in the tensile tests of nonwovens and this force can be more accurately captured by a hand-held force gage than a large capacity load cell on the MTS tensile machine. Therefore, we conducted three hall tests on 600" specimens to measure the MD Young's modulus of nonwoven. The MD Young's modulus is measured to be 10543 psi (Figure 4-25). The same radial modulus test method described for high modulus webs was used for an SMS nonwoven stack. Pfeiffer's constants were fitted to be K_1 equals 0.14 psi, K_2 equals 13.12 (Figure 4-26).

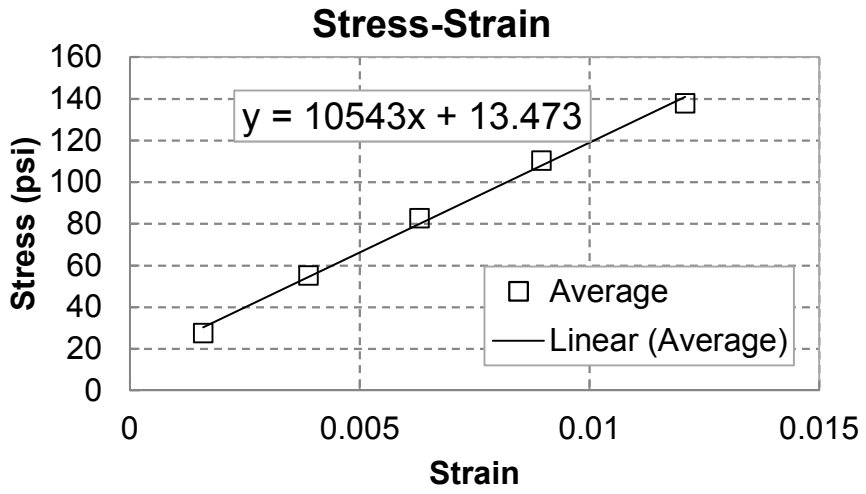

Figure 4-25 MD strain-stress curve of SMS nonwoven

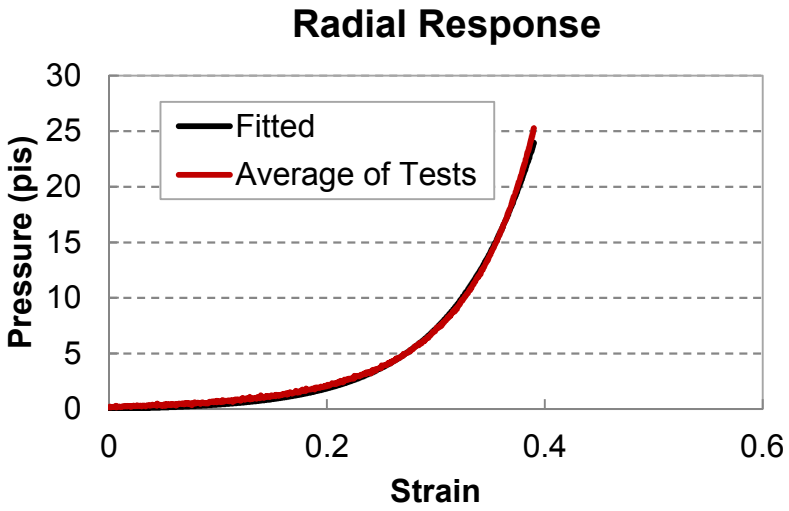

Figure 4-26 Radial response of stack of SMS nonwoven

A similar out-of-plane shear modulus test method that was first used on the PET web was used to measure the shear modulus of the SMS nonwoven. Due to the high compressibility of SMS nonwoven stack, the steel plate used for PET will cause very large deformation by its weight, therefore, the steel plate is replaced by a much lighter plate made of balsa wood, as shown in Figure 4-27. Figure 4-28 (a) and (b) show the measured natural frequency and shear modulus calculated using equation 4.16. The shear modulus of PET was a bilinear form while SMS has an exponential form.

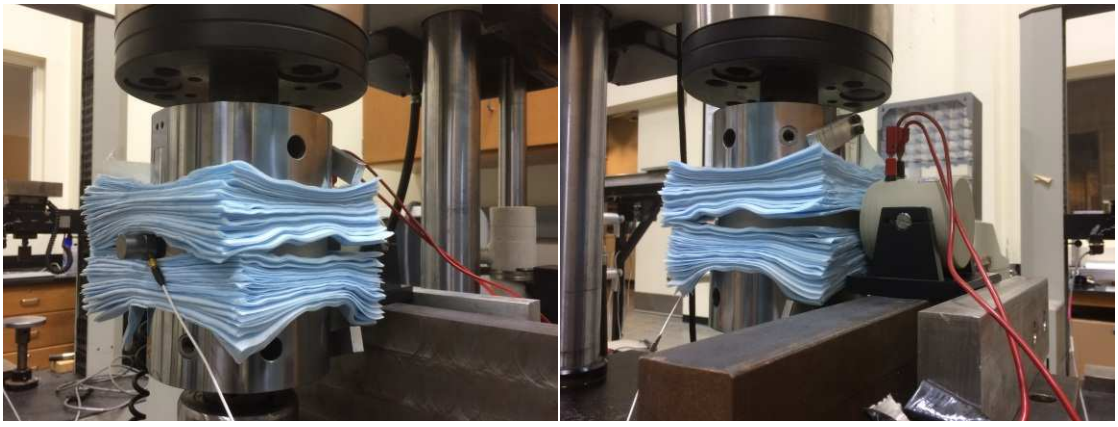

Figure 4-27 Shear modulus test of SMS nonwoven

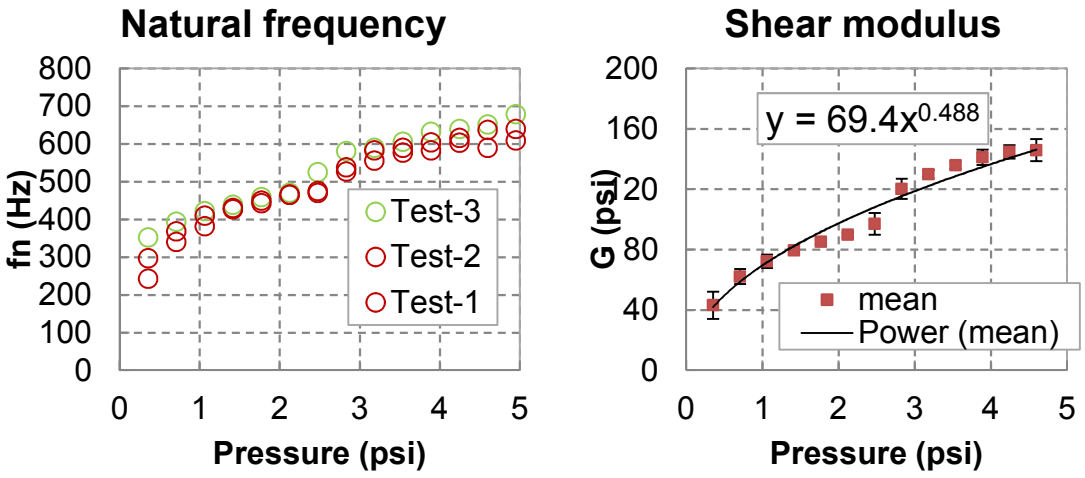

(a) (b)

Figure 4-28 (a) Measured natural frequency of SMS nonwoven, (b) converted shear modulus of SMS nonwoven

The coefficient of friction between the web and another layer of web was measured to be 0.36 shown in Figure 4-29 Test of COF between web The average coefficients of friction between the web and nip roller and core were measured to be 0.45 by the Capstan method.

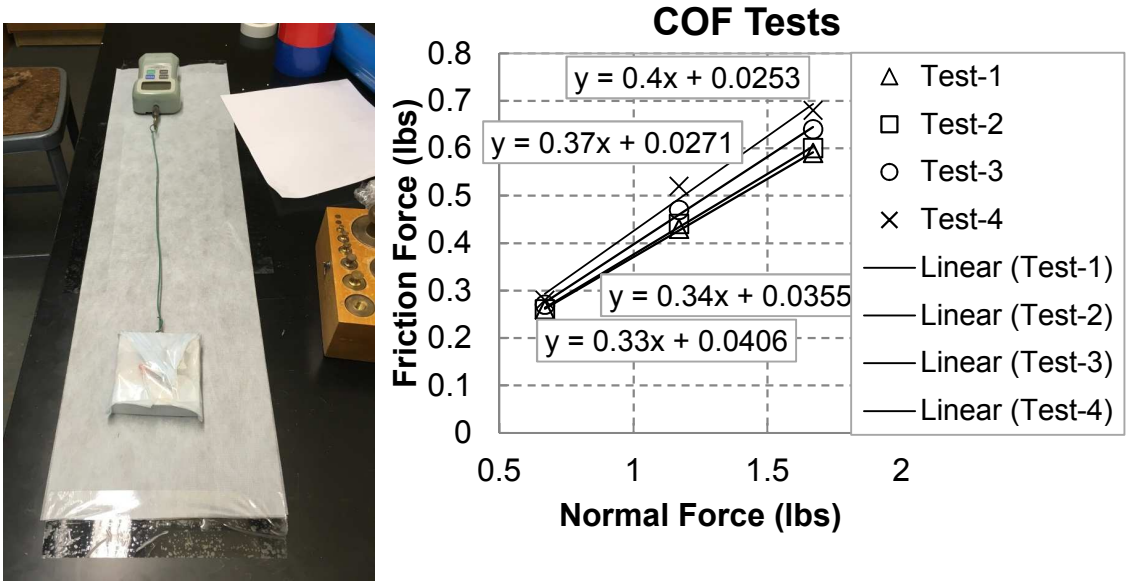

Figure 4-29 Test of COF between web layers

Table 4-4 Characterization of SMS nonwovensummarizes the properties of SMS nonwoven. Those properties will be used in the Abaqus model.

Table 4-4 Characterization of SMS nonwoven (P in psi)

Properties	Tested Values
E_1	10543 psi
E_2	$E_2 = K_2(P + K_1) = K_1K_2e^{K_2\lvert\varepsilon_2\rvert}$ $K_1 = 0.14\,psi,\ K_2 = 13.12$
E_3	10543 psi
υ_{12}	0.37
υ_{13}	0.36
υ_{23}	0.01
G_{12}	$G = 40,$ $G \leq 40\,psi$ $G = 69.4P^{0.50}$ $G > 40\,psi$
t	0.005”
$\mu_{web-web}$	0.36
$\mu_{web-roller}$	0.45

4.6 Validation of Abaqus Model Using High Modulus PET Web

The modeling of winding is identical to that described earlier in Section 4.2 on modeling. What changes is how the material properties are represented in the simulation. In the previous simulation results presented all of the properties were set as constants and input to Abaqus. In explicit analyses the dynamic behavior of a system (the winding roll herein) requires many solutions over small time steps because the solution method is

conditionally stable. After each time step all deformations, strains, stresses, velocities, accelerations, contact pressure and shear stresses, loads and moments required to enforce constraint values are known. Abaqus/Explicit allows material properties such as the properties that are state dependent in Table 4.3 to be updated after each time step in a Fortran subroutine entitled VUMAT. The element stresses at the end of a time step are passed to VUMAT and new unique material properties are created for each finite element in the model prior to the formulation of the next solution in time. The range of pressure within the finite elements is high. In the free web span prior to the nip roller the pressure is essentially zero. After the web contacts the nip roller there is a small contact pressure between the web and nip roller. Upon entry into the nip contact zone with the wound roll the contact pressure on the upper and lower surface of the web becomes very high and is influenced by nip load, nip and wound roll radius and web material properties. The contact pressure then undergoes a rapid decrease as the web exits the nip contact zone. Now the contact pressures are due to winding and are influenced by the WOT. The contact pressure will dynamically increase each time the web passes beneath the nip roller as successive layers are wound onto the core. Thus the range of the state dependent E_2 modulus and the shear modulus G_{12} will be quite high depending on the current element locations and winding conditions.

Winding experiments were conducted on and instrumented winder shown in Figure 4.23. The winder was fitted with additional rollers and load cells which allowed the measurement of σ_{out} as shown in Figure 4.24.

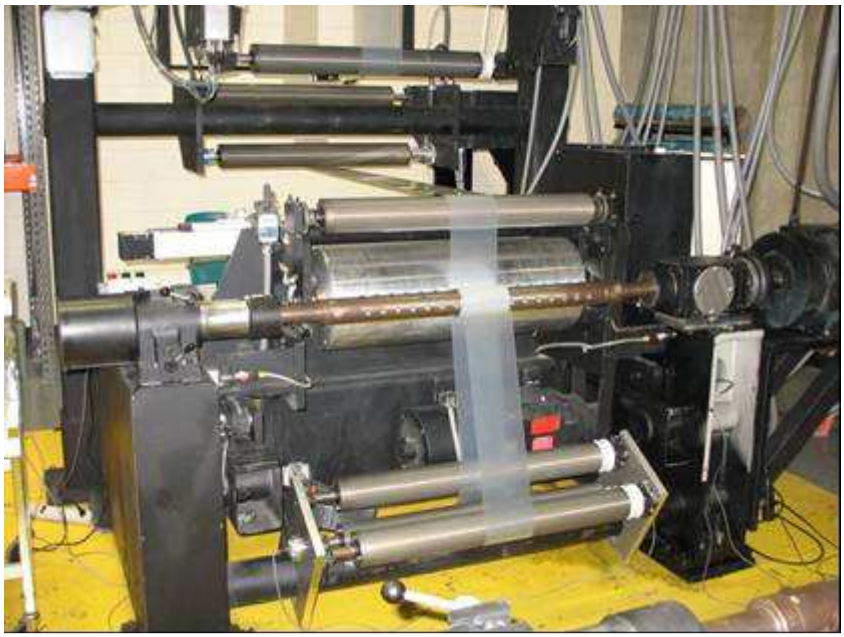

Figure 4-30 Center winding verification tests conducted on 254 μm (0.01 in) Polyester

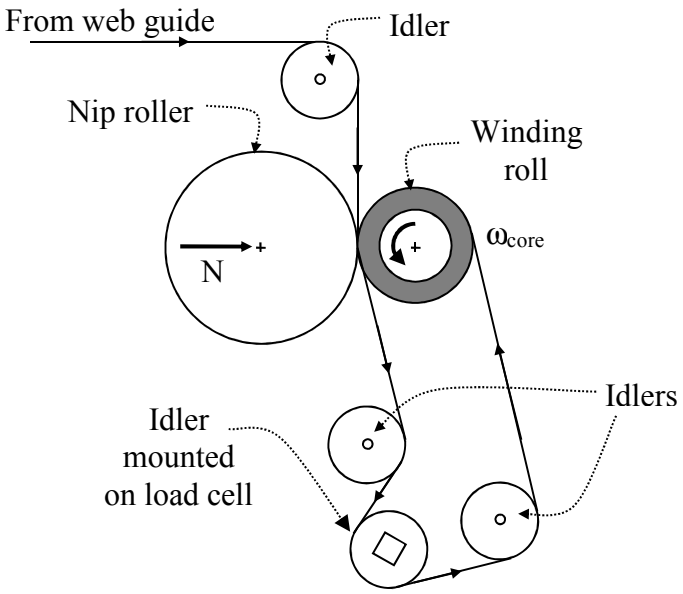

Figure 4-31 Schematic of measurement section of winder

The dimensional data and winder operating parameters are shown in Table 4.4.

Table 4-5 Center Winder Setup Parameters

Property	Value
Web length	140.6 cm
Web thickness	0.0254 cm
Rigid core diameter	8.9 cm
Rigid nip roller diameter	30.5 cm
Angular velocity (ω_{core})	3 rad/sec
Coefficient of friction ($\mu_{N/w}$, $\mu_{w/w}$, $\mu_{C/w}$)	0.18, 0.16, 0.18
Web line tension (T_{in})	5.25 N/cm
Nip load (N)	43.8, 58.4, 87.6, 109, 146, 193 N/cm

The results of the winding tests and the Abaqus simulations are shown in Figure 4.25. The agreement between the simulations, the test data and the center winding algorithm (2.29) is quite good at lower nip loads. At higher nip loads (100-200 N/cm) the simulations and the test data show larger zones of stick forming on the lower surface of the web, similar to that shown in Figure 4.9b which limits the WOT to be less than that given by expression (2.29). There is some discrepancy at the higher nip loads between the test values of WOT and those harvested as discussed earlier from the Abaqus simulations. This discrepancy can be partially resolved by considering that the outer layer had to be pulled away from the surface of the winding roll to make the WOT test measurement as shown in Figure 4.24. The Abaqus simulations modeled the case of a production winder where the outer layer remains in contact with the winding roll. Thus the friction conditions between the outer lap and the layer beneath are very different for the simulations than existed in the tests.

The simulations show that the slippage between the outer lap and the layer beneath are important in determining the final value of the WOT. In Figure 4.3 a spike in MD membrane stress was shown at 27 cm. This spike was the result of slippage that was occurring beneath the outer lap just prior to the outer layer becoming the second layer.

The nip roller was inducing slippage beneath the outer layer and the layer beneath in the nip contact zone. This occurred in the simulations which the web properties were allowed to be state dependent as well. In Figure 4.26 the tension in the outer lap is shown for the case in which the nip load was 193 N/cm. The tension rises rapidly at the left of the chart where the web passed through the nip contact zone the first time. Note the rise in MD web line tension at approximately 80 cm just prior to the outer lap entering the nip contact zone again.

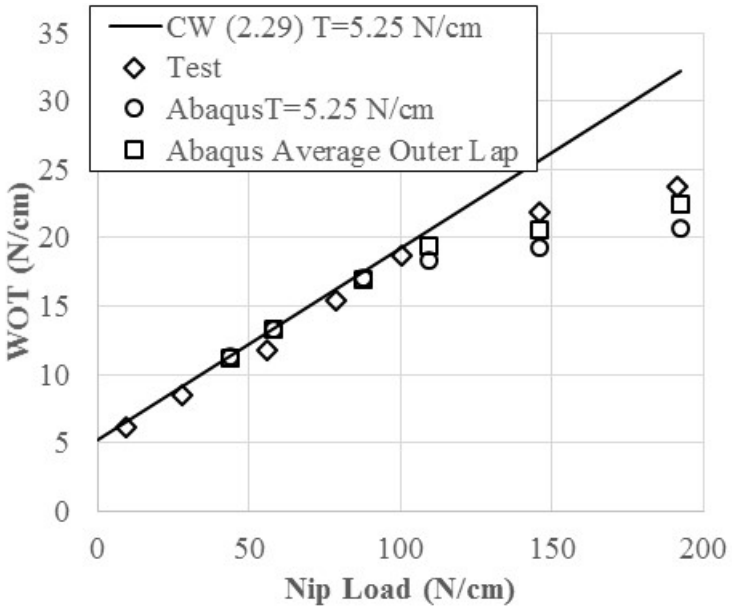

Figure 4-32 WOT for Center Winding 254 μm Polyester

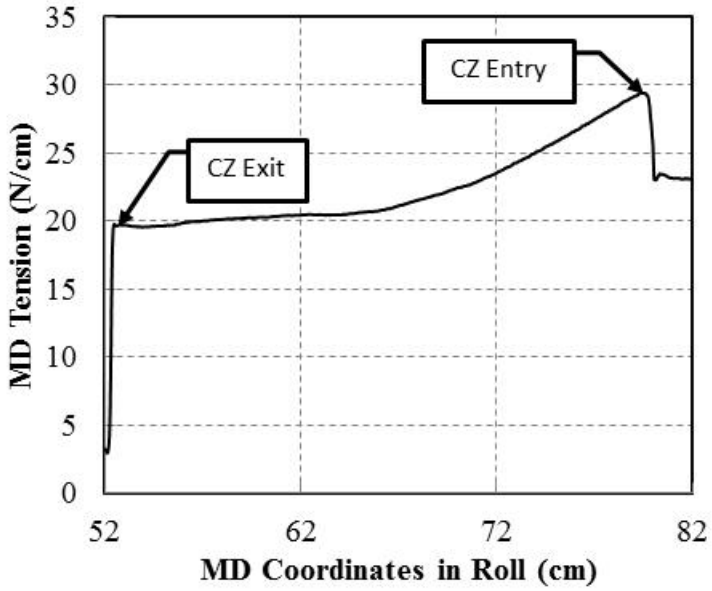

Figure 4-33 Determining the Final Value of the WOT, N=193 N/cm

This is due to slippage which is shown in Figure 4.27. The contact shear stresses cannot exceed the Coulomb friction limits without slippage resulting. Note that the contact shear stresses become equal to the friction limit prior to the outer layer entering the nip contact zone the second time at an MD coordinate of 80 cm. It was concluded that it was more appropriate to use the average of the MD tension in the outer lap between the exit and the entry of the contact zone that was shown in Figure 4.26. This average was calculated for all nip load cases in the simulations and the results are shown in Figure 4.25. These averages compare better with the test values of WOT at the higher nip load levels.

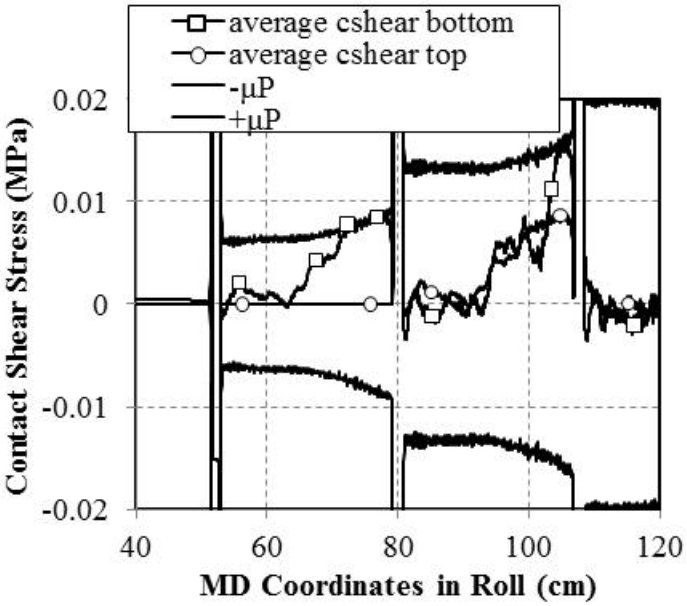

Figure 4-34 Slippage of the Outer Laps, N=193 N/cm

4.7 Validation of Abaqus Model Using Low Modulus SMS Nonwoven

Nonwovens are wound commonly on surface winders. As a result we focused the research on surface winding tests and Abaqus simulations. We conducted a 2x2 matrix of surface winding tests (Table 4-6) with two unique web line tensions and nip loads, respectively. Initially, we were concerned that wound roll size would affect the WOT due to the high radial compliance of the web material. It is not economical in terms of solution time for an Abaqus winding model to wind many layers. So we decided to surface wind a 10-lap roll under the four winding conditions and measure the core pressure using pull tab method. The tests were conducted on the High Speed Low Tension (HSLT) web line of the web handling research center, shown in Figure 4-35 (a). The core had an outer radius of 3.5” and nip roller had a radius of 8.5”. The web has wrap

of 180 degree on the nip roller, shown in Figure 4-35 (b). Meanwhile, we conducted 10-lap Abaqus surface winding simulations for the same four winding conditions.

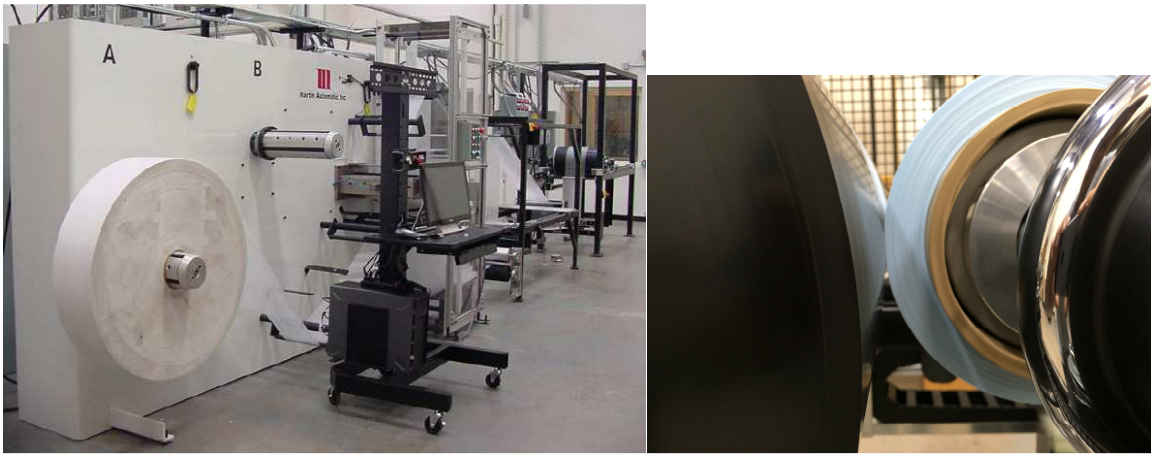

(a) (b)

Figure 4-35 (a) HSLT web line (b) Nip roller and core of the rewinding part

Table 4-6 Surface winding conditions for the SMS nonwoven

$T_w = 2\ lbs = 0.27\ pli$ $N = 30\ lbs = 4\ pli$	$T_w = 4\ lbs = 0.53\ pli$ $N = 30\ lbs = 4\ pli$
$T_w = 2\ lbs = 0.27\ pli$ $N = 60\ lbs = 8\ pli$	$T_w = 4\ lbs = 0.53\ pli$ $N = 60\ lbs = 8\ pli$

Figure 4-36 shows the MD membrane stress results from the Abaqus surface winding simulation for the T=0.53 pli (108 psi) and N=4 pli case. We can see the MD stress starts with the web line tension stress level of 108 psi and jumps to 140 psi (0.7 pli) after the nip contact zone, and then stays almost constant in the outmost lap of the roll. Therefore the WOT in this case is 140 psi. Figure 4-37 shows the radial pressure of developed in the roll in the MD coordinates. The radial pressure spikes in the nip contact zone in each lap of the roll. The core pressure value can be obtained by taking the average of radial pressure in the innermost lap, 1.70 psi in this case.

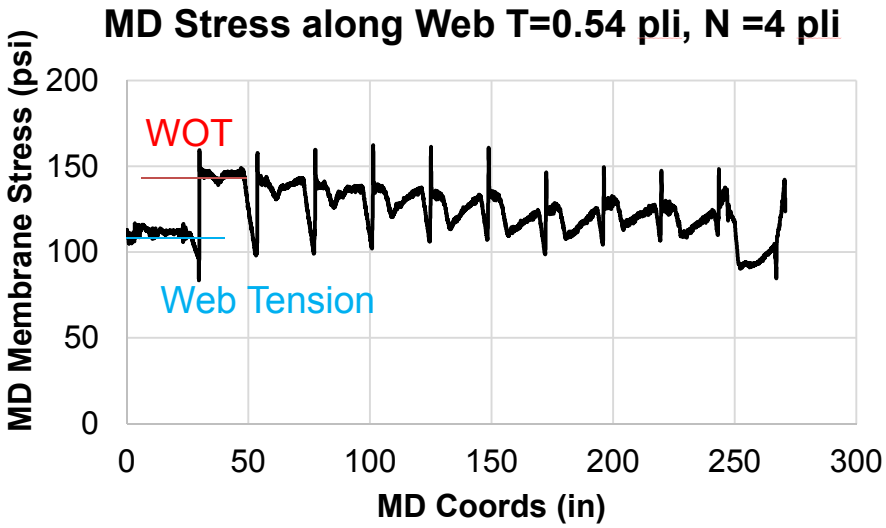

Figure 4-36 MD membrane stress of Abaqus simulation under T=0.54 pli, N=4 pli

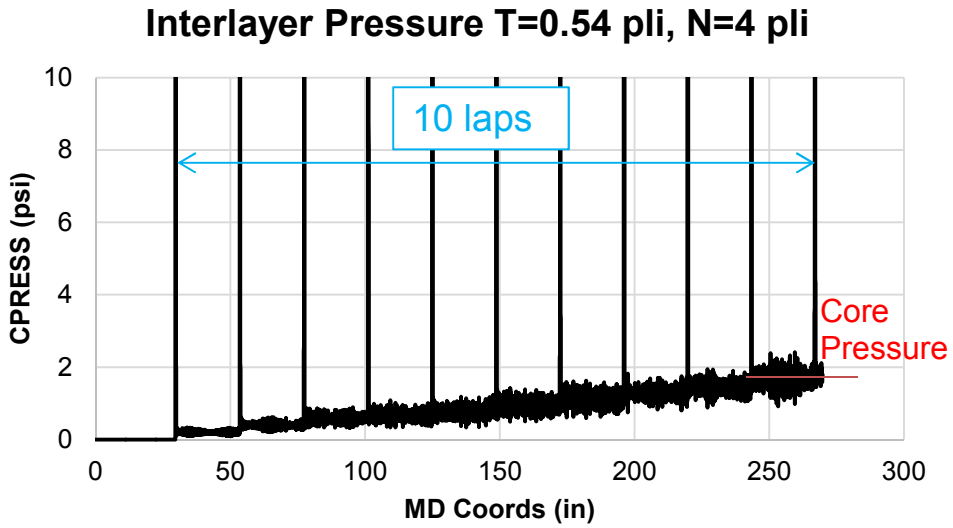

Figure 4-37 Radial pressure of Abaqus simulation under t=0.54 pli, N=4 pli

Table 4-7 WOT and core pressure of Abaqus simulation results

Abaqus Results	$T_w = 0.27\ pli$	$T_w = 0.54\ pli$
$N = 4\ pli$	WOT=0.44 pli CoreP=1.00 psi	WOT=0.70 pli CoreP=1.70 psi
$N = 8\ pli$	WOT=0.56 pli CoreP=1.40 psi	WOT=0.90 pli CoreP=2.35 psi

Table 4-7 summarizes the WOT and core pressure results from four Abaqus simulations. Figure 4-38 shows the core pressure comparison between the 10-lap surface wound roll tests and Abaqus. We can see the core pressure predicted by Abaqus agrees well with the test results. Based on the measured core pressure, we can use the winding model reviewed in Chapter 2 to infer the WOT with the measured material properties of the web. We used MAXIWINDER 3.0 to iterate the winding tension until the model calculates a core pressure equal to the measured value. We can then compare those WOT inferred from test values of the core pressure and a winding model with Abaqus results. Figure 4-39 shows the comparison of WOT between the 10-lap surface wound roll tests and Abaqus results. We can see the Abaqus model predicted the WOT values that agree very well with test values.

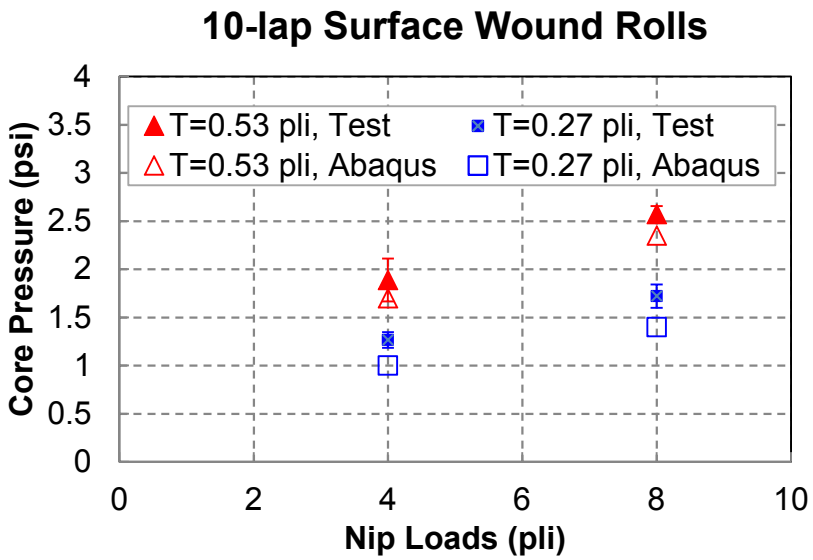

Figure 4-38 Core pressure comparison between 10-lap SW roll test and Abaqus

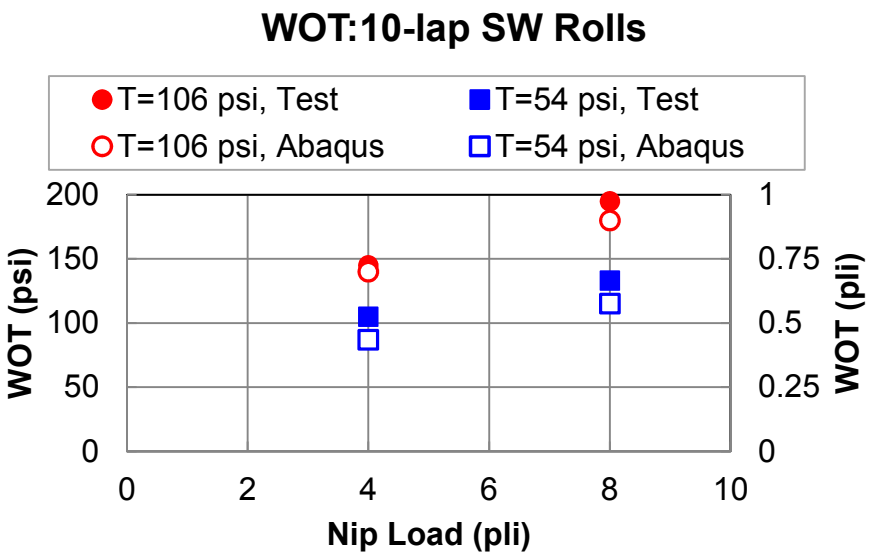

Figure 4-39 WOT comparison between 10-lap SW roll test and Abaqus

4.8 Summary

The nip center and surface winding simulations have shown that the explicit finite element modeling method is a powerful tool for studying the contact mechanics of winding.

The simulations revealed the mechanism of the formation of WOT for center winder with nip and surface winder. A nip roller could cause the outmost web lap in the nip contact zone to slip or stick on the winding roll, which induces the change of tension from the web line tension. The slip/stick behavior in the contact surface between outmost web layer and the layer beneath is critical to quantitatively determine the WOT. The behavior of web in the wrap of the nip roller in a winder was also revealed by the simulations. High modulus web tends to fully slip on the nip roller, of which the behavior was found

to be governed by the Capstan equation. Low modulus web tends to stick with the nip roller in a larger part of the wrap and only slip in some area. The slip/stick behavior was found to be relevant with the MD strain of web subject to web line tension.

The simulations have shown how to connect the experience bases from winding all web types on both nip center and surface winders using one theory. When wound low in-plane modulus webs the contact surface between the bottom surface of outermost web layer and the top surface of the layer beneath was found to be dominated by stick even at lower nip loads, therefore, the impact of nip loads on the WOT is not large. We also found that web line tension affects the WOT whether a surface or a center winder is used and that nip load may have small impact. The simulations exhibited this behavior in Figure 4.15 and Figure 4-39. Results in Figure 4-39 show that almost all web line tension becomes part of the WOT. When wound high in-plane modulus webs we found that very little web line tension enters WOT if rolls are surface wound but that when center winding with nip, much of the web line tension will become WOT. We also found that nip load directly affects WOT at low nip loads but less so at high nip loads. These behaviors were exhibited by the simulations in Figure 4.11. All of these behaviors are controlled by the slippage in the nip contact zone. This slippage is limited by friction but driven by the contact shear stresses that develop in the web as it travels through the nip. These contact shear stresses will be affected by nip and wound roll diameter, web line tension and nip load and web material properties. Young's modulus and the shear modulus of elasticity material properties have a large influence on WOT.

Depending on the slippage induced by the nip roller the final value of the WOT may or may not occur in the outer lap of the winding roll. Pfeiffer deduced this in his early tests

[27]. The simulations have shown that nip induced slippage for layers beneath the outer layer can be important too.

We conducted winding tests with both high modulus PET web and low modulus SMS nonwoven and validated the finite element model. The explicit finite element model was proven to be able to predict the WOT for different kinds of web material under nip center and surface winding conditions.

Chapter 5. Hybrid Winders

A hybrid winder was shown in Figure 1.1(d). This winder has torque provided to both the core and the nip roller making it a more expensive winder. These winders are often used to wind webs with low friction coefficients that can clockspring or telescope easily if they are center or surface wound. This work as resulted in a unique set of relations that explain how the WOT develops in all nipped winders.

5.1 Governing Equations of Winder: Winder Equilibrium

When a winder is running in steady state, both internal and external equilibrium must be satisfied. In Figure 5.1 equilibrium of the nip roller, the web wrapping the nip roller, the web in the nip contact zone and the wound roll of web after the web exits the nip contact zone are all established. The external equilibrium of the winder is also established. Two equilibrium expressions are generated for T_{out}, the tension in the web as it exits the nip contact zone. These expressions are then used to compare the effects of winder type on T_{out}. As previously discussed T_{out} is not the WOT but may be close depending on how much slippage is occurring beneath the outer layer. Note in Figure 5.2 that T_{out} and hence the WOT are all a function of Q_1, which is the Q_{bottom} in equations 4.10 and 4.11. If slippage dominates the lower surface of the web in the contact zone then Tout for the center and surface winder become expressions (2.29) and (2.30). Unfortunately knowledge of whether the lower surface of the web in the contact zone is in a state of

complete slip comes only from the contact mechanics analysis that is being performed with Abaqus. Thus although these expressions for T_{out} appear simple, they have entries like Q_1 that are hard to determine. Also it should not be assumed the Q1 is an independent variable, it will be affected by M_1 and M_2.

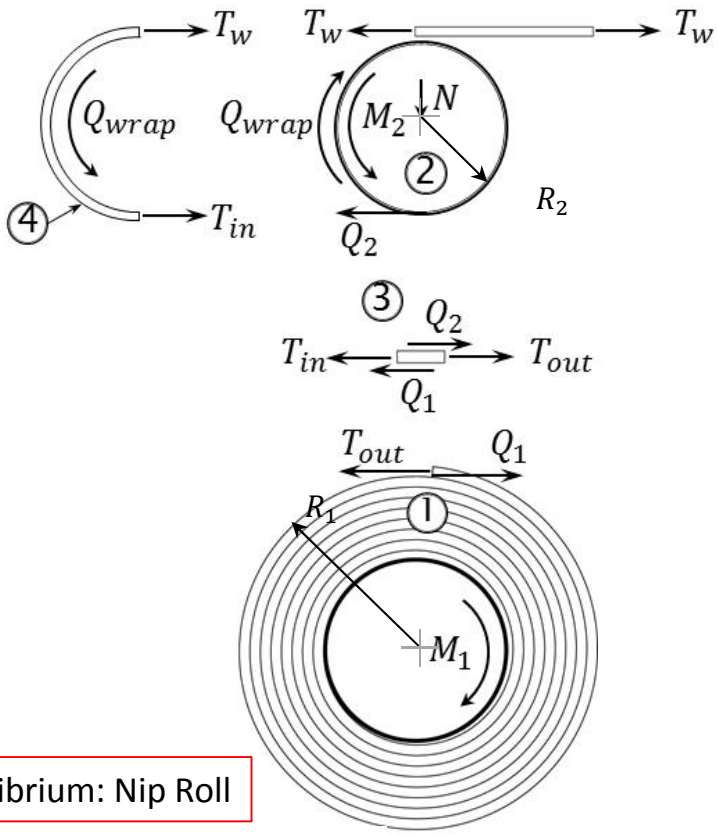

Equilibrium: Nip Roll

$$M_2 = (Q_2 + Q_{wrap})R_2 \ ②$$

Equilibrium: Web wrapping Nip Roll

$$T_w = T_{in} + Q_{wrap} \ ④$$

Equilibrium: Web in Nip Contact Zone

$$T_{out} + Q_2 = T_{in} + Q_1 \ ③$$

Equilibrium: Winding Roll

$$M_1 = (T_{out} - Q_1)R_1 \ ①$$

Equilibrium of the system

①②④ → ③

$$\frac{M_1}{R_1} + \frac{M_2}{R_2} = T_w$$

$$T_{out} = \frac{M_1}{R_1} + Q_1$$

$$T_{out} = T_w - \frac{M_2}{R_2} + Q_1$$

Figure 5-1 Winder equilibrium

Hybrid winding $M_1,\ M_2 \neq 0$	Center winding with nip roller $M_1 \neq 0,\ M_2 = 0$	Surface winding $M_1 = 0,\ M_2 \neq 0$
$\frac{M_1}{R_1} + \frac{M_2}{R_2} = T_w$	$\frac{M_1}{R_1} = T_w$	$\frac{M_2}{R_2} = T_w$
$T_{out} = \frac{M_1}{R_1} + Q_1$	$T_{out} = T_w + Q_1$	$T_{out} = Q_1$
$T_{out} = T_w - \frac{M_2}{R_2} + Q_1$	$T_{out} = T_w + Q_1$	$T_{out} = Q_1$
When nip load is low, slippage may dominate the bottom contact surface, $Q_1 = \mu N$		
$T_{out} = \frac{M_1}{R_1} + \mu N$	$T_{out} = T_w + \mu N$	$T_{out} = \mu N$

Figure 5-2 Effect of winder type on T_{out}

5.2 The WOT of Hybrid Winders

Hybrid winding is also called surface winding with center assist torque. Although theoretically we can apply arbitrary combination of torques on the nip roller and core, some of them will violate the winder equilibrium and are not valid winding conditions to wind material successfully. In application the center assist torque that is applied on the core is often referred to some percentage of the torque that used in the center winding with nip on the same winder with the same winding tension.

From the previous derivation for a hybrid winder T_{out} is determined by equation (5.1), where M_1 and R_1 is the assist torque on the core and the radius of the core respectively.

$$T_{out} = \frac{M_1}{R_1} + Q_1 \tag{5.1}$$

If the web is wound in the condition of center winding with nip, from previous derivation the equilibrium of winder requires (5.2):

$$\frac{M_1}{R_1} = T_w \tag{5.2}$$

Therefore, $M_1 = T_w R_1$ is the torque in the condition of center winding with nip. A hybrid winding with 50% assist torque applies a torque of value $50\% \cdot T_w R_1$ on the core. A hybrid winding with 100% assist torque applies a torque of value $T_w R_1$ on the core. If we substitute the torque values in two cases into (5.1), we will have the expression of T_{out} for hybrid winding with 50% assist torque as (5.3) and with 100% assist torque as (5.4) respectively.

$$T_{out} = \frac{1}{2} T_w + Q_1 \tag{5.3}$$

$$T_{out} = T_w + Q_1 \tag{5.4}$$

Under the low nip loads where the slippage dominates the bottom nip contact zone, (5.3) and (5.4) can be furthered simplified into (5.5) and (5.6).

$$T_{out} = \frac{1}{2} T_w + \mu N \tag{5.5}$$

$$T_{out} = T_w + \mu N \tag{5.6}$$

Noted, the expressions of T_{out} (5.4) and (5.6) in the hybrid winding with 100% assist torque condition is essentially the same as those in the condition of center winding with nip. And by the equilibrium of the winder, in such winding conditions, very little torque is required on the nip roller to maintain the surface velocity of the nip roller.

To study the WOT developed in hybrid winding, Jiang [30] and I conducted center winding tests with nip, surface winding, hybrid winding with 50% assist torque, and

hybrid winding with 100% assist torque on the high modulus PET web used in Chapter 4. The tests were conducted on the high speed web line with an 8” instrumented core and 12” nip roller. In the tests, we applied 3 pli web line tension on the 0.01” thick, 6” wide PET web in center winding with nip and surface winding. In hybrid winding tests, we wound 1.5” pile height rolls. In 100% assist toque cases, an assist torque of 72 lb·in was applied on the core at the beginning of tests and linearly increased to 99 lb·in at the end when the roll achieved 1.5” pile height. In 50% assist torque cases, an assist torque of 36 lb·in were applied on the core at the beginning and linearly increased to 49.5 lb·in at the end. The instrumented core measured the core pressure after the roll was wound. MAXIWINDER was used to infer the WOT. Abaqus models are essentially similar with the model used in Chapter 4.6. The only difference is in the hybrid winding conditions, an assist torque of 12 lb·in and 6 lb·in were applied on the core for 100% assist and 50% assist cases. The torque values are obtained by dividing the test torque values by the web width since we are using the plane strain element in the Abaqus model and the width of the web is set to 1”. The assist torque was applied as a constant in Abaqus since we only wound 5 layers on the core and the change of assist torque due the growing roll radius is ignorable.

Figure 5-3 shows the WOT of PET web under various winding conditions and the comparison with Abaqus. We can see that at low nip loads, the Good’s empirical solution predicted close WOT results compared to both test and simulation results. At higher nip loads, the test WOT values are lower than empirical solutions due to the sticking behavior in the bottom nip contact zone. Abaqus simulation agrees well with the test results under

high nip loads. The WOT results of hybrid winding with 100% assist torque are essentially the same as those of the center winding with nip condition.

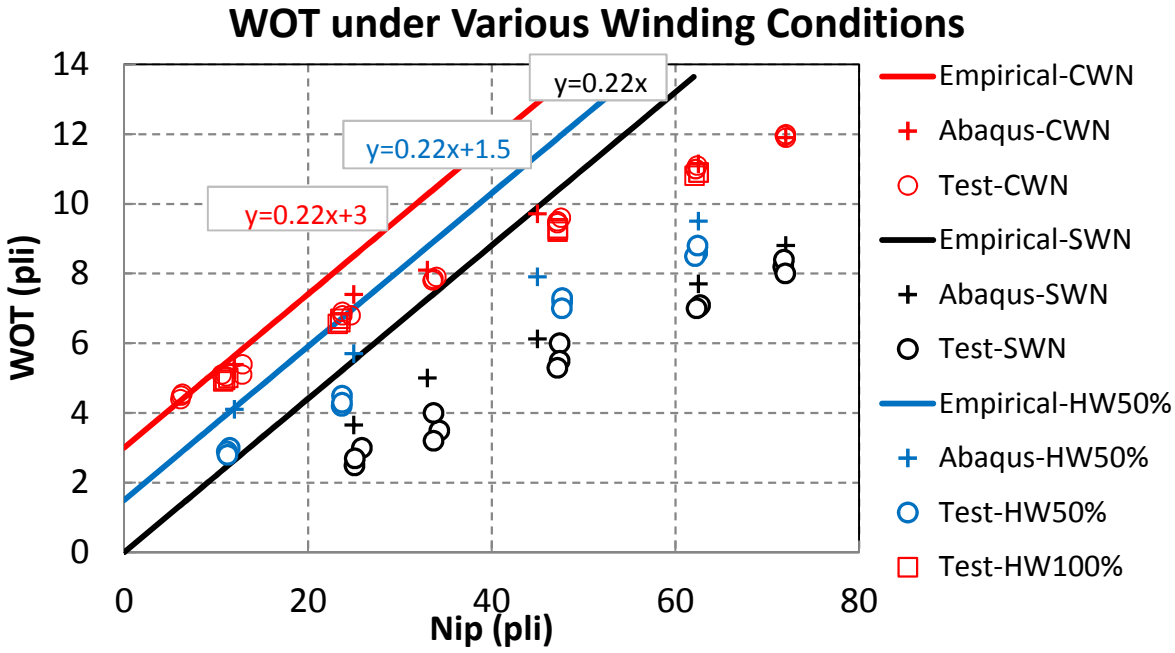

Figure 5-3 WOT under various winding conditions

5.3 Summary

By considering the equilibrium of the parts involved in the winder, we derived the governing equations of the winding problems under various winding conditions: center winding with nip, surface winding, and hybrid winding. The equations contain a contact shear force term Q_1, which is the contact shear force at the contact surface between outmost web layer and the layer beneath in the nip contact zone. This term can be approximated by Coulomb's friction under lower nip loads, where slippage dominates the contact surface. In those cases, the governing equations have the same form with Good's empirical solutions (2.29 and 2.30) and analytical solutions can be obtained. Under higher nip loads, a numerical model is required to predict the stick/slip behavior and

calculate the contact shear force. We develop the explicit finite element model in Abaqus for this purpose. We conducted various winding tests on the PET web and studied the WOT under center winding with nip, surface winding, and different hybrid winding conditions. The Abaqus model was validated by the winding tests. Both winding tests and simulations show that the assist torque applied to the core in a hybrid winding helps the winding of the web material onto the roll by increasing the WOT. A 50% assist hybrid winding may add 50% web line tension of a corresponded center winding to the WOT. A 100% assist torque hybrid winding is essentially equivalent with the corresponded center winding with nip in terms of WOT.

Chapter 6. Parametric Modeling of Wound-on-tension Using Abaqus Python Scripting

Through the previous chapters we have developed an explicit finite element model in Abaqus which is able to predict the wound-on-tension for a specific web under a specific winding condition. Bearing the existence of a great variety of webs and multiple winding conditions in application, we hope to extend the model to a general model which enable analysts to predict WOT for different kinds of web under real winding conditions.

Abaqus provides the Python scripting interface as an application programming interface which allows users to program the building of the model. If we can abstract the problem and extract all parameters related to the WOT in a winding process, we could implement those parameters as input variables in a Python script and it can automatically build the finite element model based on the parameters of the winding problem.

6.1 Problem Abstraction and Parameter Extraction

All parameters involved in a winding problem can be categorized into geometry, material, contact, loadings, and finite element control. Geometrical parameters describe the geometry of web and winder, for instance the thickness of web and radius of core and nip roller properties. Material parameters describe the material properties of web and nip cover. As discussed in Chapter 4, the orthotropic elastic constitutive model is chosen as the framework of the web. Among those material parameters radial and out-of-plane shear modulus are state dependent on the radial strain or pressure, which are implemented in a VUMAT subroutine. Contact parameters contain three coefficients of friction

between different parts in contact interactions during winding. The COF between web layers is an important parameter for WOT. Loadings parameters set up the winding conditions. Finite element control parameters include the length-width ratio of element, the number of elements used to discretize the web thickness etc. Those categories of parameters are listed in Table 6-1, Table 6-2, Table 6-3, Table 6-4, and Table 6-5.

Table 6-1 Geometric parameter of the parametric WOT model

Geometry	
R_{core}	radius of the core, [length]
R_{nip}	radius of the nip roller, [length]
h	thickness of the web, [length]
W_{web}	width of the web, [length]
n_{laps}	number of laps that will be wound on the core, [number]

Table 6-2 Material parameters of the parametric WOT model

Material	
ρ	density of the web, [mass / length^3]
E_1, E_3	Young's modulus in MD and CMD, [force / length^2]
K_1, K_2	constants in Pfeiffer's expression for modulus in ZD, $E_2 = K_1 K_2 e^{K_2 \lvert \varepsilon_2 \rvert}$ K_1 in [force / length^2], K_2 dimensionless
$\upsilon_{12}, \upsilon_{13}, \upsilon_{23}$	Poisson's ratio in MD-ZD, MD-CMD, and ZD-CMD, dimensionless
$G_{12-A}, G_{12-C}, G_{12-M}$	constants in an exponential form of shear modulus in MD-ZD, $G_{12} = G_{12-A} P^{G_{12-C}}$, G_{12-M} is the minimum shear modulus

Table 6-3 Contact parameters of the parametric WOT model

Contact	
$\mu_{web-web}$	coefficient of friction between web and web, dimensionless
$\mu_{web-core}$	coefficient of friction between web and core, dimensionless
$\mu_{web-nip}$	coefficient of friction between web and nip roller, dimensionless

Table 6-4 Loading parameters of the parametric WOT model

Loadings	
T_w	web line tension, in [force]
N	nip force, in [force]
ω	angular velocity applied on core in center winding with nip or nip roller in surface winding, in [rad / s]
winder type	0: center winding with nip 1: surface winding

Table 6-5 FEA control parameters of the parametric WOT model

FEA	
$n_{thickness}$	number of elements used to discretize the thickness of web, [number]
$\alpha_{element}$	ratio of length over height of the element, dimensionless
n_{CPUs}	number of cores of processer to do parallel computing, [number]
$t_{objective}$	objective time increment after using mass scaling, [time]

6.2 Using the Python Script of Parametric Model of WOT

The Python script is a text file with the all the parameters set as variables at the beginning. We only need to input those parameters and run it through Abaqus/CAE from menu: "File – Run Script". Then Abaqus/CAE will automatically generate the finite element model based on the input parameters. An example of the input section of the script which

generates the Abaqus model for the low modulus SMS material is shown in Figure 6-1. The section of the script is in shown in Appendix and a full version of script can be accessed by contacting [31].

```
#   Material
density = 0.00013  # Density of the web, 386 is the coefficient to transform the density in unit of [lb/in^3] to
E1 = 10543.  # MD Young's modulus, important parameter
Pk1 = 0.14  # Pfeiffer's constant 1, important parameter
Pk2 = 13.12  # Pfeiffer's constant 2, important parameter
# If Pk2<>0 then a vumat subroutine implemented Pfeiffer's law will be used for the state dependent radial modulu
E3 = 10543.  # ZD Young's modulus
v12 = 0.36  # Poisson's ratio as loading in MD and deformation in ZD
v13 = 0.3  # Poisson's ratio as loading in MD and deformation in CMD
v23 = 0.01  # Poisson's ratio as loading in ZD and deformation in CMD
G12_A = 69.4 # Constant 1 of shear modulus in MD-ZD plane
G12_C = 0.488 # Constant 2 of shear modulus in MD-ZD plane
G12_M = 40 # The minimum value of shear modulus in MD-ZD plane
#  Shear modulus is an important parameter. SMS nonwoven is found to be a exponential function of radial pressure

#   Contact
cofCoreWeb = 0.45  # Coefficient of friction between web and core
cofNipRollerWeb = 0.47  # Coefficient of friction between web and nip roller
cofWebWeb = 0.36  # Coefficient of friction between web and web, important parameter

#   Loadings
nipLoad = 30  # Nip force as a concentrated force, in the unit of force, important parameter
windingTension = 2 # Web tension in the upstream span, in the unit of force, important parameter
angularVelocity = 2*pi  # [radian/s]
windingType = 1  # 0-center winding; 1-surface winding

#   FEA
numElementThickness = 3.  # Number of elements in the thickness direction, at least 3 to guarantee the results ac
elementLWRatio = 10.  # Length-width ratio of a element
objectiveInc = 0  # Objective time increment after mass scaling, if 0 no mass scaling will be used
```

Figure 6-1 Input section of Python script that generates the SMS surface winding model

6.3 Running Environment and Solution Time

To deal with the material nonlinearity, the Python script will generate a Fortran VUMAT subroutine that accounts for the state dependent material properties of radial modulus and out-of-plane shear modulus. To successfully run the model with the VUMAT subroutine, it is required that a specific version of Intel Fortran compiler needs to be installed and configured for Abaqus to call. A detailed process of installation and configuration can be found in Abaqus documentation. If no Intel Fortran compiler is installed, the model can still be run but only for linear elastic material, losing the ability to account for material

nonlinearity. To do this set the PK2 and G12-C to zero, then values of PK1 and $G_{12\text{-}A}$ will be the constant radial modulus and out-of-plane shear modulus respectively.

Depending on the material properties of web, the size of element, and the number of laps being modeled, the solution time varies. For the results in this thesis, the solution time varies from 4 to 33 hours.

6.4 Summary

We extend the explicit finite element Abaqus/CAE model to a general model that implemented by Python script. The script takes input from geometry, material, contact, loadings, and FEA control parameters and generates a specific explicit finite element model in Abaqus/CAE. The script enable us to conveniently study the WOT of a wide range of web under real winding conditions. We also hope the significant increase of efficiency in modeling provided by the python script can help analysts to focus on the physical problem itself and quickly iterate.

Chapter 7. Summary and Future Work

7.1 Summary

The 2D pure center winding processes were simulated in Abaqus. The purpose is to find the best way to model the winding problems and nonlinearity of the web material and to fill the gap between the spiral and the axisymmetric winding models.

1. Both explicit and implicit numerical schemes were tested. It is found that the implicit method generates smooth results while explicit method generates noisy stress results. The lap average values of radial stress from the explicit and implicit methods are close to each other and match the results of axisymmetric winding model (Winder 6.2 & 6.3) very well.
2. The dynamic effect in explicit method and the gap between web and the circular core affect the accuracy of circumferential stress. The implicit method and use of a spiral core to eliminate the gap helps to revolve the noise and produce accurate circumferential stress.
3. The explicit method with an Archimedean spiral core has the best performance if both computational cost and the result accuracy are taking into account.
4. A VUMAT subroutine which handles the nonlinearity of the radial modulus of the web was successfully developed. The agreement of wound roll stresses between

5. Abaqus with VUMAT results and Winder 6.2 & 6.3 verified the VUMAT subroutine.

We successfully developed the explicit finite element model of center winding with nip roller and surface winding. The mechanism of the development of wound-on-tension was studied.

1. The simulations revealed the mechanism of the formation of WOT for center winder with nip and surface winder. A nip roller could cause the outmost web lap in the nip contact zone to slip or stick on the winding roll, which induces the change of tension from the web line tension. The slip/stick behavior in the contact surface between outmost web layer and the layer beneath is critical to quantitatively determine the WOT.
2. The behavior of web in the wrap of the nip roller in a winder was also revealed by the simulations. High modulus web tends to fully slip on the nip roller, of which the behavior was found to be governed by the Capstan equation. Low modulus web tends to stick with the nip roller in a larger part of the wrap and only slip in some area. The slip/stick behavior was found to be relevant with the MD strain of web subject to web line tension.

The simulations have shown how to connect the experience bases from winding all web types on both nip center and surface winders using one theory.

1. When wound low in-plane modulus webs the contact surface between the bottom surface of outermost web layer and the top surface of the layer beneath was found to be dominated by stick even at lower nip loads, therefore, the impact of nip loads on the WOT is not large. The web line tension affects the WOT for low

modulus web whether a surface or a center winder is used. Test and simulations results show almost all web line tension becomes part of the WOT.

2. When wound high in-plane modulus webs we found that very little web line tension enters WOT if rolls are surface wound but that when center winding with nip, much of the web line tension will become WOT. Nip load is found to directly affects WOT at low nip loads but less so at high nip loads. These behaviors were exhibited. All of these behaviors are controlled by the slippage in the nip contact zone. This slippage is limited by friction but driven by the contact shear stresses that develop in the web as it travels through the nip.
3. These contact shear stresses will be affected by nip and wound roll diameter, web line tension and nip load and web material properties. Young's modulus and the shear modulus of elasticity material properties have a large influence on WOT.

The effect of material properties on the wound-on-tension was studied. New test methods to measure some material properties that were not measured before were developed.

1. Out-of-plane shear modulus was found to be critical to the WOT. We successfully developed a dynamic test method to infer the out-of-plane shear modulus.
2. The Poisson's ratio as web subject to the MD tension and contracts in the thickness direction was measured by constructing a capacitor on the web.

Winder equilibrium dictates the governing equation of WOT for any type of winder. The governing equation involves the contact shear force term Q_1, which is the contact shear force at the contact surface between outmost web layer and the layer beneath in the nip contact zone.

1. In all types of winders, at lower nip loads when the bottom nip contact surface is in full slippage, Q_1 evaluates the coefficient of friction between web layers multiplied by the nip load. The expressions under this condition fall back to Good's empirical equations and analytical solutions can be obtained.
2. Both winding tests and simulations show that the assist torque applied to the core in a hybrid winding helps the winding of the web material onto the roll by increasing the WOT. A 50% assist hybrid winding may add 50% web line tension of a corresponded center winding to the WOT. A 100% assist torque hybrid winding is essentially equivalent with the corresponded center winding with nip in terms of WOT.

The explicit finite element model was extended to a parametric and automatic scripted model by using Abaqus/Python. All parameters involved in the WOT problem were made as input variables. The script enable us to conveniently study the WOT of a wide range of web under real winding conditions. We also hope the python script can help analysts to focus on the physical problem itself and quickly iterate.

7.2 Future Work

7.2.1 Other Types of Winders

This study revealed the mechanics of formation of wound-on-tension. Although the fundamental mechanism of the formation of wound-on-tension is same, different types of winder exhibit their specific rule of wound-on-tension. We have studied wound-on-tension of the specific winder types as center winder with nip roller, surface winder, and surface winder with assist torque. However, there are other types of winder that are used

in industry. An example of a type of winder that is used in one of our sponsor's facility is the belt driven winder. The winder is used to wind delicate webs such as tissue paper. Though the belt may be viewed as a softer and larger nip roller, the contact area, stick-slip behavior can be quite different from the winder covered in this study. It may be valuable to study the specific formation of wound-on-tension in this type of winder if the wound roll stresses needs to be better controlled. The similar finite element modeling technique developed in this study can be adapted to study other types of winder.

7.2.2 A 3D Winding with Continuum Shell Elements

Due to the expensive computational cost of winding simulations relative to the current state of computational resources, this study is restricted to only model a section of the wound roll. The underlying assumption is that if the thickness of web is uniform, the wound-on-tension will have a uniform distribution across most part of roll in the CMD direction. The planar model will accurately predict the value of wound-on-tension. However, the variation of web thickness across the roll width is not a rare issue. When the web thickness does vary across the roll width, the wound-on-tension also varies across the roll width. This case a planar model fails. Continuum shell elements in Abaqus are continuum-based elements that have a node at each corner of a cube. Therefore, it can accurately model the double-sided contact occurred to web layers in a roll. On the other hand, it still uses the formulation of shell elements, which means the bending stresses can be calculated by only one layer of element through thickness direction, instead of multiple layers of elements when using the solid elements. This may reduce the overall computational cost to a manageable level even with the current computational resources.

The finite element model using continuum shell elements will be a truly 3D model that is able to study the effect of variation of web thickness on wound-on-tension.

7.2.3 Development of a New Type of Element Suited for Winding

The explicit finite element simulations of winding processes using solid elements are extremely expensive computations. This is mainly due to two factors: the large model size and the small time increment. The large model size is caused by that multiple layers of solid elements have to be used to accurately compute the stress results; bearing the thin nature of webs, the height of element is even smaller. Furthermore, an accurate finite element result also requires a reasonable aspect ratio for the solid elements and the stress concentration in the nip contact zone require finer elements in the MD, the length of the element that can be used is also restricted to be small. Therefore, a large number of elements have to be used. On the other hand, the small dimension of the elements further causes a small time increment due to the conditional stability of the explicit. The beam element is a kind of structural element based on the beam theory. It is able to accurately calculate the bending stress by only one layer of element in the thickness direction. However, a typical beam element only has 2 or 3 nodes at the reference axis of the beam. It cannot model the double-sided contact of web layers in a roll. If we can develop a new kind of continuum-based beam element which has distinct nodes at the top and bottom plane, similar with the continuum-based shell elements in the 3D case, the double-sided contact can be modeled and only one layer of element is necessary to accurately predict the bending stresses. The computational cost will be reduced at least two thirds. With this kind of elements, the 2D modeling of a complete web line may be viable.

References

1. **Good, J.K.** Basic Definitions. *Web Handling Research Center - WHRC.* [Online] Oklahoma State University. http://webhandling.okstate.edu/definition/definition.html.

2. **Good, J.K. and Roisum, D.R.** *Winding: Machines, Mechanics and Measurements.* s.l. : TAPPI Press, 2008.

3. *Predicting internal stresses in center-wound rolls with an undriven nip roller.* **Good, J. Keith and Fikes, M.** 6, 1991, Tappi journal, Vol. 74, pp. 101-109.

4. **Gutterman, R.P.** *Theoretical and Practical Studies of Magnetic Tape Winding Tension and of Environmental Roll Stability.* 1959. U.S. Contract No. DA-18-119-SC-42.

5. *A Study of Stress Distribution in Pirns.* **Catlow, M.G. and Walls, G.W.** 1962, Journal of Textile Institute, Vol. Part 3, pp. 410-429.

6. *Web Winding Simulation and Wound Roll Stresses.* **Yanabe, S., Takahashi, K. and Yamashita, T.** 1, 2010, Journal of Advanced Mechanical Design, System, and Manufacturing, Vol. 4, pp. 281-289.

7. *Winding Virtual Rolls.* **Kandadai, B.K. and Good, J.K.** 6, 6 2011, TAPPI Journal, Vol. 96, pp. 25-31.

8. *Using a Two-dimensional Winding Model to Predict Wound Roll Stresses that Occur due to Circumferential Steps in Core Diameter or t Cross Web Caliper Variation.* **Kedl, D.M.** Oklahoma State University, Stillwater : s.n., 1991. Proceddings of the First Interational Conference on Web Handling. pp. 99-112.

9. *On the Effect of Width Direction Thickness Variations in Wound Rolls.* **Hakiel, Z.** Stillwater, OK : s.n., 1991. Proceedings of the First International Conference on Web Handing. pp. 79-98.

10. *A Nonlinear Wound Roll Model Accounting for Widthwise Web Thickness Nonuniformities.* **Cole, K.A. and Hakiel, Z.** 1992. Preceedings of the Web Handling Symposium, ASME Applied Mechanics Division. pp. 13-24.

11. *A Nonlinear Wound Roll Model Allowing for Large Deformation.* **Benson, R.C.** 12, 12 1995, Journal of Applied Mechanics, Vol. 62, pp. 853-859.

12. *Formulas for Computing the Stresses in Center-Wound Rolls.* **Altmann, H.C.** 4, 4 1968, TAPPI Journal, Vol. 51, pp. 176-179.

13. *Internal Pressures in a Wound Roll of Paper.* **Pfeiffer, J.** 8, 8 1966, TAPPI Journal, Vol. 47, pp. 342-348.

14. *Losses in Wound-On-Tension in the Center Winding of Wound Rolls.* **Good, J.K., Pfeiffer, J.D. and Giachetto, R.M.** 1992. Proceeding of the Web Handling Symposium. pp. 1-12.

15. *An Axisymmetric Finite Element Model for Center Winding Webs.* **Hoffecker, P. and Good, J.K.** Stillwater, OK : s.n., 2005. Proceedings of the Eighth International Conference on Web Handling.

16. *Axisymmetric Wound Roll Models.* **Mollamahmutoglu, C. and Good, J.K.** Stillwater, OK : s.n., 2009. Procceedings of the Tenth International Conference on Web Handling.

17. *Nonlinear Model for Wound Roll Stresses.* **Hakiel, Z.** 5, 5 1987, TAPPI Journal, Vol. 70, pp. 113-117.

18. *A Width-wise Variation of Magnetic Tape Pack Stresses.* **Lee, Y.M. and Wickert, J.A.** 3, 3 2002, ASME Journal of Applied Mechanics, Vol. 69, pp. 358-369.

19. *Stress Field in Finite Width Axisymmetric Wound Rolls.* **Lee, Y.M. and Wickert, J.A.** 2, 2 2002, ASME Journal of Applied Mechanics, Vol. 69, pp. 130-138.

20. *Mechanics of a Rolling Nip on Paper Webs.* **Pfeiffer, J.** 8, 8 1968, TAPPI Journal, Vol. 49, pp. 77-86.

21. *Large Deformation Winding Models.* **Mollamahmutoglu, C. and Good, J.K.** Stillwater, Oklahoma : s.n., 2009. Proceedings of the Tenth International Web Handing Conference.

22. *Dynamics of Web Tension Control with Velocity or Torque Control.* **Shelton, J.J.** Seattle, WA : s.n., 1986. Proceedings of the American Control Conference. pp. 1423-1427.

23. **Struik, L.** *Lecture Notes on Winding Studies Presentation.* TNO Rubber Institute. Delft, Netherlands : s.n., 1984.

24. *The mechanism of nip-induced tension in wound rolls.* **Good, J.K. and Wu, Z.** 12 1993, Transactions of ASME, Vol. 60.

25. *Physical properties of newsprint rolls during winidng.* **Rand, T. and Ericsson, L.G.** 6, 1973, Tappi, Vol. 56.

26. *Nip Forces and Their Effect on Wound-in Tension.* **Pfeiffer, J.** 2, 1977, Tappi, Vol. 60.

27. *Centrifugally-Induced Stresses within Center-Wound Rolls-Part II.* **Yagoda, H. P.** 4, 4 1980, Mechanics Research Communications, Vol. 7, pp. 233-240.

28. *On the Effect of Centrifugal Force on Winding.* **Olsen, J.E.** 7, 7 1995, TAPPI Journal, Vol. 78, pp. 191-195.

29. **Bathe, K.J.** *Finite Element Procedures.* Englewood Cliffs, NJ : Prentice-Hall, Inc., 1996.

30. **Jiang, Wenxing.** *Development of Non-Interfering Wound-On-Tension Measurement Method.* Stillwater : Oklahoma State Univeristy, 2014.

31. **Ren, Yao and Good, J. K.** *Python script for modeling nip winding.* Stillwater, OK : Oklahoma State University, 2016.

32. *Development of sheet tenison under a rolling nip on a paper stack.* **Ärölä, K. and von Hertzen, R.** 47, 2005, International Journal of Mechanical Science, pp. 110-113.

33. **Welch, A.D.** *Study on the Development in Axial Stresses in Wound Rolls.* Mechanical and Aerospace Engineering, Oklahoma State University. Stillwater, OK : s.n., 2006.

34. **Roisum, D.R.** *The Mechanics of Winding.* s.l. : TAPPI Press, 1994.

35. **Smith, R.D.** *Roll and Web Defect Terminology.* s.l. : TAPPI Press, 1995.

36. *Prediction of Roll Defects from Roll Structure Formulas.* **Pfeiffer, J.** 10, 10 1979, TAPPI Journal, Vol. 62, pp. 83-87.

37. *Effects of Cross Direction Caliper Variation in Winding.* **Spitz, D.A.** 6 1969, TAPPI Journal, Vol. 52, pp. 1168-1170.

38. *Nonlinear Model for Wound Roll Stresses.* **Hakiel, Z.** 1986. Fishing and Converting Conference Proceeding.

39. **Timoshenko, S.P. and Gere, J.M.** *Theory of Elastic Stability.* New York : McGraw-Hill Book, 1961.

40. **Allen, H.G. and Bulson, P.S.** *Background to Buckling.* Maindenhead : McGraw-Hill Book (UK), 1980.

41. *Wound Roll Stress Analysis including Air Entrainment and the Formation of Roll Defects.* **Forrest, A.W.** Stillwater,OK : s.n., 1995. Proceedings of the Third International Conference on Web Handling. pp. 113-131.

42. **Hetenyi, M.** *Beams on Elastic Foundation.* Ann Arbor, MI : The University of Michigan Press, 1946.

43. **Good, J.K.** *Mechanics of a Web during Winding-Report on Web Handling Semiannual Sporsors Meeting.* Web Handling Research Center, Oklahoma State University. Stillwater, OK : s.n., 2004.

44. *Buckling of Webs from Lateral Compressive Forces.* **Shelton, J.J.** Stillwater, OK : s.n., 1995. Proceedings of the Third International Conference on Web Handling. pp. 303-319.

45. *New developments in the non-linear theories of the buckling of thin cylindrical shells.* **Thielemann, W.F.** 1960. Aeronautics and Astronautics, Proc. Durand Centennial Conference. p. 76.

46. **Lee, B.O.** *Buckling Analysis of Starred Roll Defects in Center Wound Rolls.* Oklahoma State University. 1991. PhD Dissertation.

47. *Air Entrainment during Film Winding with Layon Rolls.* **Forrest, A.W.** Stillwater, OK : s.n., 1995. Proceedings of the Third International Conference on Web Handling. pp. 78-94.

48. *Corrugation and Buckling Defects in Wound Rolls.* **Lin, P.M. and Wickert, J.A.** 2, 2 2006, ASME Journal of Manufacturing Science and Engineering, Vol. 128, pp. 419-436.

Appendix

Attached below is the Python script that generates the finite element model of surface winding the SMS web.

```
# This Abaqus/Python script creates an Abaqus/Explicit model for users to simulate the 2D spiral winding process with a nip roller, specifically, center winding with nip and surface winding. The simulation results help to predict the Wound-on-tension value. This script is developed by Yao Ren and Dr. J.K. Good at Oklahoma State University.
# Model Assumptions:
#    0. This model uses a plane strain assumption
#    1. The core and nip roller are assumed to be rigid
#    2. The nonlinearity of radial modulus is assumed to follow Pfeiffer's relation
#    3. Out-of-plane shear modulus for SMS is found to be state dependent on the radial pressure and subjected to a power law relation. It can be measured by a natural frequency test on stacks of webs or inferred by iterating this parameter until an equal WOT is obtained compared to a known WOT test.
# Use:
#    0. Fill out the following parameters and save
#    1. In Abaqus/CAE, run through "File-Run Script..." and select this script
#    2. Submit the job generated in the Abaqus/CAE.
# Notice:
#    To deal with the state dependent radial modulus of web, an Abaqus subroutine VUMAT is generated. Solving with Abaqus subroutine requires an appropriate installation of Intel Fortran compiler. If the Fortran compiler is not appropriately installed, this script can only deal with the constant radial modulus case.

# Model parameters
#   Geometry
coreRadius = 3.75  # Radius of the core
nipRollerRadius = 8.5  # Radius of the nip roller
webThickness = 0.005  # Thickness of the web
webWidth = 7.5  # The width of the web
lapNum = 5  # Number of laps that will be wound on the core
```

```
#   Material
density = 0.00013  # Density of the web, 386 is the coefficient to transform the density in unit of [lb/in^3] to a consistent unit with [in., s, lbf.]. Mass scaling can be done by manually scaling up this parameter to save computational time.
E1 = 10543.  # MD Young's modulus, important parameter
Pk1 = 0.14  # Pfeiffer's constant 1, important parameter
Pk2 = 13.12  # Pfeiffer's constant 2, important parameter
# If Pk2<>0 then a vumat subroutine implemented Pfeiffer's law will be used for the state dependent radial modulus; if Pk2==0 then the Pk1 value will be taken as the constant radial modulus (E2=Pk1).
E3 = 10543.  # ZD Young's modulus
v12 = 0.36  # Poisson's ratio as loading in MD and deformation in ZD
v13 = 0.3  # Poisson's ratio as loading in MD and deformation in CMD
v23 = 0.01  # Poisson's ratio as loading in ZD and deformation in CMD
G12_A = 69.4 # Constant 1 of shear modulus in MD-ZD plane
G12_C = 0.488 # Constant 2 of shear modulus in MD-ZD plane
G12_M = 40 # The minimum value of shear modulus in MD-ZD plane
#  Shear modulus is an important parameter. SMS nonwoven is found to be a exponential function of radial pressure: G12 = G12_A * P^G12_C. G12_A and G12_c are two constants determined by tests. If G12_C is entered as 0, the shear modulus will be a constant equals to the value of G12_A.

#   Contact
cofCoreWeb = 0.45  # Coefficient of friction between web and core
cofNipRollerWeb = 0.47  # Coefficient of friction between web and nip roller
cofWebWeb = 0.36  # Coefficient of friction between web and web, important parameter

#   Loadings
nipLoad = 30  # Nip force as a concentrated force, in the unit of force, important parameter
windingTension = 2 # Web tension in the upstream span, in the unit of force, important parameter
angularVelocity = 2*pi  # [radian/s]
windingType = 1  # 0-center winding; 1-surface winding

#   FEA
numElementThickness = 3.  # Number of elements in the thickness direction, at least 3 to guarantee the results accuracy
elementLWRatio = 10.  # Length-width ratio of a element
```

```
objectiveInc = 0  # Objective time increment after mass scaling, if 0 no mass scaling will
be used
numCPUs = 4  # Number of CPU cores to do parallel computing
#       End of input



# Convert loadings from force unit to force/length unit
nipLoadAba = nipLoad / webWidth
windingTensionAba = windingTension / webWidth / webThickness



if windingType:
   jobName = 'SWN' + str(int(nipLoad)) + 'T' + str(int(windingTension)) + '-SMS'
#Name of job
else:
   jobName = 'CWN' + str(int(nipLoad)) + 'T' + str(int(windingTension)) + '-SMS'
#Name of job

from abaqus import *
from abaqusConstants import *
from regionToolset import *

# Calculate weblength and step time period
webLength=round(lapNum*2*pi*coreRadius+2*pi*(lapNum-
1)*webThickness+.2*(pi*nipRollerRadius))
Cd1=sqrt(E1/density)
# pretensionTimePeriod=4*webLength/Cd1*6
pretensionTimePeriod=1
nipLoadTimePeriod=0.5
if windingType==0:
   coreAngularVelocity=angularVelocity
else:
   coreAngularVelocity=angularVelocity*nipRollerRadius/coreRadius
windingTimePeriod=(lapNum*2*pi-
pretensionTimePeriod/2*coreAngularVelocity)/coreAngularVelocity+pretensionTimePer
iod

# Create model
modelWOT=mdb.Model(name='DynamicWinding')

import part

# Create core
sketchCore=modelWOT.ConstrainedSketch(name='Core', sheetSize=250.)
```

```
partCore=modelWOT.Part(name='Core', dimensionality=TWO_D_PLANAR,
type=ANALYTIC_RIGID_SURFACE)
```

VITA

Yao Ren

Candidate for the Degree of

Doctor of Philosophy

Thesis: THE WOUND-ON-TENSION OF WINDERS WITH NIP ROLLERS

Major Field: Mechanical and Aerospace Engineering

Biographical:

Education:

Completed the requirements for the Doctor of Philosophy in Mechanical and Aerospace Engineering at Oklahoma State University, Stillwater, Oklahoma in December, 2016.

Completed the requirements for the Master of Science in General Mechanics and Foundation of Mechancis at Beijing Institute of Technology, Beijing, China in 2008.

Completed the requirements for the Bachelor of Science in Vehicle Engineering at Beijing Institute of Technology, Beijing, China in 2006.